NOAA Technical Memorandum ERL AOML-59

ACOUSTIC REMOTE SENSING OF WASTE DISPOSAL IN THE OCEAN

John J. Tsai

Atlantic Oceanographic and Meteorological Laboratory
Miami, Florida
September 1984

UNITED STATES
DEPARTMENT OF COMMERCE

Malcolm Baldrige,
Secretary

NATIONAL OCEANIC AND
ATMOSPHERIC ADMINISTRATION

John V. Byrne,
Administrator

Environmental Research
Laboratories

Vernon E. Derr
Director

Property of
NOAA Miami Library
4301 Rickenbacker Causeway
Miami, Florida

021711

QC
807
.5
.U6
A5
59
C.2

NOTICE

Mention of a commercial company or product does not constitute an endorsement by NOAA Environmental Research Laboratories. Use for publicity or advertising purposes of information from this publication concerning proprietary products or the tests of such products is not authorized.

CONTENTS

TABLES

FIGURES

ACOUSTIC REMOTE SENSING OF WASTE DISPOSAL IN THE OCEAN

John J. Tsai

ABSTRACT. Four ocean dumping experiments at three different locations of both shallow and deep water (30 to 3000 m) are discussed and used to illustrate the application of acoustic remote sensing in the study of waste disposal in the ocean. The dumped materials include pharmaceutical wastes, dredged matter, and drilling fluid. Relative isoconcentration maps based on acoustic backscattered intensity measurements reveal plume structure and space-time particulate distribution of the dumped materials as well as the physical oceanographic features of the water column. Joseph and Sendner's model is applied to describe a two-process diffusion, and to calculate the apparent diffusivity, diffusion velocity, and the variance. Both the time dependence of the variance and the length scale dependence of the apparent diffusivity show good agreement with those from Okubo. On the basis of acoustic measurements, particle budget is found to decrease exponentially as a function of time in the shallow-water case. Direct and linear relationships are found among the observed acoustic intensity, measured total suspended material, theoretically calculated acoustic intensity, and total suspended material calculated from particle number and particle sizes. The analysis can be applied to other types of waste materials, and provide a new approach to monitor waste disposal in lakes, coastal zones, and open oceans.

I. INTRODUCTION

High-frequency acoustic studies of particulate materials in the water column have been carried out continuously by the U.S. National Oceanic and Atmospheric Administration - Atlantic Oceanographic and Meteorological Laboratory (NOAA-AOML) since the detection of low-density sediment distributions from a dredging operation in 1974 (Proni et al., 1976a). Among these studies were several successful ocean-dumping experiments that measured the space-time distribution of the dumped materials as a function of depth, and that obtained the dispersive growth for different stratifications of the water mass. The dumped materials included sewage sludge in New York Bight (Proni et al., 1976b), river bottom dredged materials in Lake Ontario (Proni et al., 1977) and materials from harbor dredging (Proni et al., 1975; Proni and Stewart, 1978), pharmaceutical wastes off Puerto Rico, and more recently, drilling muds from an oil rig in the Gulf of Mexico (Trefry and Proni, 1983). Results from these studies have provided good evidence that acoustic remote sensing can be useful for studying waste disposal in the ocean. Acoustic techniques may be used with other conventional oceanographic measurements such as temperature from conductivity-temperature-depth (CTD) analysis, and total suspended material and particle size from chemical instruments. All measurements can take place simultaneously on board a research vessel. Acoustic data provide real-time plume structure of dumped waste material and water column information as well as necessary data for post-experimental analysis.

In most of the dumping operations, the research ship maintains its position perpendicular to and stays as close as possible to the course of the dumping vessel before the dumping takes place. Upon commencement of dumping, the ship then proceeds right into the plume and takes stations inside the plume for chemical sampling. After the chemical sampling, the ship proceeds

out of the plume and reenters the plume repeatedly for several transects before taking another station. In some cases, the ship will make several transects before taking the first station for a specific dump. When taking stations, the ship maintains its position in the most dense area of the plume as determined by acoustic profiles. The sampling depths are chosen by real-time acoustic backscattered signals from the suspended material in the water column so that the best results and correlations between acoustics and chemistry can be expected. The procedure has become standard for such ocean-dumping studies by acoustic remote sensing.

The acoustic systems used for remote sensing include both the 20-kHz system, with an operating frequency of 20 kHz and a peak power at the transducer of about 1 kW, and the 200-kHz system, with an operating frequency of 200 kHz and a peak power output of 80 W into its transducer. The transducer for each system is mounted in a hydrodynamically stable towbody and towed alongside the ship (Proni et al., 1977). The two systems often respond differently to a given type of suspended material in a given phase of the dispersion process (Proni et al., 1976b). One system is often more effective than the other in detecting and tracking suspended material during a given period of evolution of the plume resulting from the dumping. Therefore, both acoustic systems are used to guarantee success of the experiment.

The acoustic data can be recorded in two forms: real-time echograms on pressure-sensitive papers and analog signals on magnetic tapes. The paper records provide in-situ observations of plume structure and environmental conditions in which the dispersion study is to be conducted. The paper records also serve as guidance for precise depth for chemical sampling. The magnetic tape records the acoustic backscattered intensity that shows on the paper record. The tape can be played back in the laboratory after the field

experiment, and the data can be digitized using a PDP-11 minicomputer system. The digitized data are manipulated to compensate the spreading loss and are contour-plotted in the UNIVAC computer to show the levels of equal acoustic backscattered intensities. These contour lines also represent the isoconcentration levels of suspended particulate material within the water column. The equivalent radius of the area bounded by the isoconcentration line can be calculated by a line digitizer for all desired levels of particulate concentration. Joseph and Sendner's (1962) dispersion model can then be applied to find the relevant diffusion parameters for different dispersion studies.

Results from different ocean dumping experiments will be presented to demonstrate the usefulness of the acoustic remote-sensing technique. The diffusion parameters for one particular experiment will be completely analyzed and compared with other results whenever available. Okubo's (1962a,b) diffusion model will be discussed to differentiate the significance.

II. EXPERIMENTAL RESULTS

Results from four ocean-dumping experiments at three different locations are presented to illustrate the acoustic remote-sensing technique in dispersion studies. The dumped matter includes pharmaceutical wastes, dredged materials, and discharged drilling muds. The experiments took place in both shallow and deep water, and cover a 3-year period from 1978 to 1981.

A. Puerto Rico Arecibo Industrial Waste Dumpsite

Two ocean-dumping operations took place at the Puerto Rico Arecibo Industrial Waste Dumpsite (Fig. 1) in February and October 1978. The dumped industrial waste, taken from several pharmaceutical plants, was equivalent to

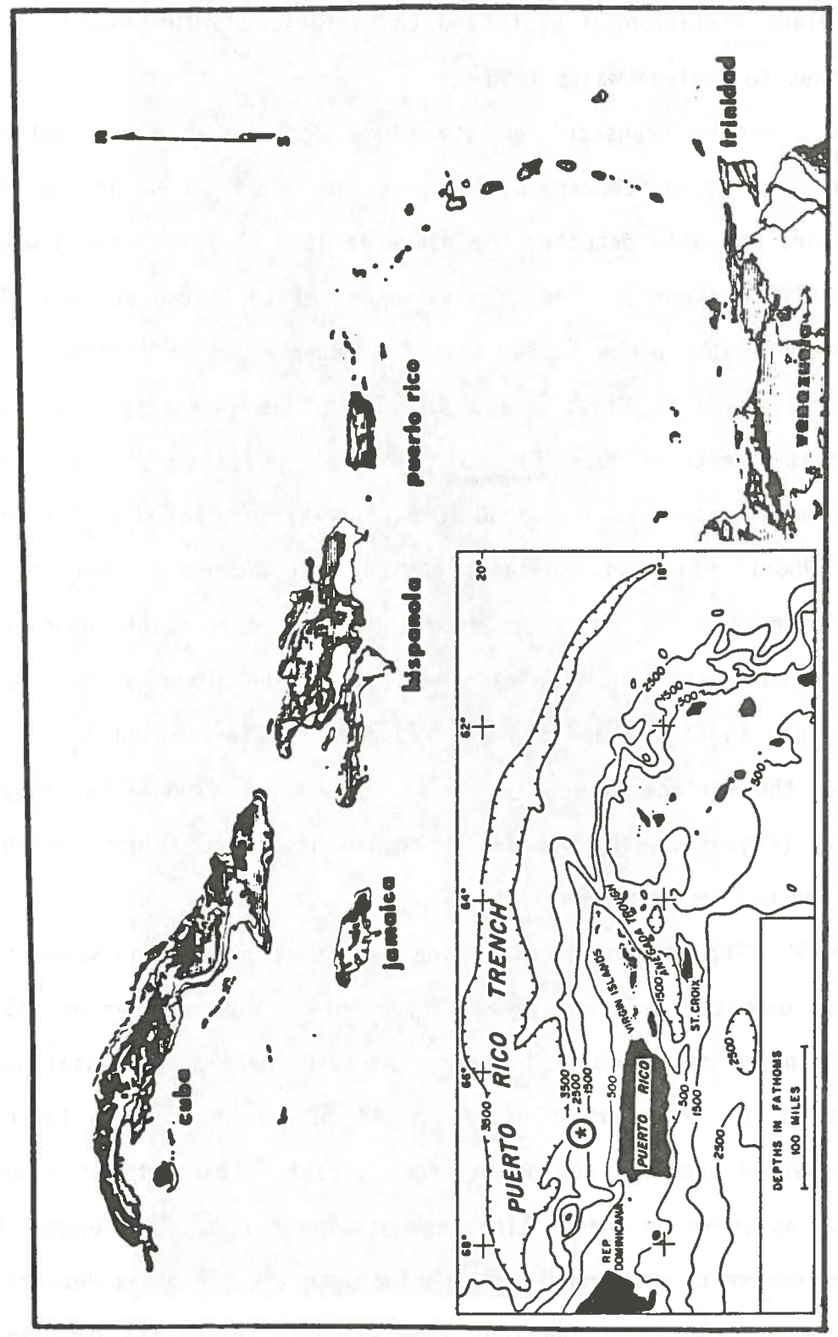

Fig. 1. Geologic map of the Caribbean region and location of the Puerto Rico Arecibo Industrial Waste Dumpsite (indicated by the *).

seawater in density, slightly acidic, 1 to 3 percent in total organic carbon, and 0.05 to 4 percent in suspended solids. The range in composition is due both to within-plant variation of waste and to variation in the amount of a given plant's input to a given waste load.

One of the acoustic transects of the plume detected 5 hours and 25 minutes after the dumping on February 6, 1978, is shown in Fig. 2. The acoustic system on board the ship detected the plume at 1636 LT (local time) when the ship moved at 4 kn (knots). The ship moved out of the plume at 1651 LT. The estimated width of the plume is 1.8 km. Two other acoustic transects of the same plume are shown in Figs. 3 and 4. The plume intensity peaks at 1830 LT and reaches a depth of 30 m (Fig. 3). The ship moved out of the plume at 1838 LT and reentered the same plume at 1845 LT. The ship moved out of the plume again at 1900 LT (Fig. 4). Because of the high background concentration, the plume boundaries are not clear from the acoustic profiles. However, they will be revealed in the contour maps shown later. The plume was retained above the 50-m depth in Fig. 2 and above 40-m depth in Figs. 3 and 4. Both depths are within the surface mixed layer measured with an expendable bathythermograph (XBT) (Fig. 5). The mixed-layer depth has great effects on the plume structure and will be discussed later.

On October 29, 1978, one particular line dump took place from south to north at the same dumpsite. The plume was detected 45 minutes later at 1155 LT (Fig. 6). The plume consisted of two parts because the dumping vessel had two tanks. This initial plume width was about 300 m. About 18 hours later, the plume was observed acoustically during four parallel transects at about the same location as shown by shaded line segments in Fig. 7. The length of the line segment represents the actual time period when the plume was detected acoustically for each transect. The four line segments reveal the east and

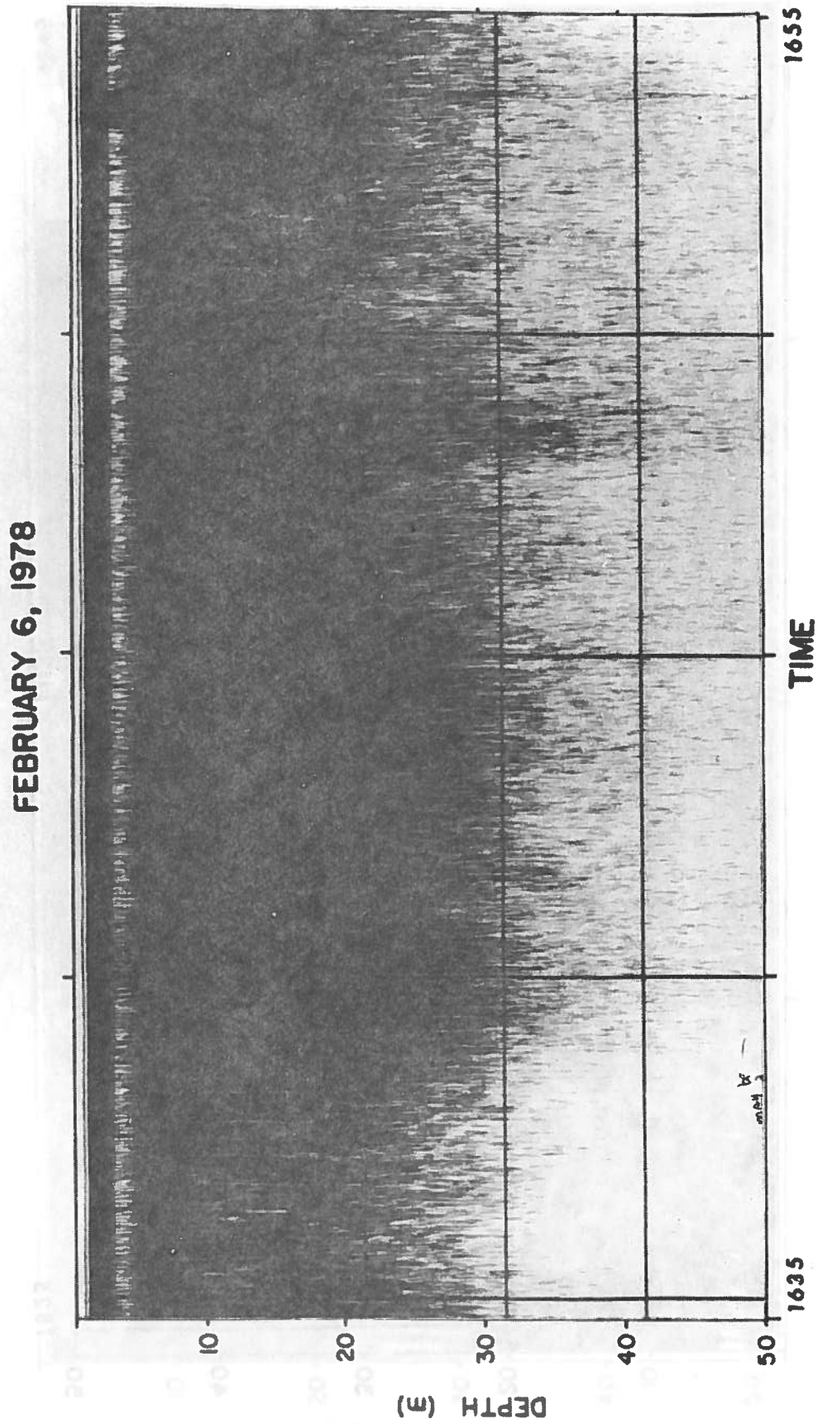

Fig. 2. Continuous acoustic transect of the line dump on February 6, 1978, during the Puerto Rico Arecibo Industrial Waste Dumping Experiment.

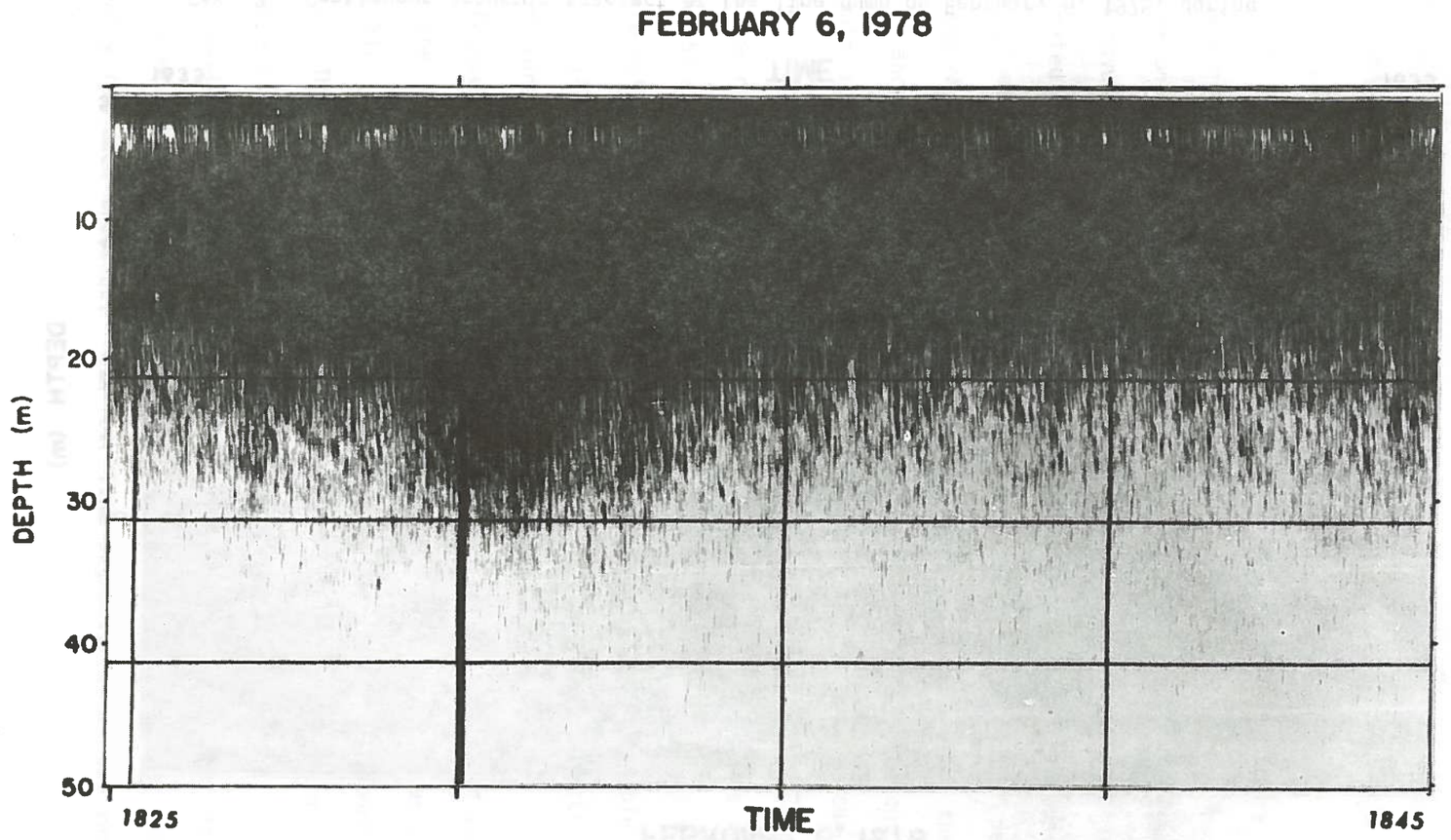

Fig. 3. Continuous acoustic transect of the same plume in Fig. 2 at later time.

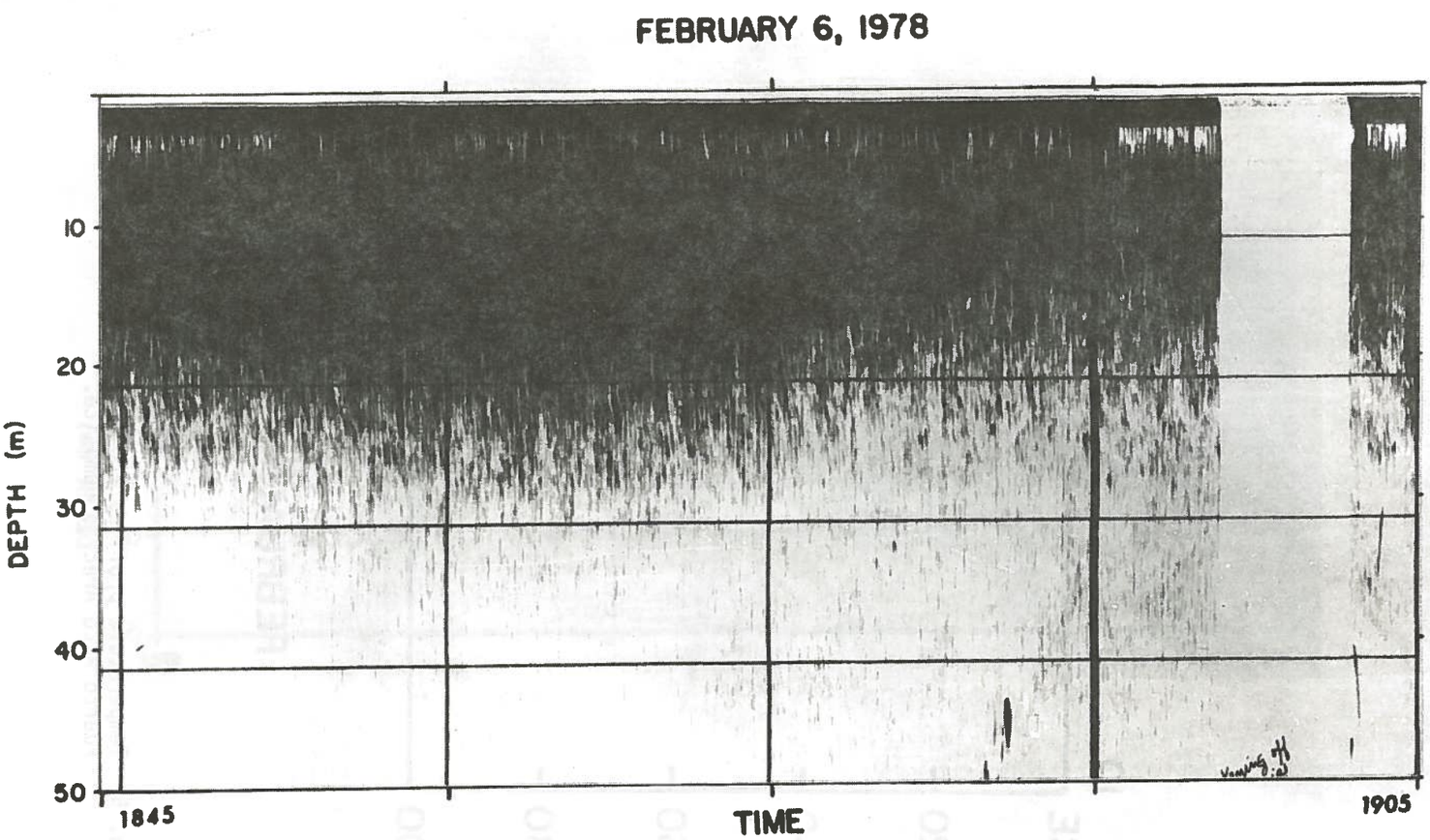

Fig. 4. Continuous acoustic transect of the same plume in Fig. 3.

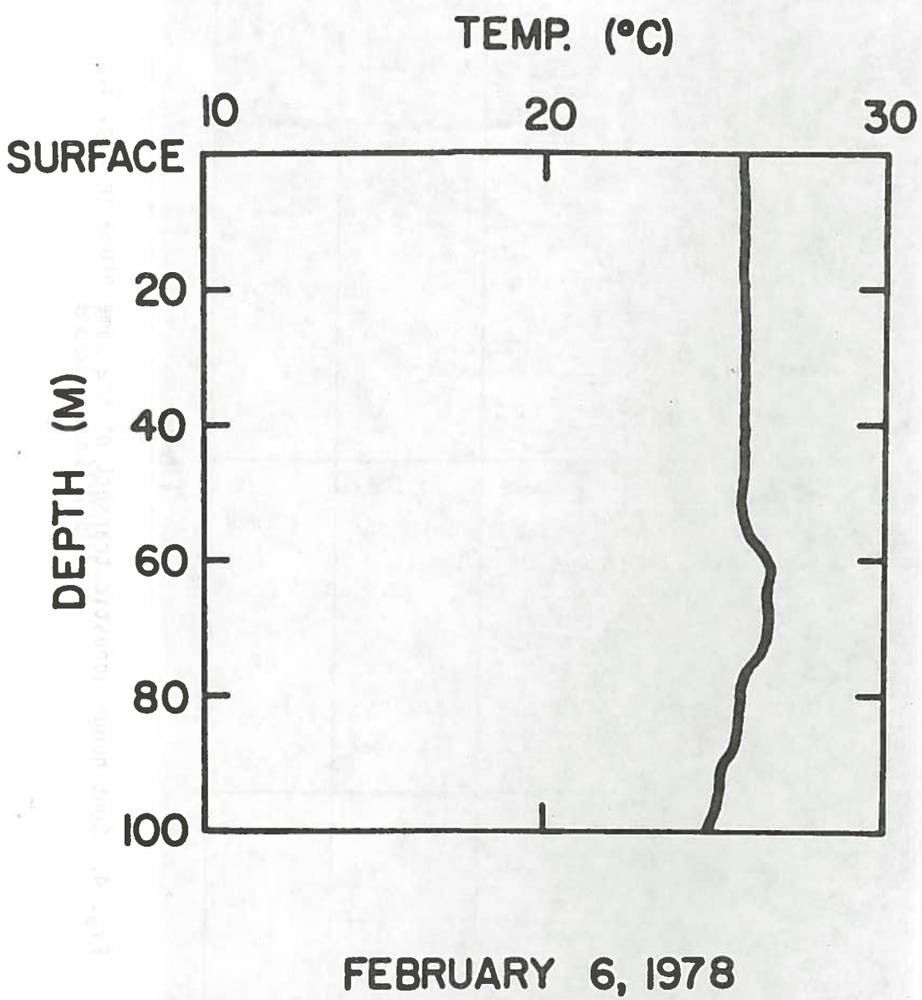

Fig. 5. Temperature profiles from XBT measurements at Puerto Rico Arecibo Dumpsite.

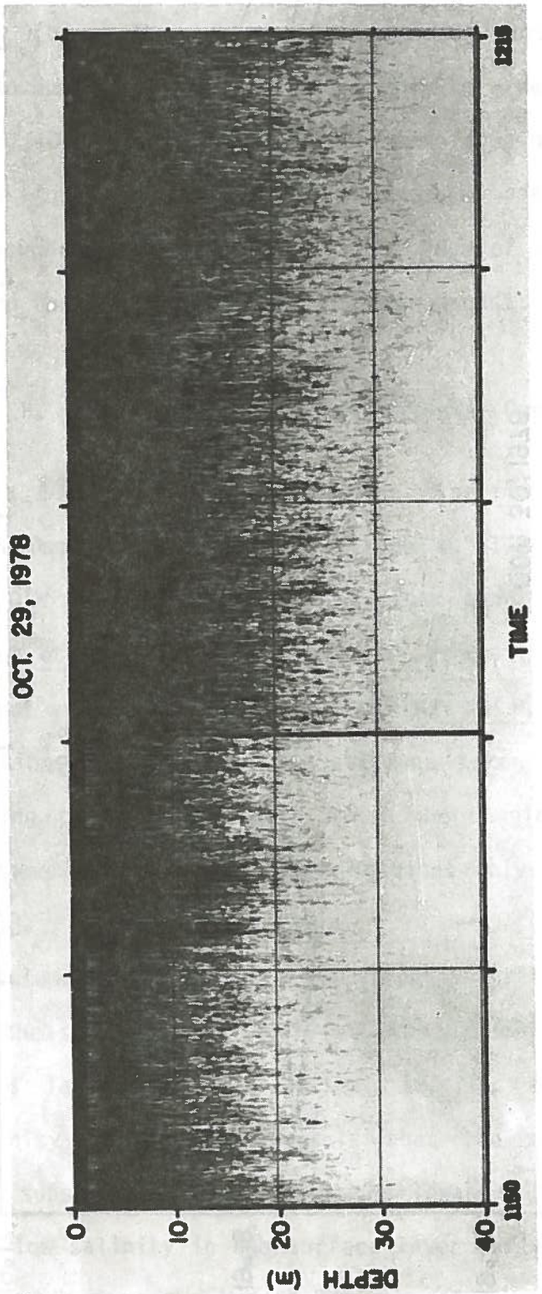

Fig. 6. Acoustic profile of the initial transect of the line dump on October 29, 1978, during the Second Puerto Rico Arecibo Industrial Waste Dumping Experiment.

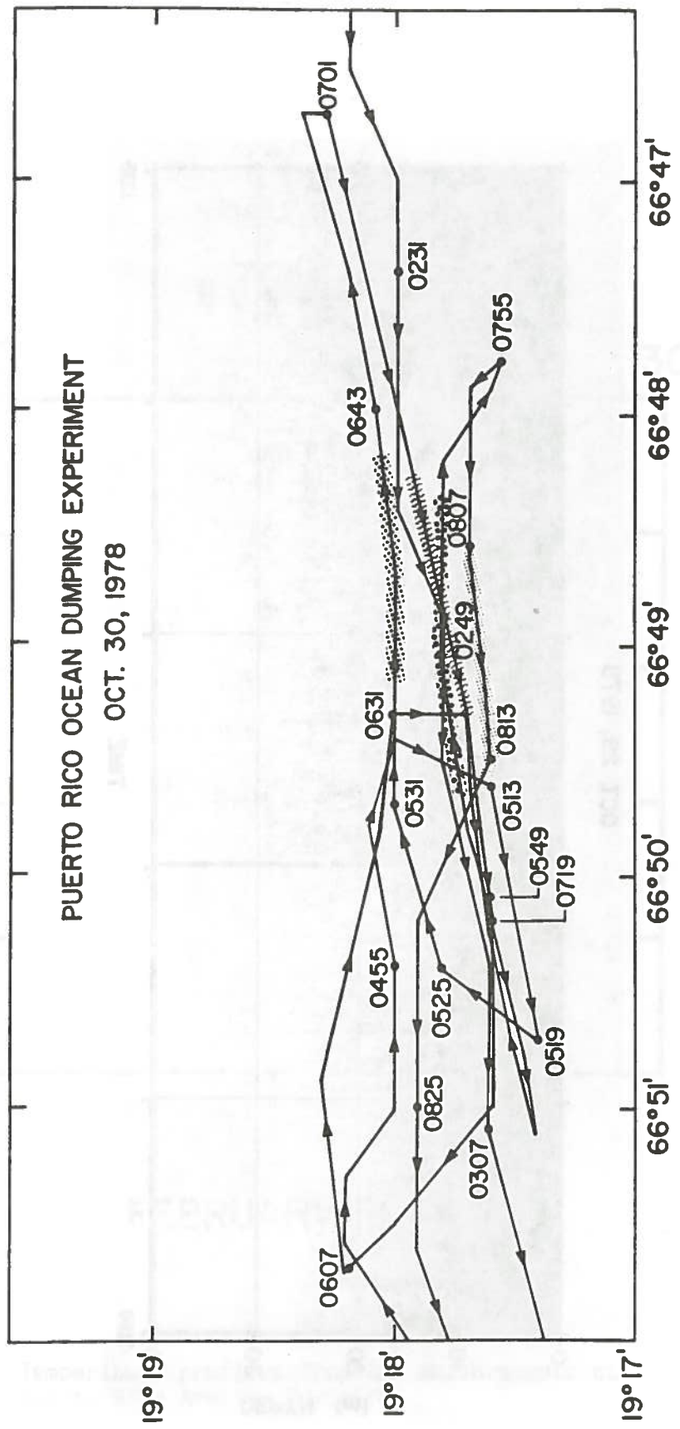

Fig. 7. Portion of the ship tracks on October 30, 1978, during the Second Puerto Rico Arecibo Industrial Waste Dumping Experiment. The shaded line segments indicate the acoustic observations of the same line dump in Fig. 6.

west boundaries of the plume along the northeast to southwest direction. These four acoustic transects are shown in Figs. 8 and 9. The ship moved from west to east in Figs. 8(a) and 9(a), and moved in the opposite direction in Figs. 8(b) and 9(b). The observations are 18 hours or later after the initiation of the dump. The plume extended only to a depth within the surface mixed layer (Fig. 10) as observed in the previous dump on February 6, 1978.

Because the Antilles Current in the area is predominantly toward the west, a sharp boundary exists at the eastern edge of the plume. This sharp and clear eastern boundary appeared on all four acoustic profiles.

B. New York Bight Dredged Material Dumpsite

During June 1979, a number of dumping experiments took place at the Dredged Material Dumpsite located at latitude 40°21.8'N-40°23.8'N, longitude 73°50.0'W-73°52.0'W [Fig. 11(a)] where enormous quantities of material were disposed (Kester et al., 1983). Both the acoustic systems and chemical sampling equipment were on board on the NOAA R/V G. B. Kelez. Table 1 lists times and locations of all chemical stations taken for the five dumping experiments during the 3-day period. Since the dumping took place approximately at the same location, the eight stations only covered about a 3-km^2 area [Fig. 11(b)].

The water column at the dumpsite was strongly stratified and consisted of three layers: the surface layer (0-10 m), the pycnocline (10-14 m), and the bottom nepheloid layer (14-26 m) (Figs. 12, 13, and 14). A detailed temperature-salinity (T-S) study reveals that the surface layer actually consists of two subsurface layers, with the lower salinity near the surface (Fig. 15). The low salinity in the surface layer reflects the bightward flow input of fresh water from the Hudson-Raritan estuary systems which produces

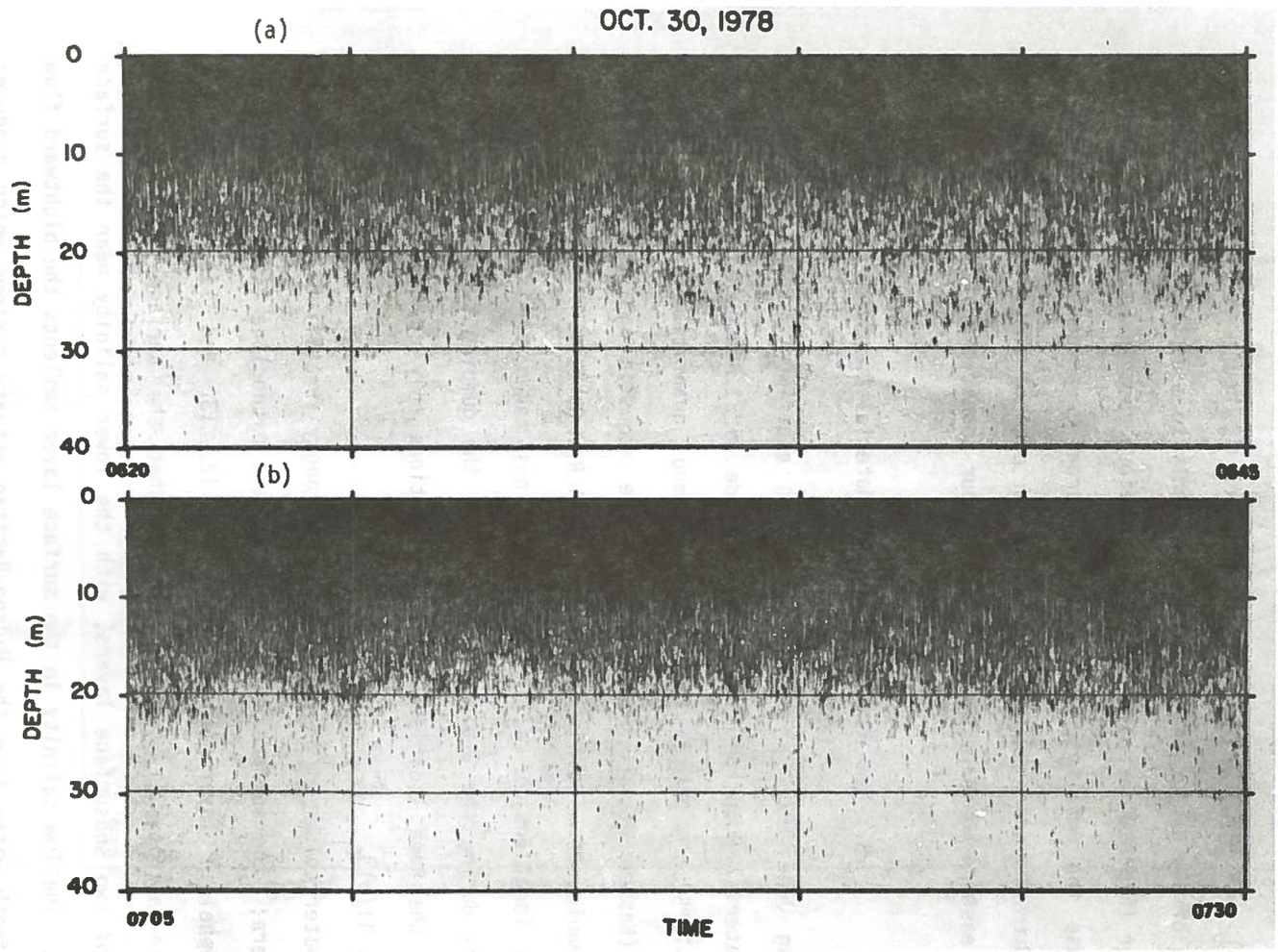

Fig. 8. Two of the four acoustic transects (shaded line segments) in Fig. 7, when the waste plume was observed.

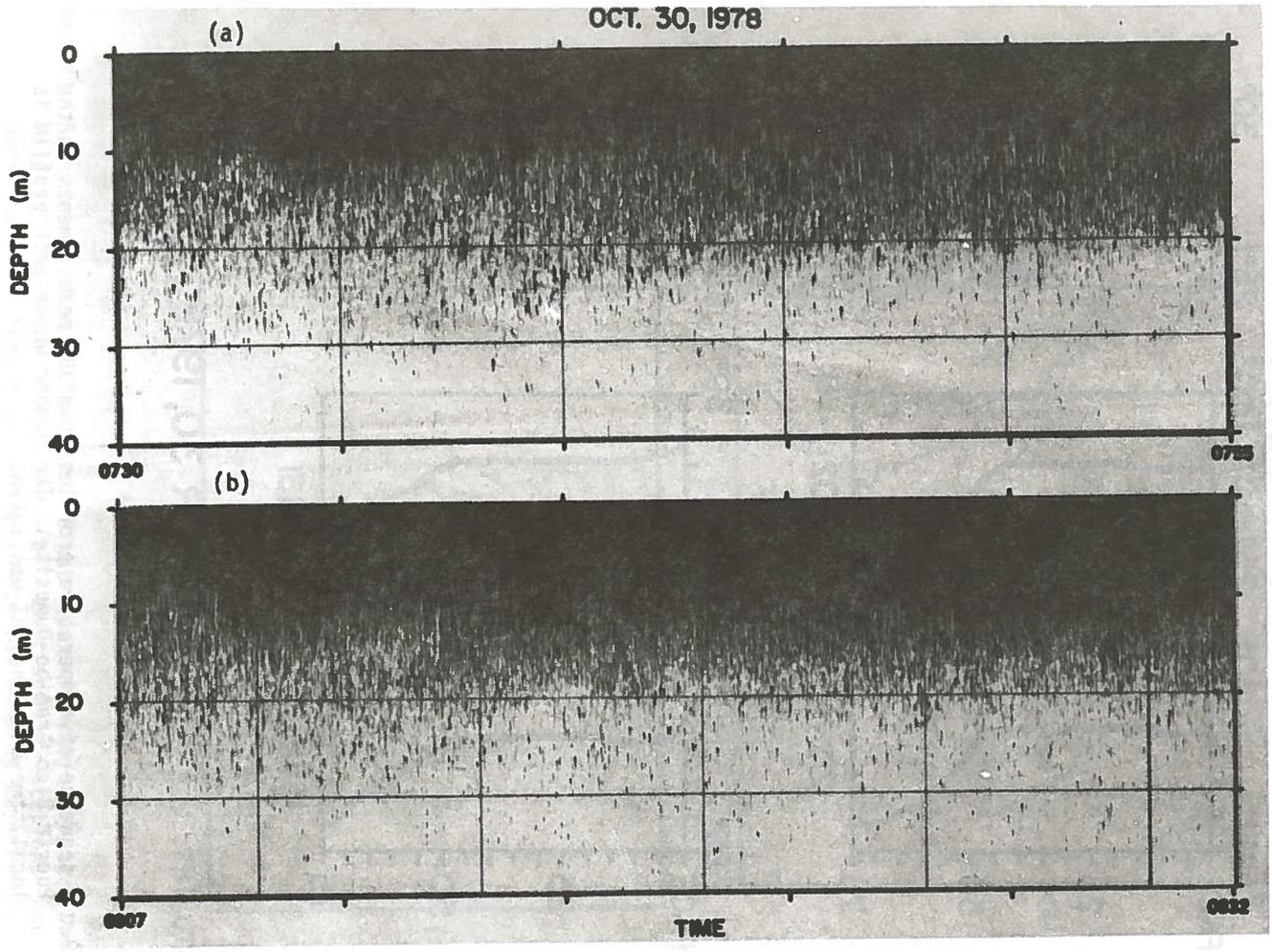

Fig. 9. The other two of the four acoustic transects in Fig. 7, when the waste plume was observed.

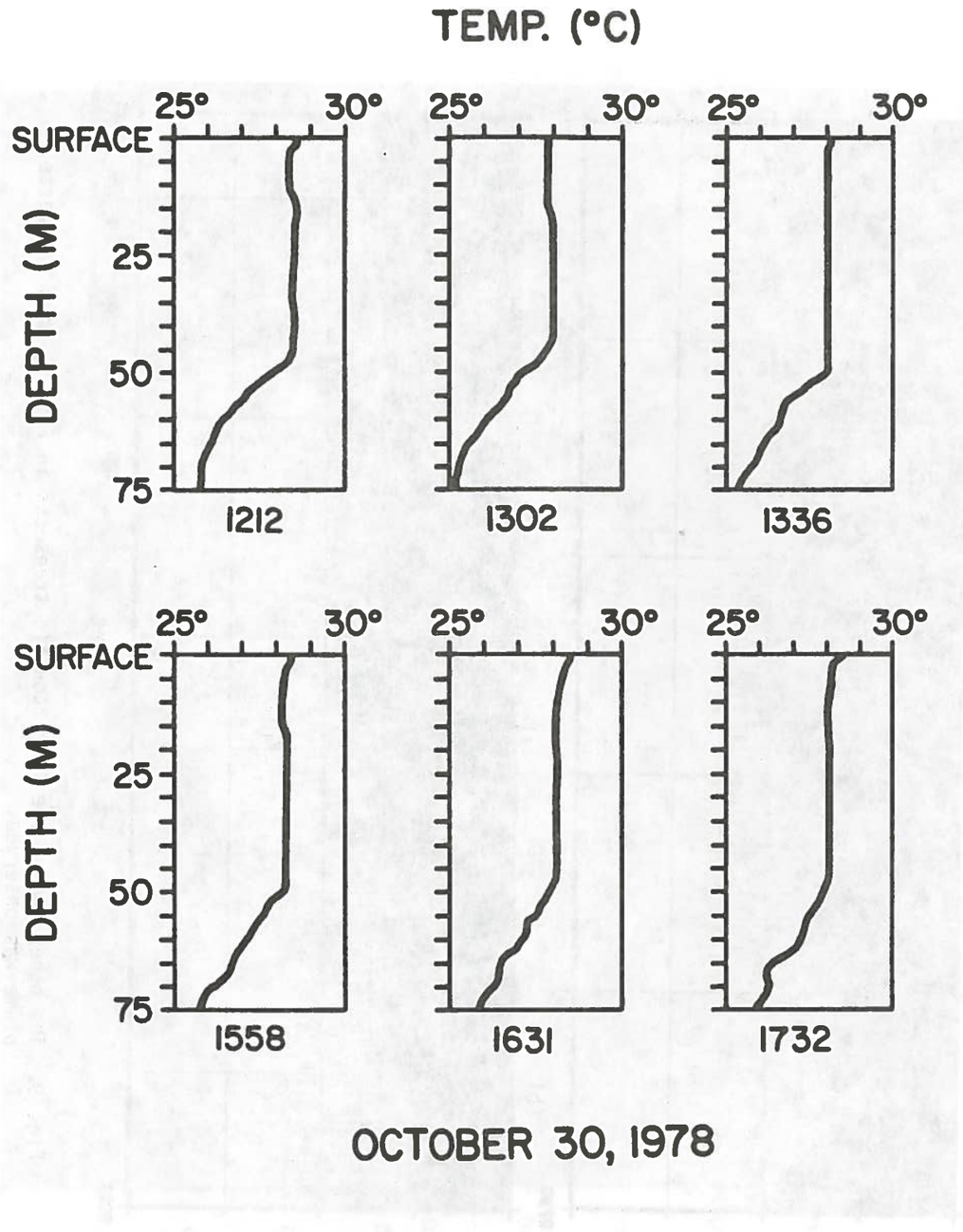

Fig. 10. A sequence of temperature profiles from XBT measurements at the Puerto Rico Arecibo Dumpsite. The number under each profile is local time when the XBT was taken.

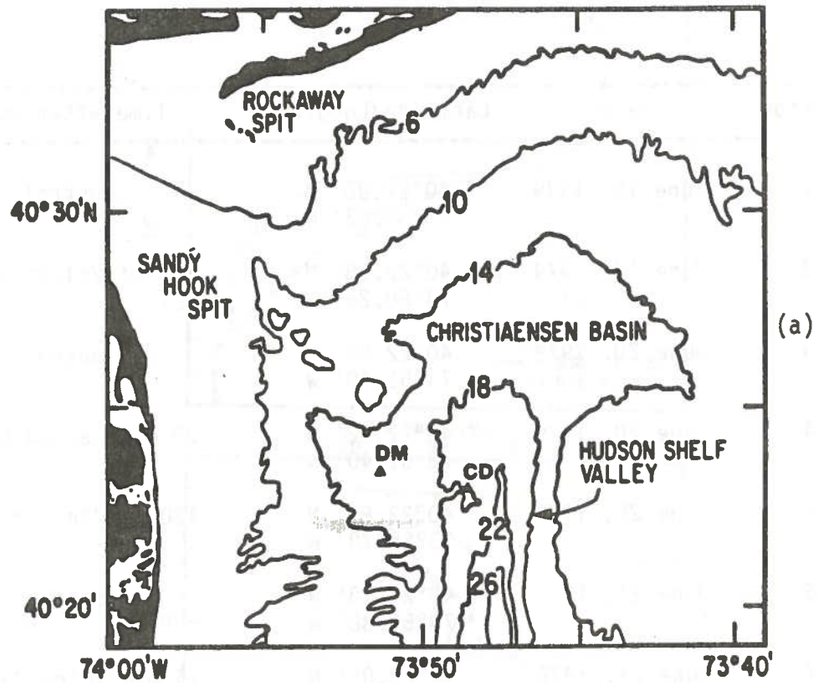

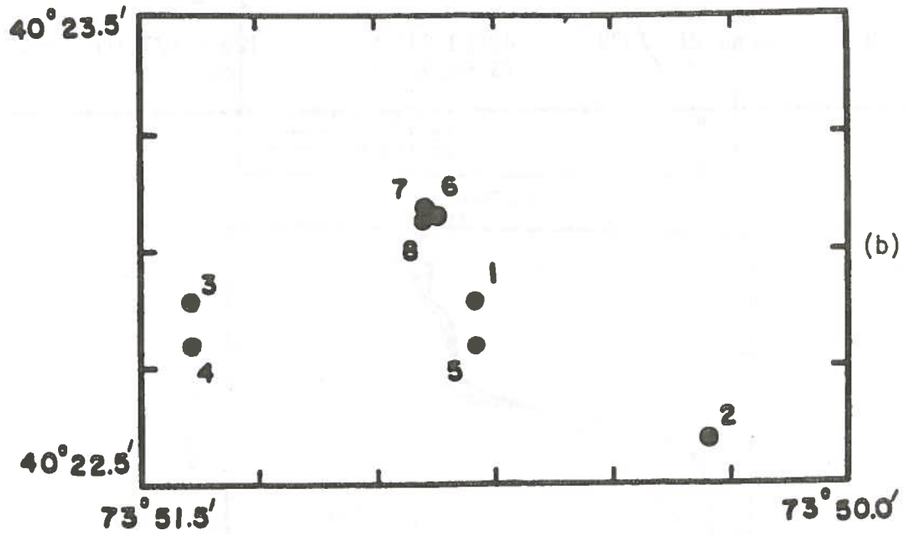

Fig. 11. Bathymetry of the New York Bight Apex showing (a) the Dredged Material Dumpsite (DM), and (b) locations of stations occupied during the New York Bight Dredged Material Dumping Experiments.

Table 1. Summary of the stations occupied during the Dredged Material Dumping Experiments in the New York Bight.

Station	Date	Latitude/Longitude	Time after Dump
1	June 19, 1979	40°22.90' N 73°50.83' W	Control
2	June 19, 1979	40°22.58' N 73°50.28' W	120 min/First Dump
3	June 20, 1979	40°22.90' N 73°51.40' W	Control
4	June 20, 1979	40°22.82' N 73°51.40' W	30 min/Second Dump
5	June 20, 1979	40°22.80' N 73°50.78' W	120 min/Second Dump
6	June 21, 1979	40°23.13' N 73°50.88' W	Control
7	June 21, 1979	40°23.05' N 73°50.88' W	15 min/Third Dump
8	June 21, 1979	40°23.03' N 73°50.98' W	120 min/Third Dump

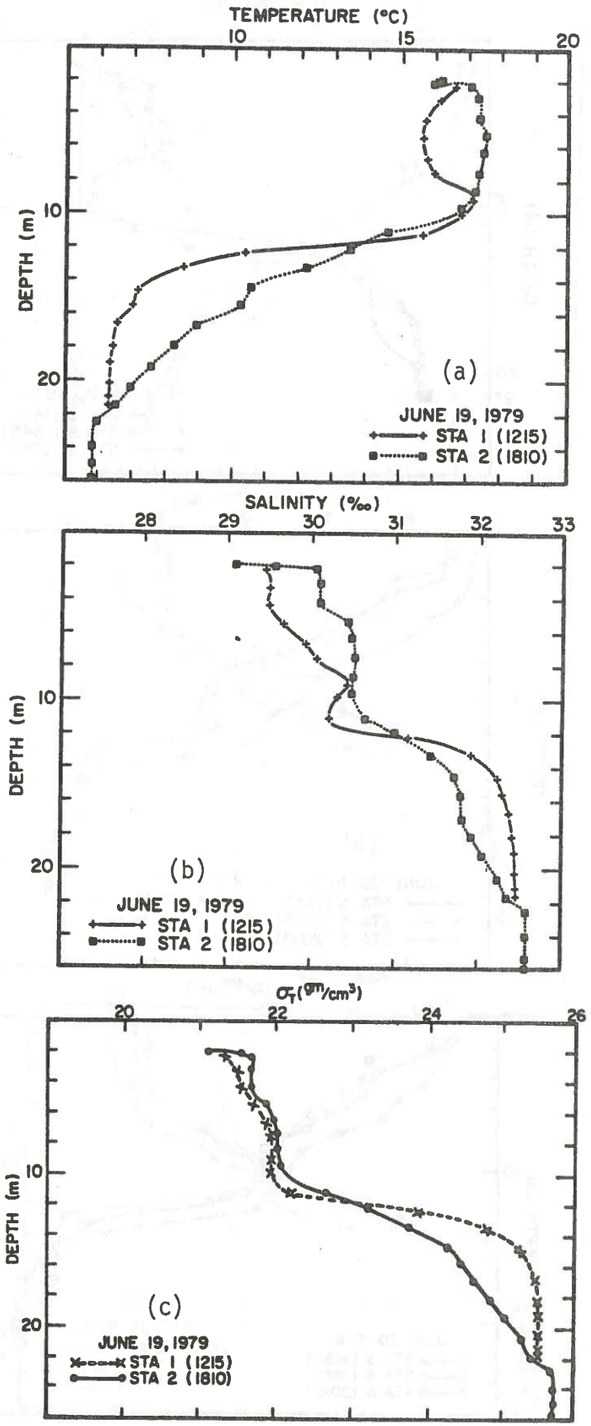

Fig. 12. Vertical profiles of (a) temperature, (b) salinity, and (c) σ_t for Stations 1 and 2 in Fig. 11(b).

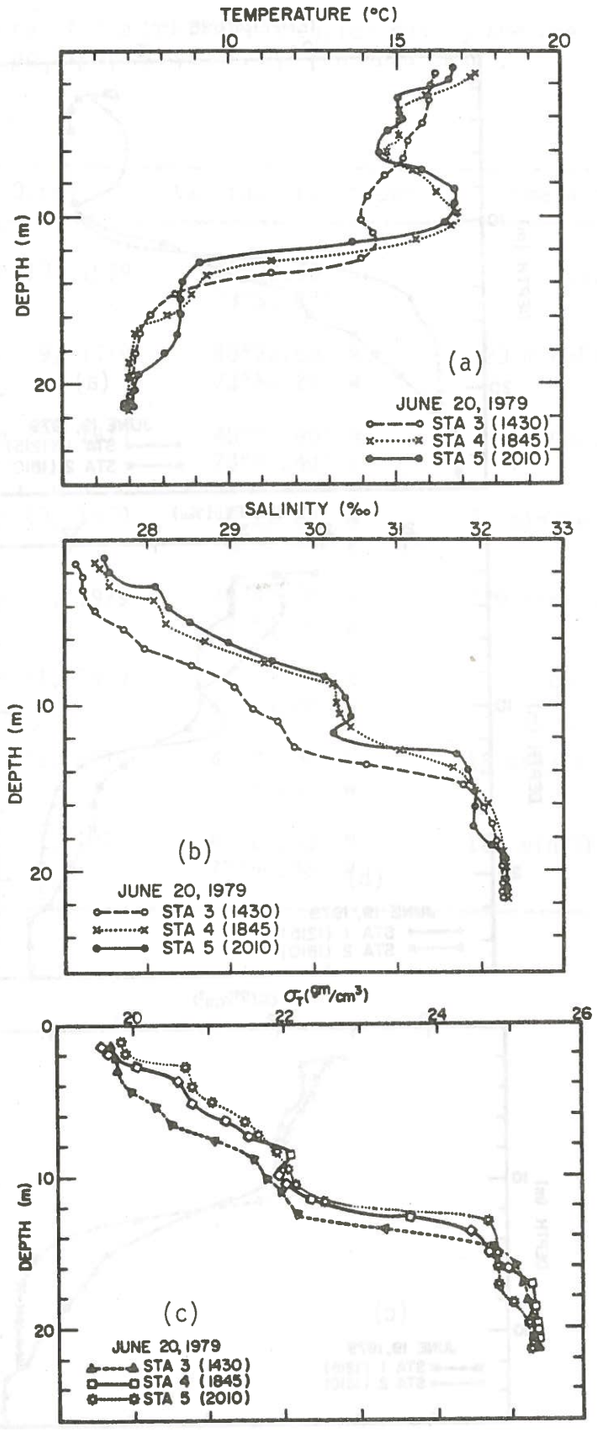

Fig. 13. Vertical profiles of (a) temperature, (b) salinity, and (c) σ_t for Stations 3, 4, and 5 in Fig. 11(b).

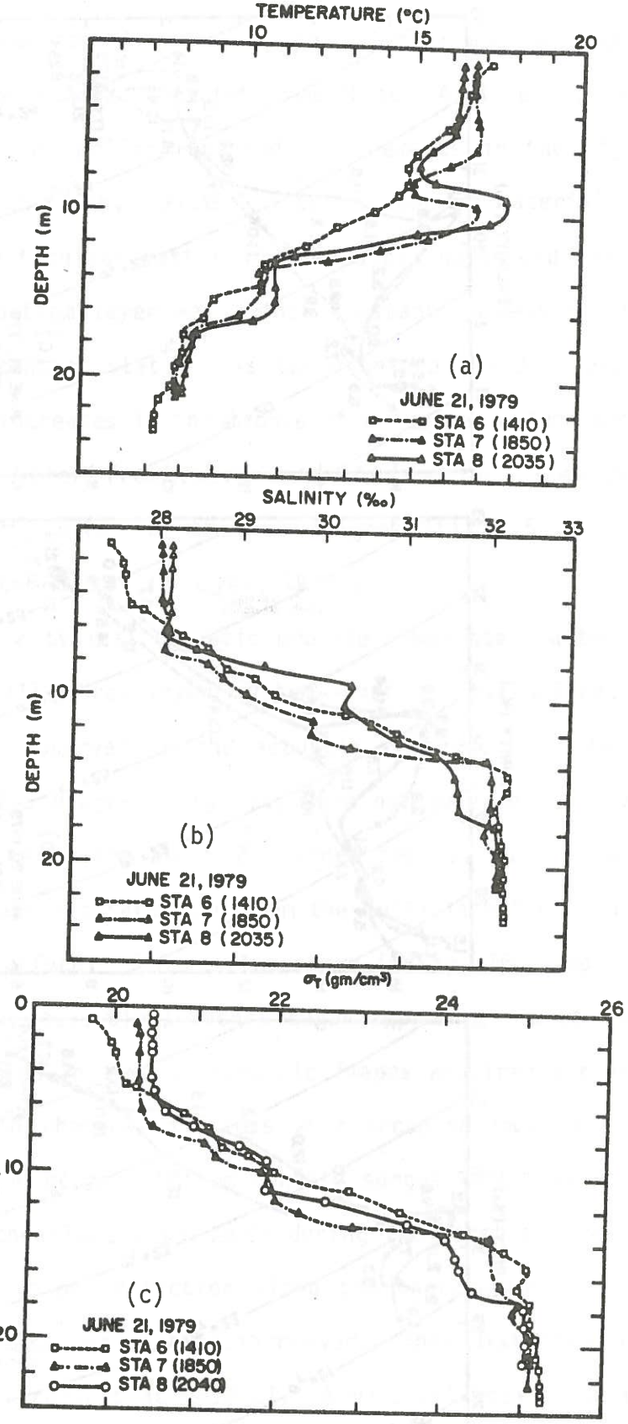

Fig. 14. Vertical profiles of (a) temperature, (b) salinity, and (c) σ_t (c) for Stations 6, 7, and 8 in Fig. 11(b).

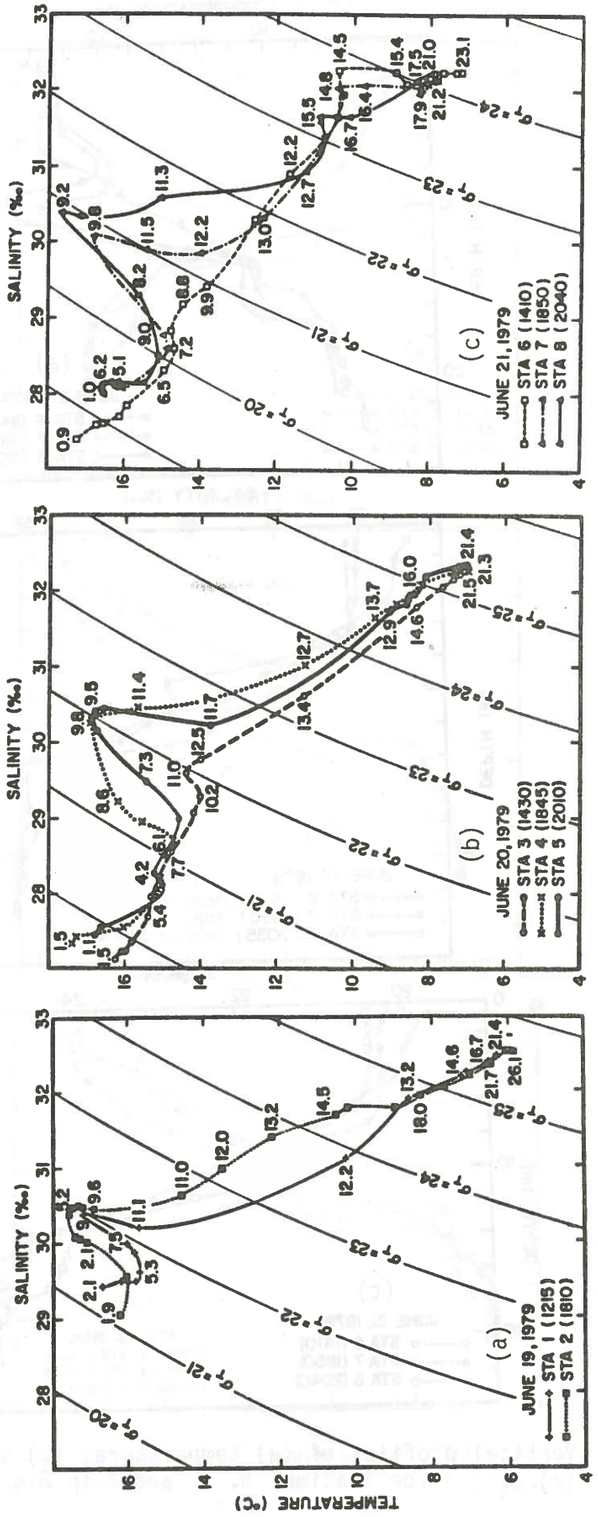

Fig. 15. Temperature-salinity diagrams for all eight stations in Fig. 11(b).

large vertical and horizontal gradients in salinity and density within the Bight apex. The pycnocline extended from 8 to 14 m depth; the range in temperature agrees with earlier reported measurements in the Bight apex for June (Bowman and Wunderlich, 1976). Total suspended material showed high concentrations of particulate matter in the bottom nepheloid layer (Mukherji et al., 1981); the bottom layer was almost constant in density, temperature, and salinity. One control station was taken before the dump each day. The temperature usually increases in the middle of the water column because of the intrusion of warmer water from above once the dumping takes place. This mixing is particularly clear in the T-S diagram (Fig. 15), appearing as a triangle of three water masses (Mamayev, 1975).

Figure 16 shows a typical acoustic profile immediately after the dump on June 21. The overall three-layer system--surface, pycnocline, and bottom nepheloid layer--was observed in the acoustic records. The two subsurface layers seen in the T-S diagram (Fig. 15) were not observed, however, because the acoustic transducers were about 2 m under the sea surface and the upper 3 to 5 m of sea surface was saturated from the multiple reflection of acoustic signals at the sea surface. For results shown in Fig. 16, dumping started at 1558 LT and the first acoustic transect began approximately at 1602 LT. The dump plume was detected in several acoustic images acquired during successive transects, because no chemical stations were occupied immediately after the initial contact of the plume. Bottom density surges were clearly seen in the increased width of the plume with depth during the first two transects. The plume was distorted in one direction along the thermocline and carried away horizontally from the center as time increased. This distortion was revealed clearly in the third transect at 1618 LT. A vertical shear flow is suggested as the main cause of the asymmetric plume structure here. The first two

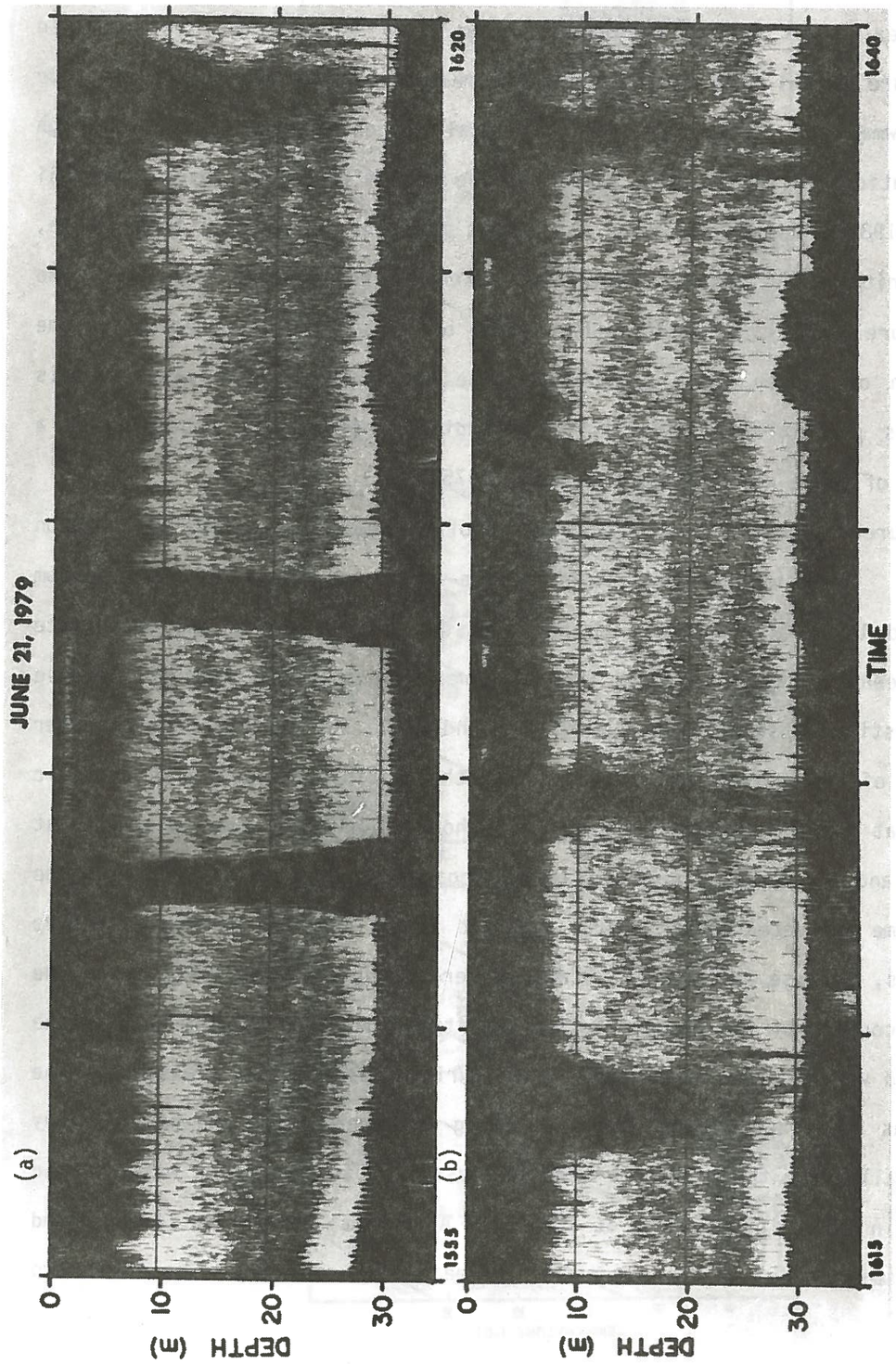

Fig. 16. Acoustic transects of the fourth spot dump at the New York Bight Dredged Material Dumpsite on June 21, 1979. The ship reversed course between two successive transects to enter from the opposite side of the plume.

transects, 4 and 10 minutes after the dump, showed sharp plume boundaries at the edges and intensive mixing inside the plume. The third transect, 10 minutes after the second one, showed a completely different plume structure. The sharp edges of the plume disappeared and dissipated into the surrounding water, indicating the passive phase of diffusion was taking place (Okubo, 1970, 1971a). The disappearance of the centroid of the plume near the bottom may suggest that the acoustic transect did not cut through the center of the plume. The fourth and fifth transects, 26 and 39 minutes respectively after the dump, show considerable reduction in both width and concentration of the plume.

Generally, the plume was not detectable acoustically in the New York Bight 1 hour after the dump because of the high concentration of background material in the water column. This is quite different from the waste dumping in the Puerto Rico Arecibo Industrial Waste Dumpsite. However, the water depths and stratification are quite different for both cases. Two other dumps of different dates taking place at the same New York Bight location are shown in Figs. 17 and 18.

The initial plume structure of the dump, on June 20, 1979 (Fig. 17), is different from the dump on June 21, 1979 (Fig. 16). There was no resuspension evident from the acoustic profiles. It is likely that the sediment may be quite different in nature at these two locations because the first transect of the two plumes took place 4 minutes after the dump. There is also a difference in plume structure near the surface. The shear flow effect is seen during the second transect in Fig. 17. The third transect at 1335 LT only showed a rough plume boundary. Actually the plume is almost indistinguishable from the dense background water 40 minutes after the beginning of the dump.

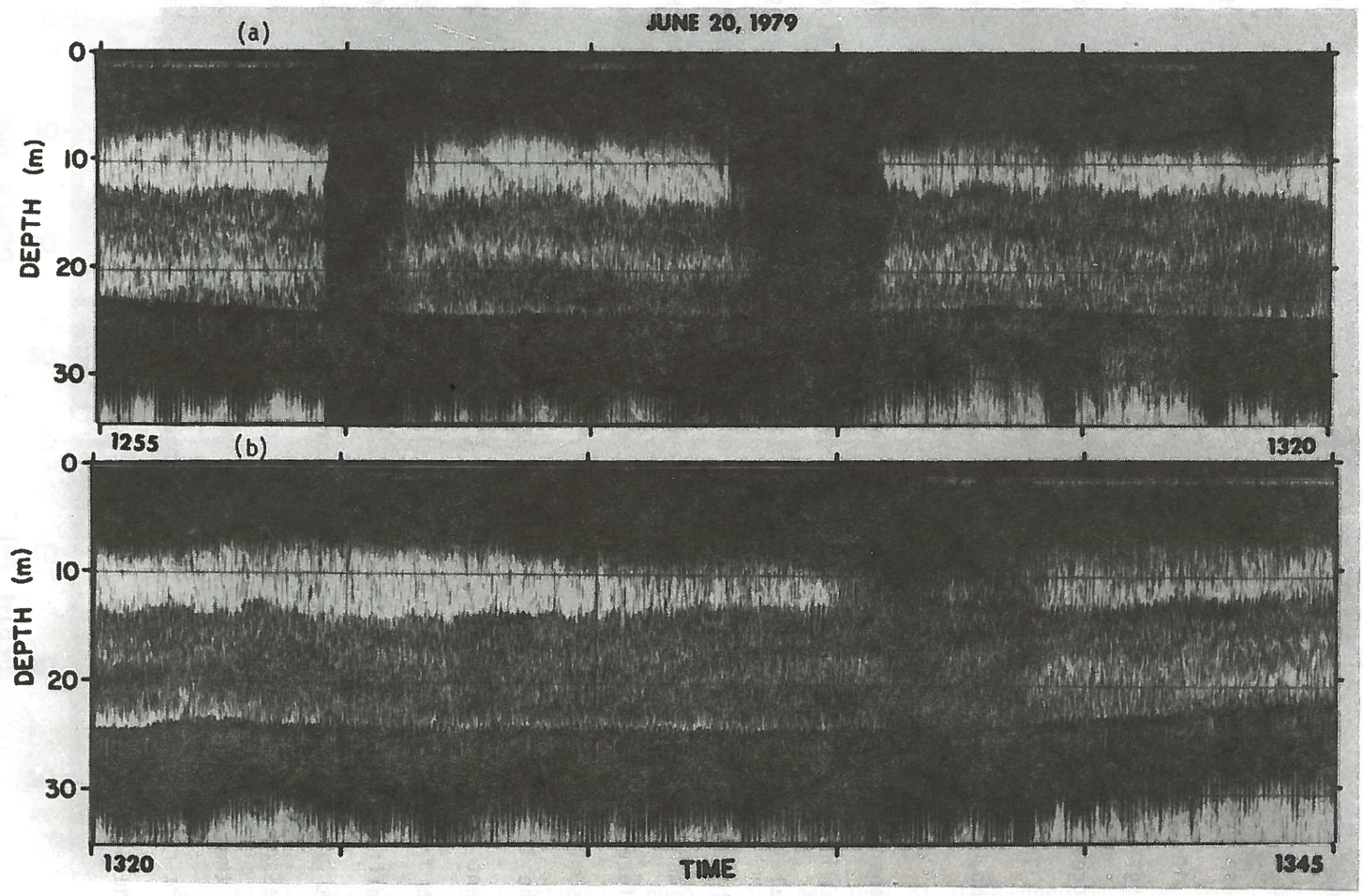

Fig. 17. Acoustic transects of the second spot dump at the New York Bight Dredged Material Dumpsite on June 20, 1979.

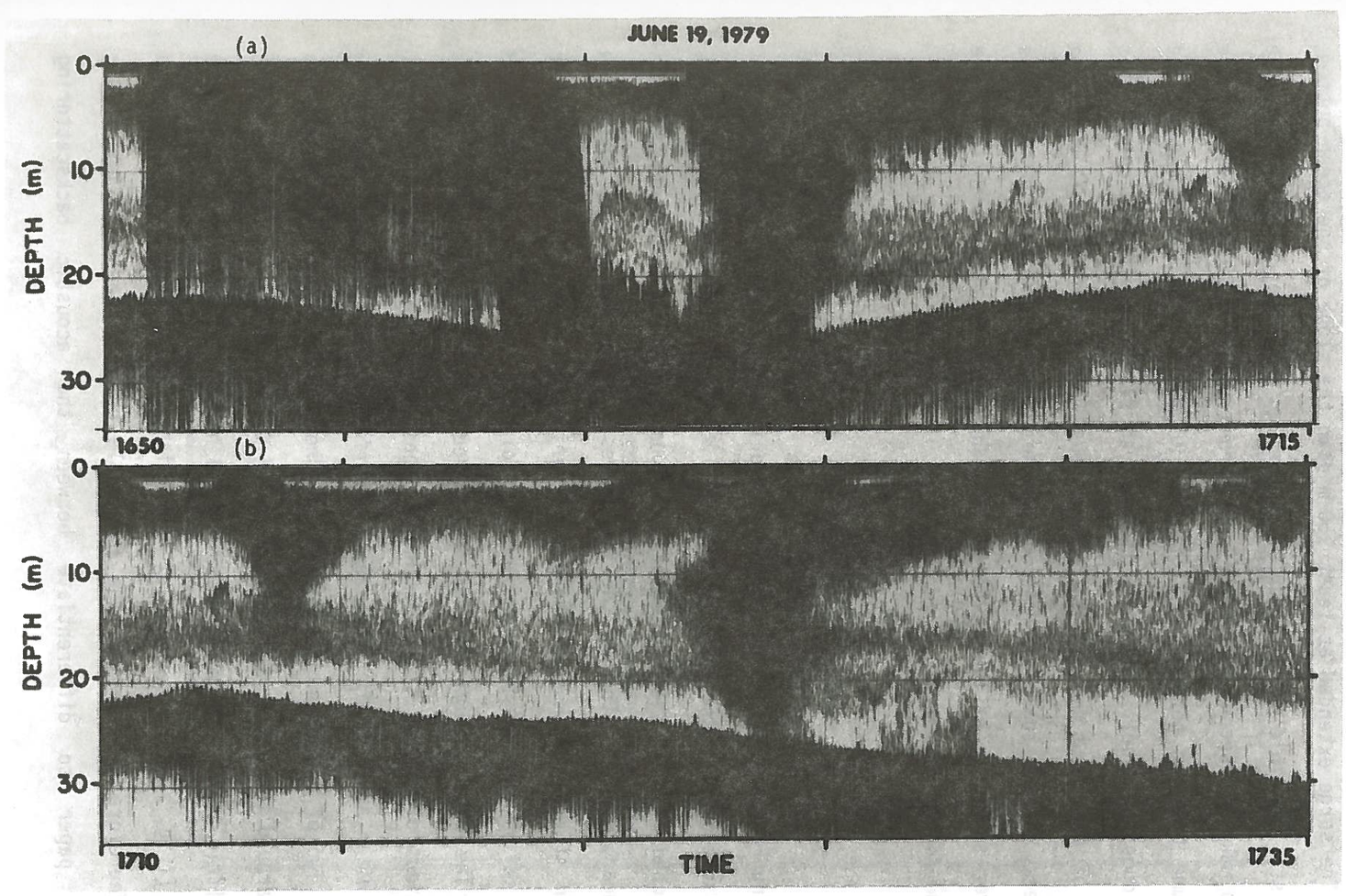

Fig. 18. Acoustic transects of the first spot dump at the New York Bight Dredged Material Dumpsite on June 19, 1979.

The other dump, on June 19, 1979 (Fig. 18), showed surges from the bottom. The surge extended at least 150 m down the slope of the ocean bottom, and was still visible on the acoustic profile when the ship reversed the course to make the second transect. The strong acoustic signal preceding the first plume transect between 1651 and 1658 LT is due to the wake generated from the dumping vessel. The third transect at 1714 LT apparently only cut at the edge of the plume and did not pass through the plume center. The ocean bottom here is much shallower than where the actual plume was located. The three-layer structure of the plume and the shear effect are evident from the second and fourth transects.

C. Flower Gardens Banks

During February 1980, an experiment of drilling mud discharge from an oil rig near station A of the inset in Fig. 19, 300 mi from the East Flower Bank, was conducted to study the particulate transport and its environmental effects in the nearby area. One of the objectives was to obtain the space-time dispersion of drilling mud discharged at various locations within the water column. Before the discharging, the ship circled the rig for a background survey. The water column was heavily loaded with fine suspended materials from previous discharges. Two discharge pipes began to dump "gelling agent" with sea water about 10 ft above the sea surface. The discharge rate was 25 bbl h^{-1}. Two of the acoustic profiles are shown in Fig. 20 when the ship was circling around the rig at a distance between 0.1 and 0.4 mi. The plumes were patches within this distance from the rig and hardly visible from the acoustic profiles [(Fig. 20(a)] because of the high concentration of background water. Therefore we decreased the adjustable pressure sensitivities of the recording paper to differentiate between the acoustic backscattering

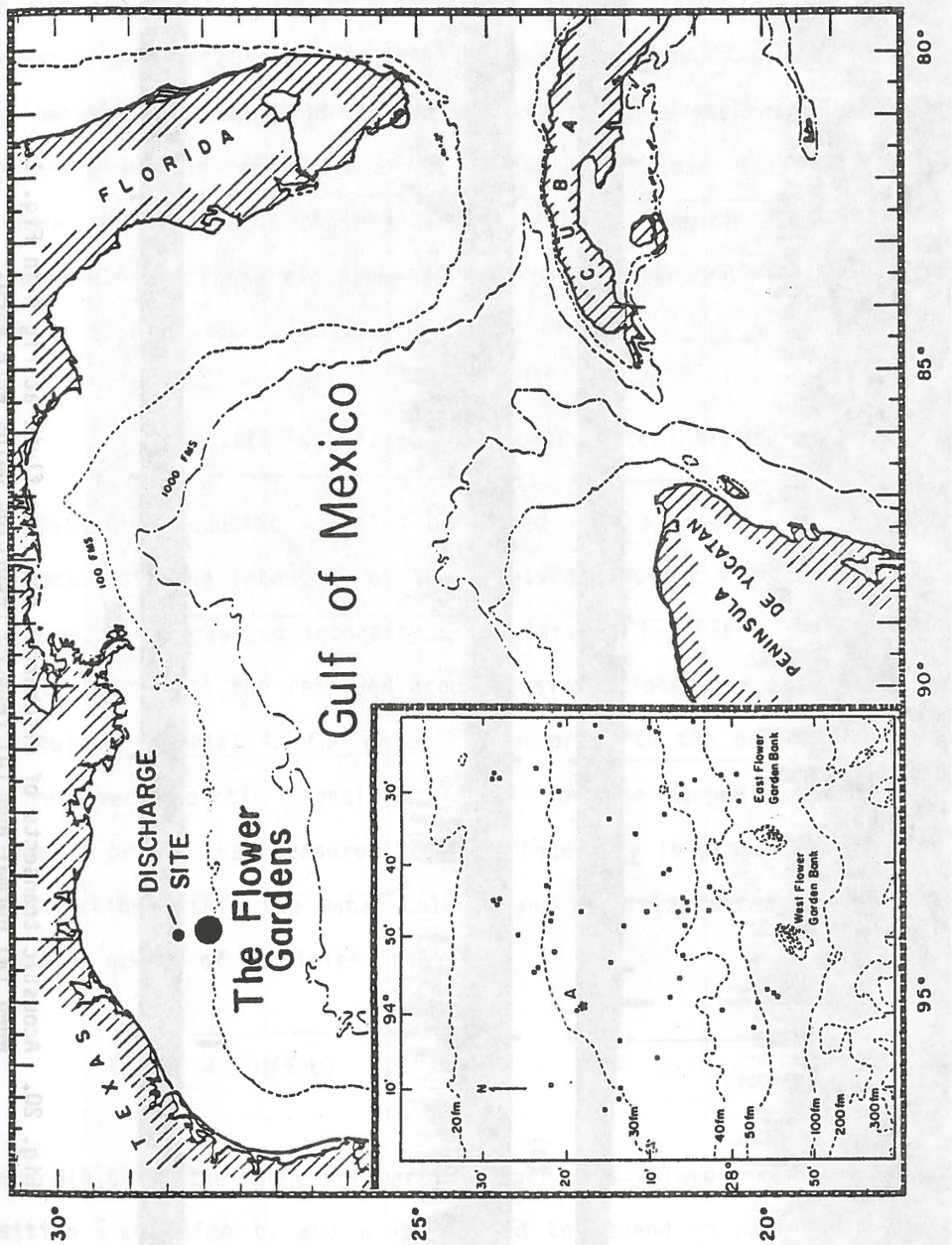

Fig. 19. Locations of the Drilling Fluid Discharge Site and the Flower Gardens Banks, Gulf of Mexico. Each square dot in the insert is an oil rig and the discharge site is at rig A.

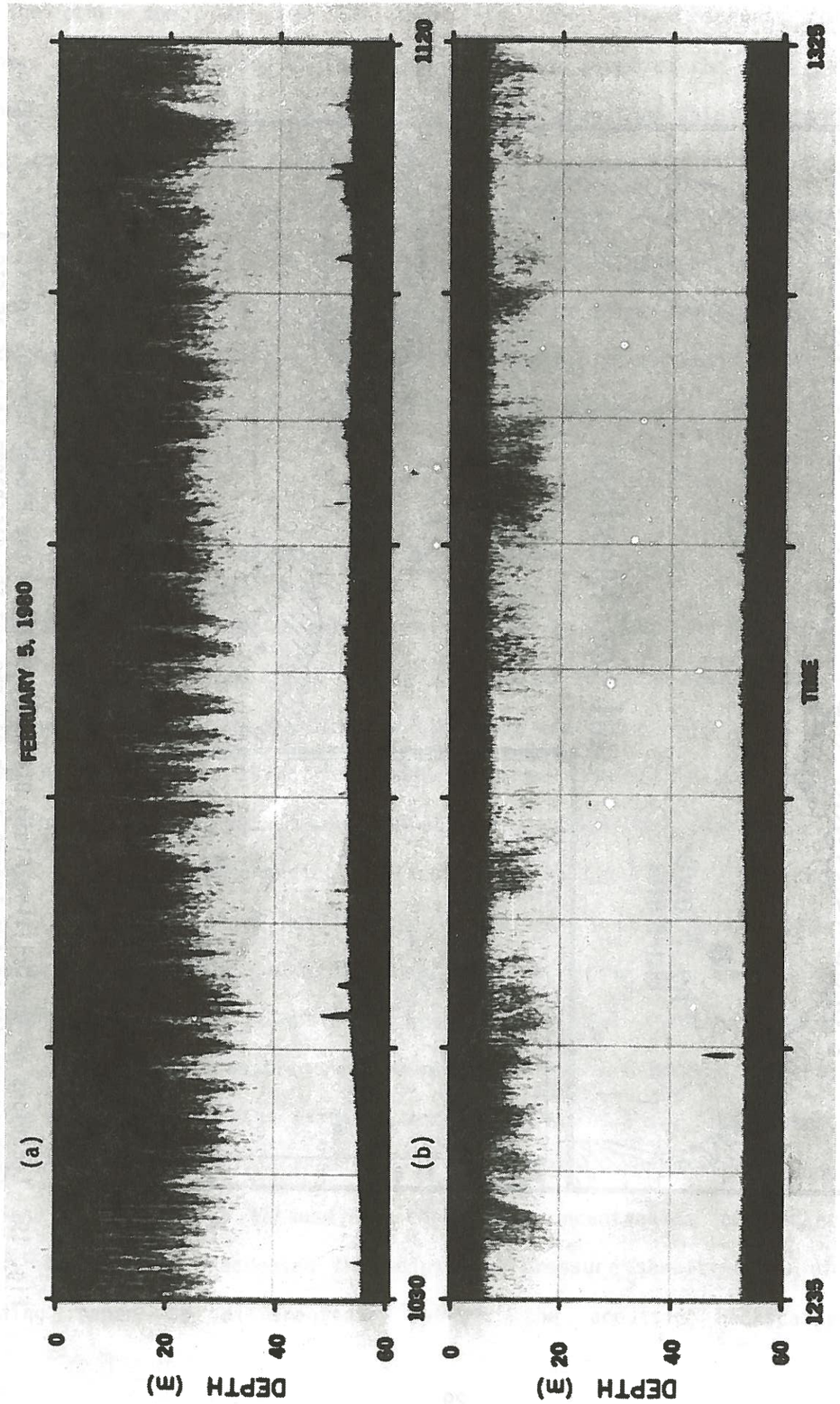

Fig. 20. Acoustic transects of discharged drilling fluid at rig A in Fig. 19 when (a) normal and (b) reduced recording gains were used.

intensities of the particulate matter within and outside the plume. This adjustment does not affect the actual acoustic signals that are recorded on the magnetic tapes. One section of the data is illustrated in Fig. 20(b). The patchiness is obvious, and the plume spreads across a 0.6-mi distance as seen between 1237 and 1248 LT. At 1305 LT the ship was making a second turn when the plume was detected again. The two small plumes between 1248 and 1305 LT were located on the other side of the rig. The time-space distribution corresponding to these two segments of acoustic tracking will be discussed in the next section.

III. RELATIVE PARTICULATE CONCENTRATIONS

Real-time acoustic profiles described in the previous section represent the backscattering intensity of the received acoustic signals. In a dumping experiment the measured intensity I consists of two basic components, I_B and I_D. I_B represents the received acoustic signal intensity from the background particulate material in the water column prior to the dumping event, and I_D the received acoustic signal intensity from the dumped material only. We assumed a priori that measured acoustic intensity is proportional to particle concentration within the water column, and particle concentration is proportional to number of particles, that is,

$$I(\vec{x},t) = \alpha\, N(\vec{x},t) \tag{1}$$

where $N(\vec{x},t)$ is the number of particles per unit volume under consideration at position $\vec{x}$ and time t, and α is assumed to depend on particle shape, size, density, compressibility, and frequency, but not on space and time. We make the following further assumptions in our analysis: (1) the particulate

concentration at the time of transects is not sufficiently high for multiple acoustic scattering to occur; (2) the change of physical characteristics of the water column does not cause serious ambiguity in the applicability of the backscattering theory; (3) the ship's motion will not affect the spatial resolution due to the change of beam width from the motion of the transducer; and (4) the size distribution of particulate matter does not change significantly from one scattering volume to another, and no particle size exceeded the acoustic wavelength.

After the experiments, analog acoustic signals recorded on magnetic tapes are digitized in the laboratory using a PDP-11 computer. We then average the digitized data over a 12-s time period and correct spherical spreading with depth to give the backscattering intensity from the whole water column. The 12-s average time is chosen to give the best plume structure in detail. Two of these acoustic intensities as a function of depth are shown in Fig. 21, each representing an averaged intensity at a particular time. When the ship is under way, the two intensity measurements represent the particulate concentrations of suspended materials within the water column at two different locations along the ship track. The solid curve indicates two acoustic backscattered intensity peaks at two different depths, corresponding to two concentration maxima at this particular location. The dotted curve indicates only one peak at deeper water, and implies that the concentration maximum at shallower water has disappeared. A contour plot of isointensity I_D in depth and time represents the relative particle concentrations of the dumped material with respect to the surrounding background water. The background water column concentration is chosen just outside the plume for each transect. The relative concentration of dumped particulate material is defined as the difference between the measured acoustic intensities of the water columns

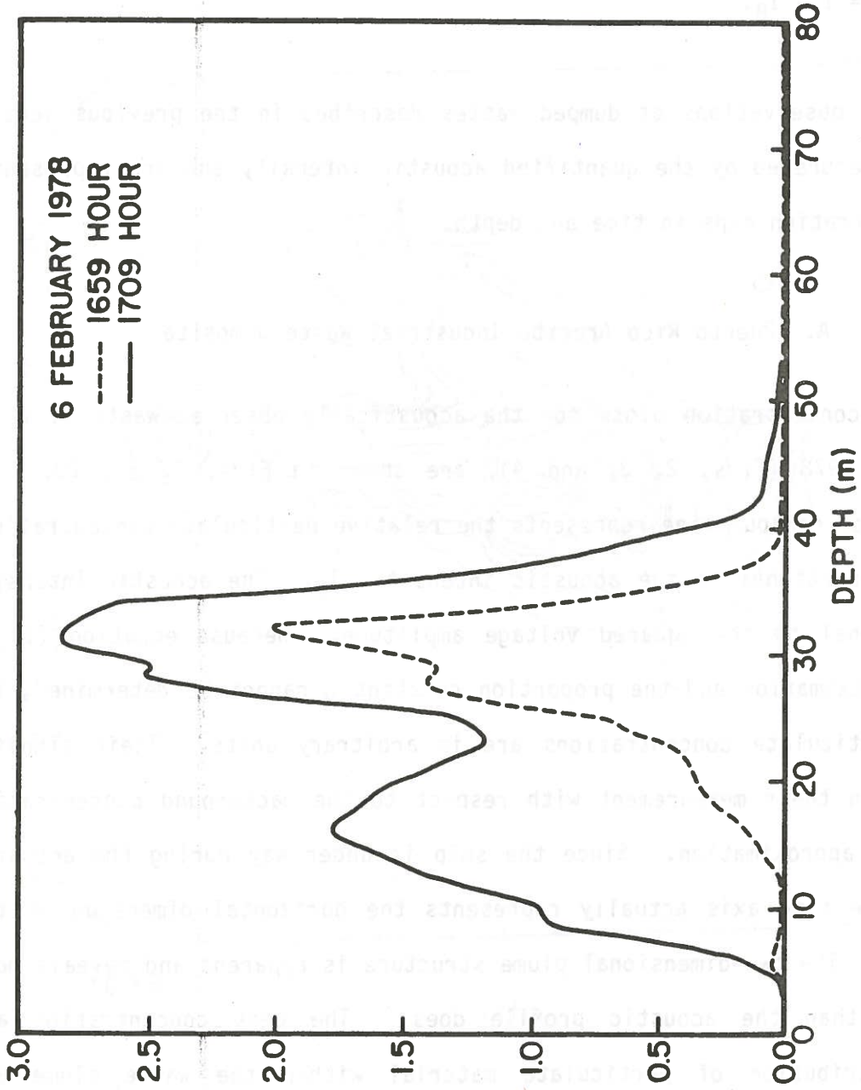

Fig. 21. Acoustic backscattered intensities from digitized data, as a function of depth at two different times, corresponding to the squares of two received pulse signals.

Property of
NOAA Miami Library
4301 Rickenbacker Causeway
Miami, Florida 33149

inside and outside each plume, assuming that the background concentration does not change significantly inside or outside the plume; hence

$$I_D = I - I_B. \qquad (2)$$

The acoustic observations of dumped wastes described in the previous section are then interpreted by the quantified acoustic intensity and are represented by isoconcentration maps in time and depth.

A. Puerto Rico Arecibo Industrial Waste Dumpsite

The isoconcentration plots for the acoustically observed waste plume on February 6, 1978 (Figs. 2, 3, and 4), are shown in Figs. 22 and 23. The number on each contour line represents the relative particulate concentration, which is proportional to the acoustic intensity, I_D. The acoustic intensity is proportional to the squared voltage amplitude. Because equation (1) is only an approximation and the proportion constant α cannot be determined, the relative particulate concentrations are in arbitrary units. Their significance lies in their measurement with respect to the background concentration at the same approximation. Since the ship is under way during the acoustic transect, the time axis actually represents the horizontal dimension of the waste plume. The two-dimensional plume structure is apparent and reveals more information than the acoustic profile does. The peak concentration and spatial distribution of particulate material within the waste plume are clearly displayed. For instance, we easily see in Fig. 22 that the peak concentration is located at a depth of 32 m, and a secondary peak at the same depth but with only half the peak value. We also see a concentration gradient at a depth of 22 m, which seems to separate the plume into two parts. The

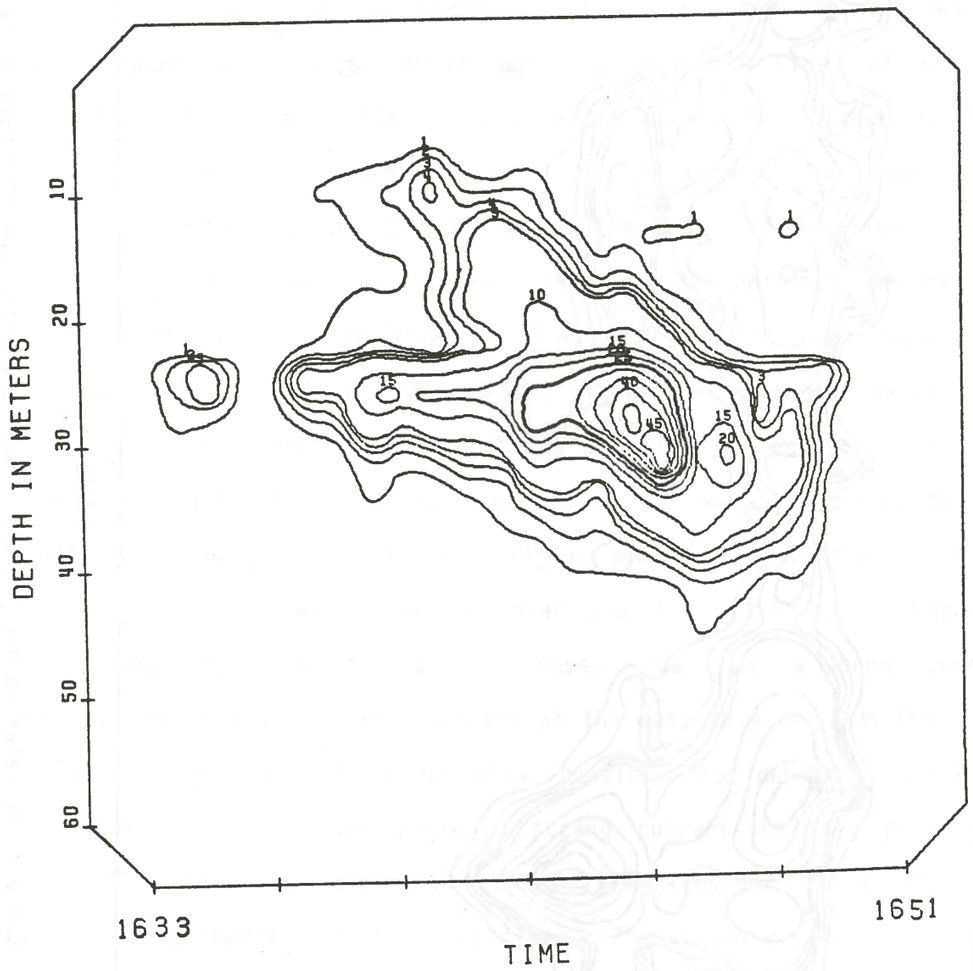

Fig. 22. Contours of relative particulate isoconcentration, in arbitrary units, corresponding to the first transect in Fig. 2, for February 6, 1978. The relative particulate concentration is proportional to the acoustic backscattered intensity of the suspended waste material; it is taken to be the difference between intensities of the whole water column inside the plume and the background material outside the plume.

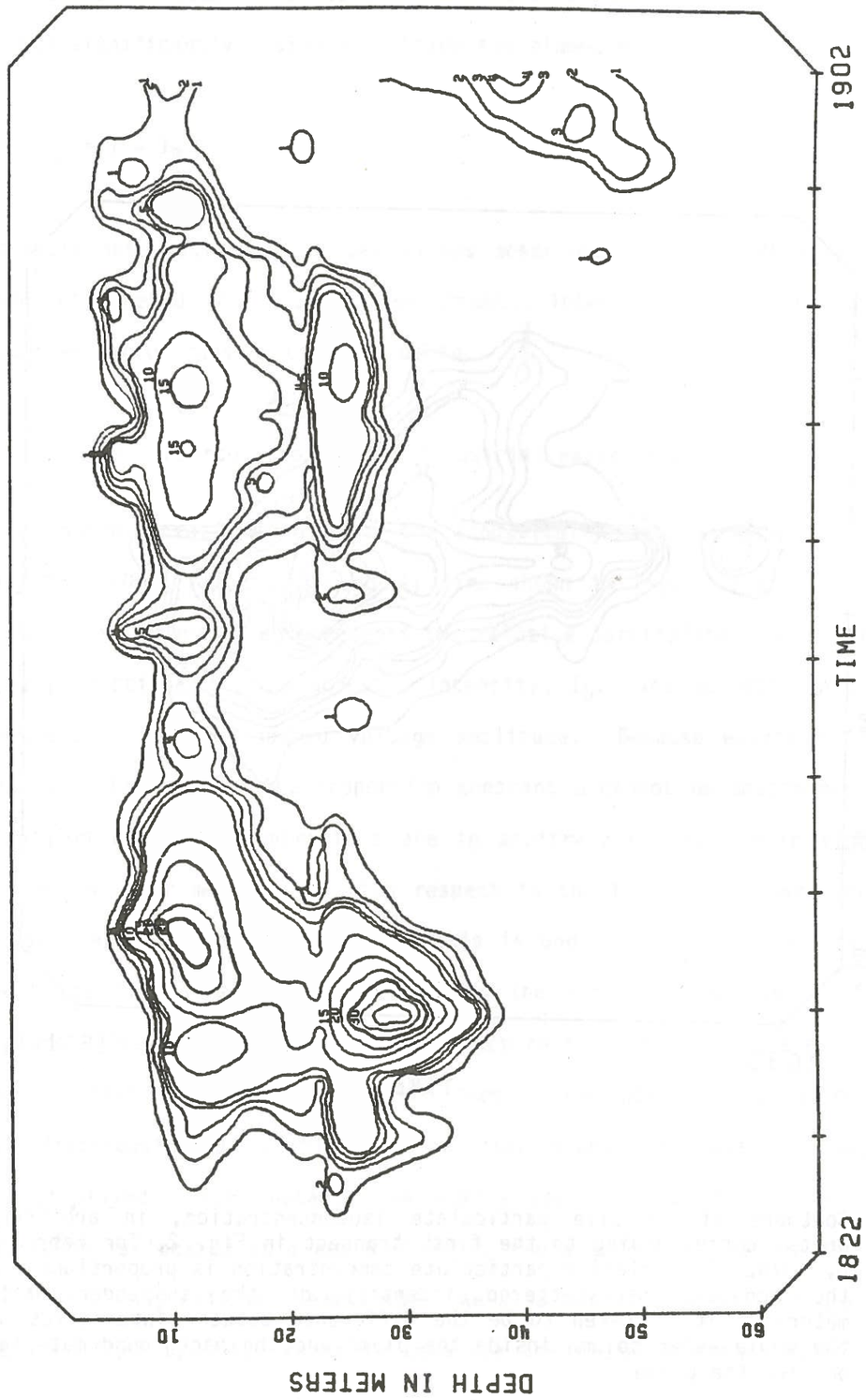

Fig. 23. Contours of relative particulate isoconcentration, in arbitrary units, corresponding to the two continuous acoustic transects in Figs. 3 and 4, for February 6, 1978.

upper part not only has a lower concentration, but also a lower gradient. The peak concentration is in the lower part, but not at the center of the plume.

The plume structure appears to indicate a shear effect due to current flows. In fact, strong shear effect was observed at the same area during the second waste dump experiment on October 29, 1978. The acoustic profiles and their corresponding isoconcentration maps are shown in Figs. 24 and 25, respectively. This shear effect was observed during two almost parallel transects in opposite directions (Fig. 26). The location of the strong shear current is indicated by the two arrows. The upper shaded line segment represents the eastward ship track, and starts from the point of the shear to the beginning of clearer water [Figs. 24(a) and 25(a)]. The lower shaded line segment represents the westward ship track, and starts from the clearer water to the point of the shear [Figs. 24(b) and 25(b)]. The acoustic profiles, Fig. 24(b) in particular, clearly reveal that the water mass was divided diagonally into two parts. The much higher acoustic intensities near the surface and in deeper water, and a lower acoustic intensity in between, suggest a circular motion of the water mass. There was a strong current westward to create a very sharp boundary at the eastern side. On the other hand, there was an eastward current flow, possibly from deeper to shallower water, which counteracts the westward strong current at this particular location. The effect on the water column is manifested in Fig. 25. The source of this eastward current is not clear. The strong westward current is the Antilles Current that generates a sharp eastern boundary of the observed plume in most cases.

The two-layer structure and the concentration gradient in Fig. 22 are also clear in Fig. 23 when the ship went through the same plume twice. The major peak concentration is still at the lower layer. The secondary peak is

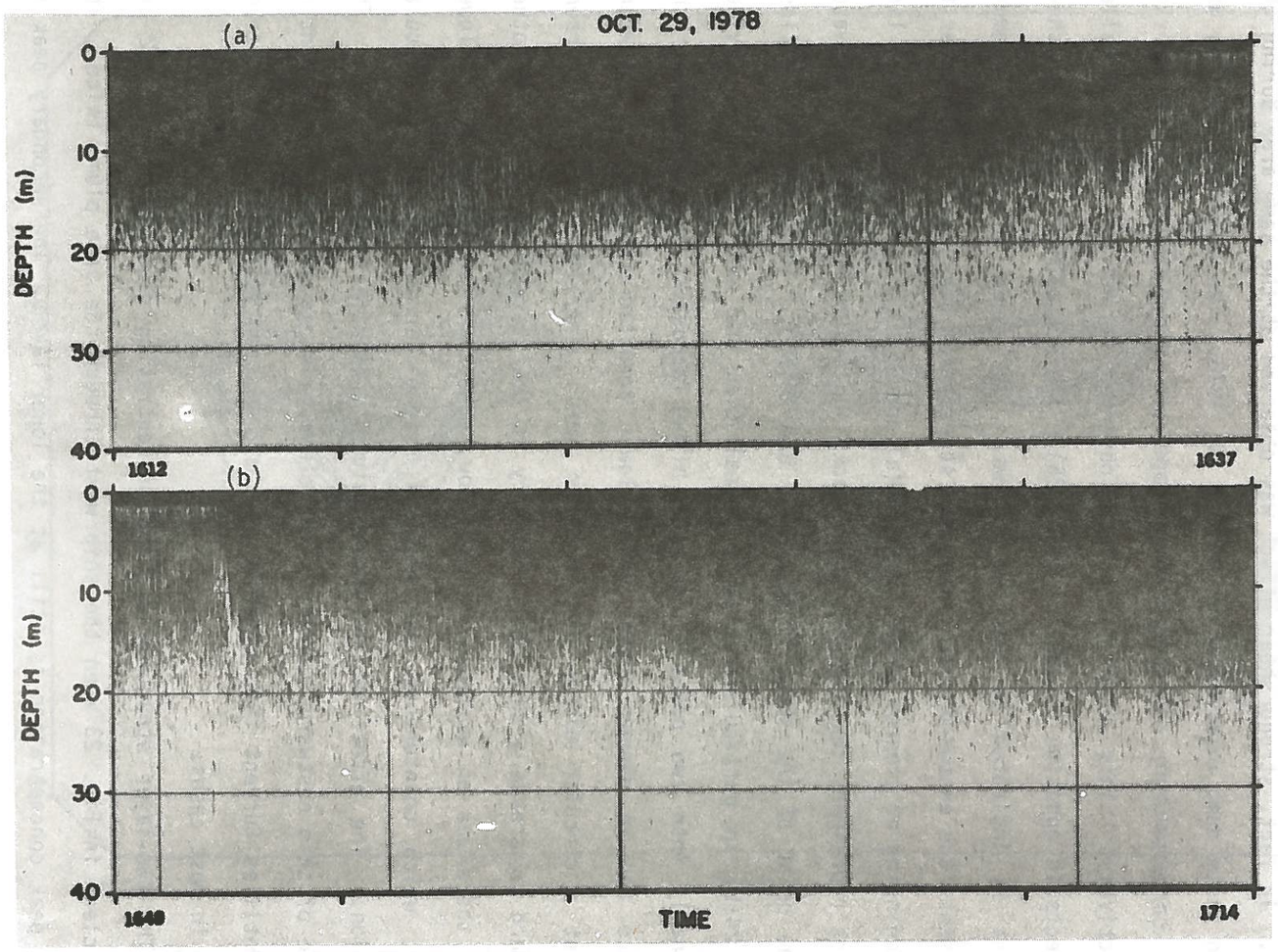

Fig. 24. Two almost parallel acoustic transects that indicate a strong shear at the Puerto Rico Arecibo Dumpsite.

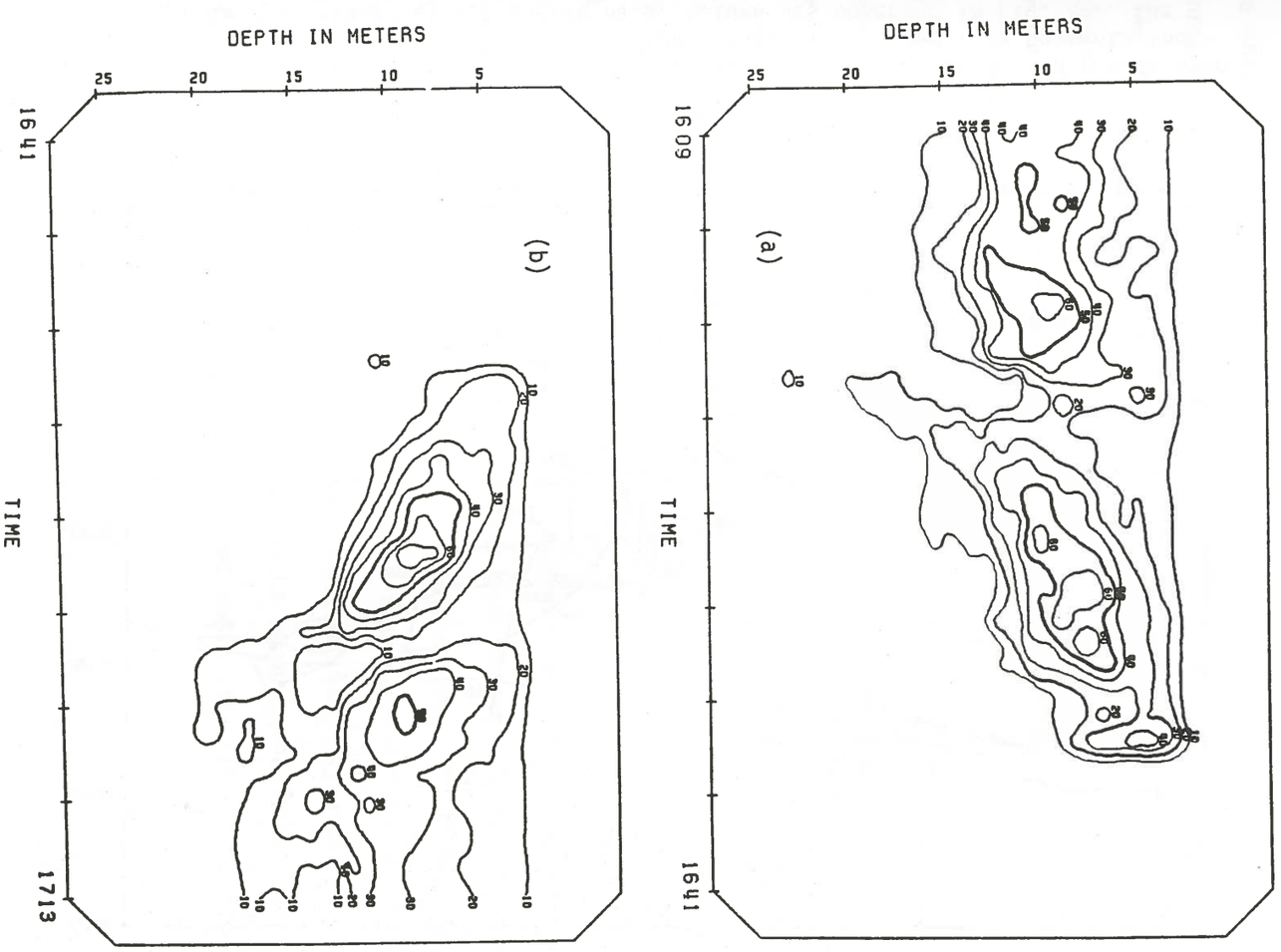

Fig. 25. Isointensity contours for the two acoustic transects in Fig. 24.

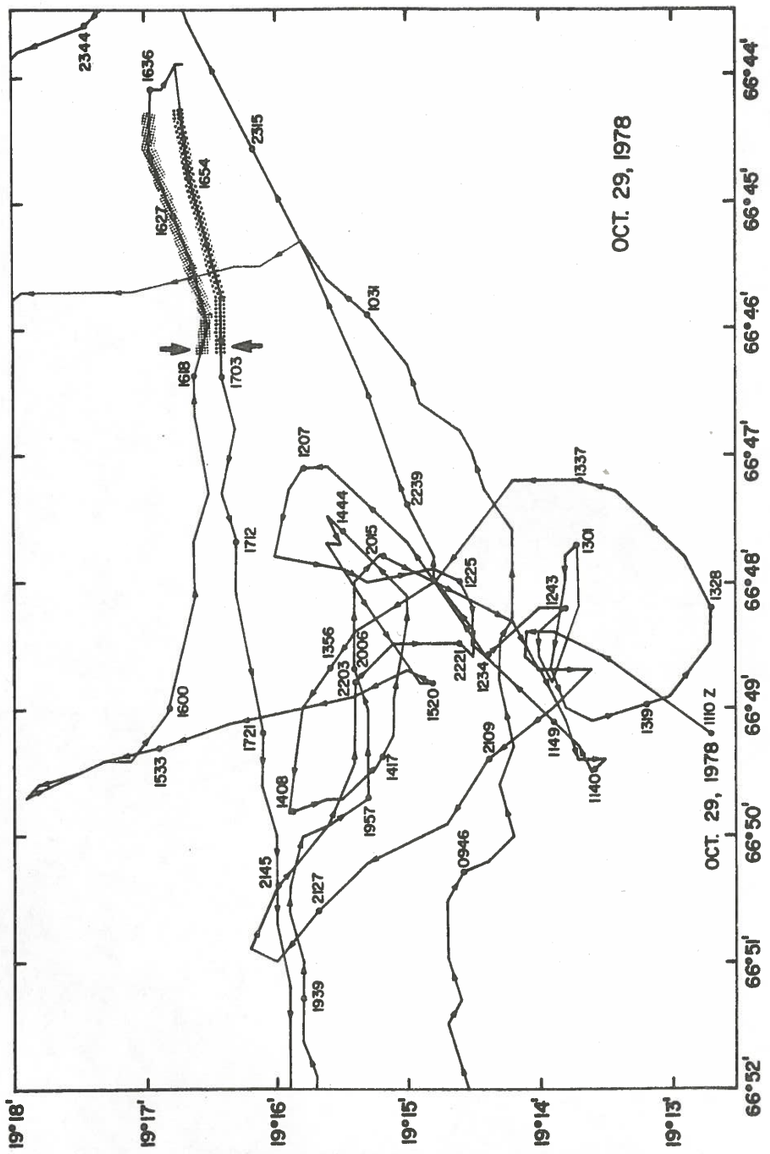

Fig. 26. Portion of the ship tracks on October 29, 1978, during the Second Puerto Rico Arecibo Industrial Waste Dumping Experiment. The shaded line segments indicate where shear effect on the water column was observed in Fig. 25. The arrows are at the locations where the shear effect appears most apparent.

now located in the upper layer. The second transect has a much lower peak concentration than the first. This is probably due to the different direction of the ship in contact with the plume when the ship made a turn and did not cut through the center of the plume the second time.

The isoconcentration contours for the initial transect of the waste dump on October 29, 1978 (Fig. 6), are shown in Fig. 27. The two parts of the plume are apparent, with a peak concentration in each part. One peak concentration is greater than the other. Even though the two peak concentrations are at the same depth, they are located much shallower than those in Figs. 22 and 23. The third plume, with peak concentration eight orders smaller than those of the other two, probably is from the dump of the previous day.

Four transects on October 30, 1978, of the same plume and corresponding to Figs. 8 and 9, are shown in Figs. 28 to 31. These transects are indicated as shadowed line segments in Fig. 7. They have several common features. First, they all have a sharp boundary with great horizontal concentration gradients at the eastern edge. Second, they have a diffusive western edge with a much lower concentration. Third, the peak concentrations are located at much shallower water than those from the previous dump. The depths of peak concentrations are also shallower than the earlier observations of the same dump (Fig. 27). This indicates an upward mechanism, possibly a current flow, that prevented the settling of the dumped waste because the pycnocline would not be able to stop the penetration of dumped waste into the deeper water 18 hours after the dump.

B. New York Bight Dredged Material Dumpsite

Figure 32 shows the detailed plume structure for the five acoustic transects of the dump on June 21, 1979 (Fig. 16). There are two relative

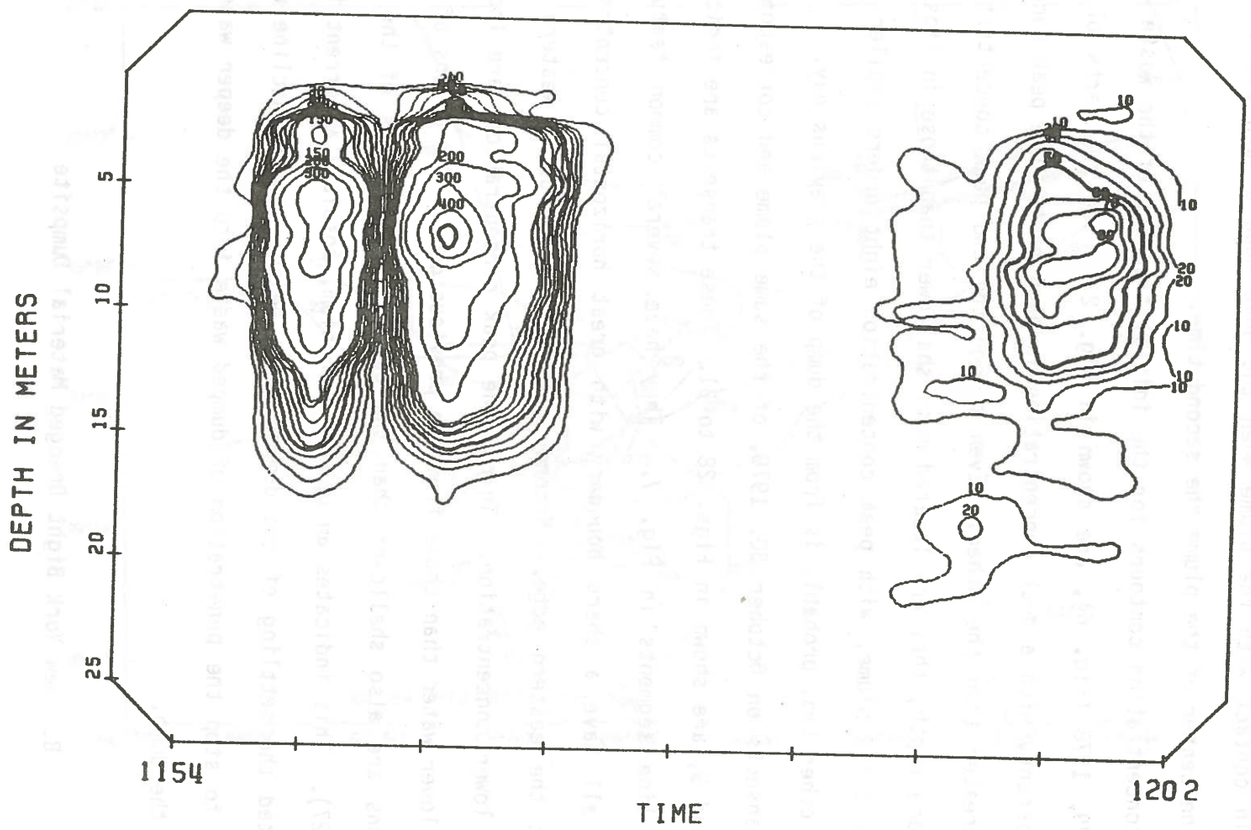

Fig. 27. Contours of relative particulate concentration, in arbitrary units, corresponding to the acoustic transect in Fig. 6, for October 29, 1978.

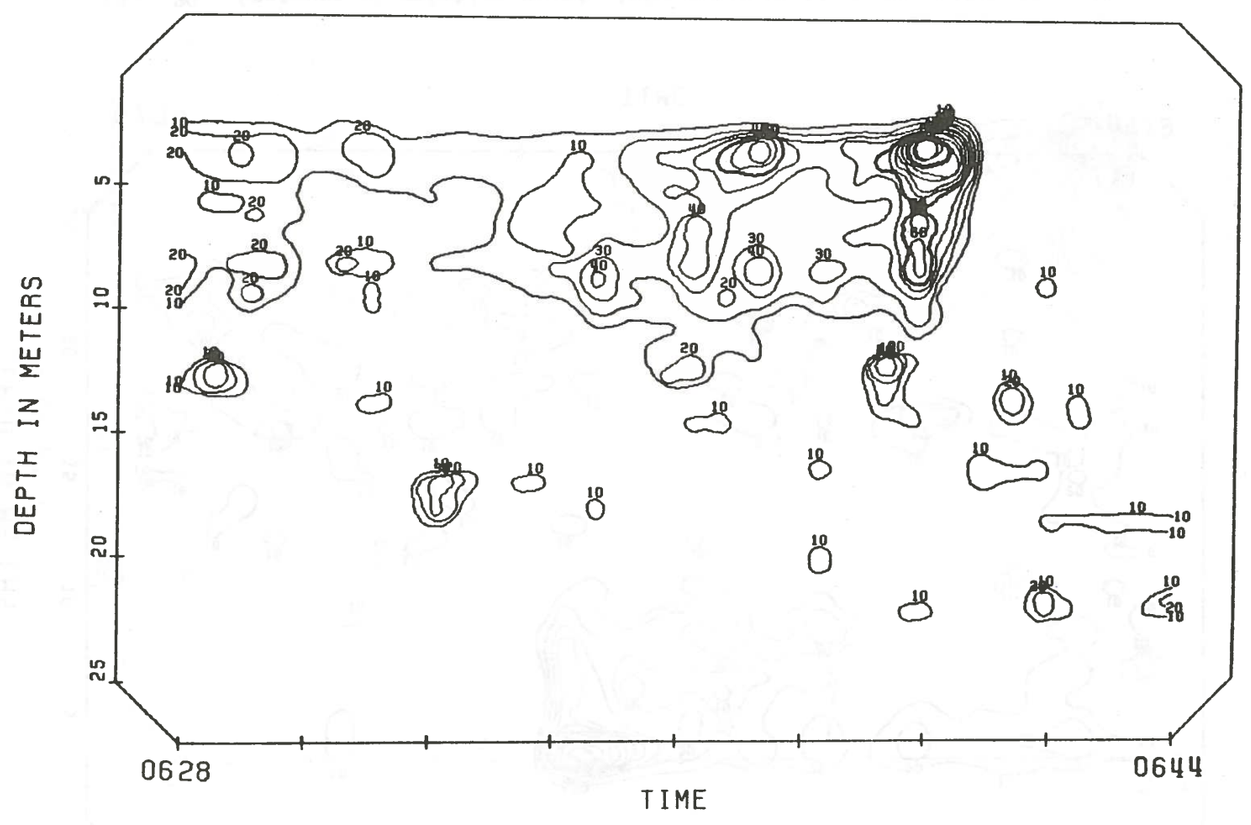

Fig. 28. Contours of relative particulate concentration, in arbitrary units, corresponding to the acoustic transect in Fig. 8(a), for October 30, 1978.

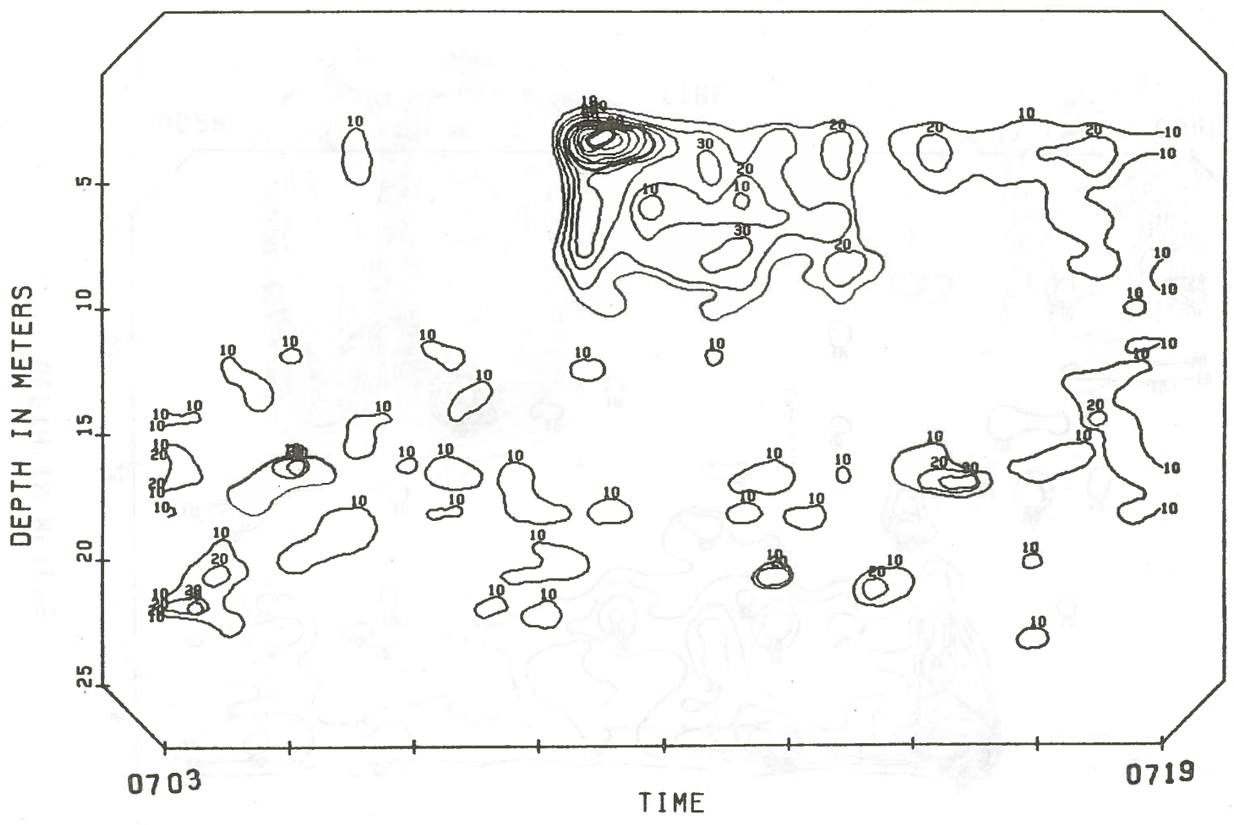

Fig. 29. Contours of relative particulate concentration, in arbitrary units, corresponding to the acoustic transect in Fig. 8(b), for October 30, 1978.

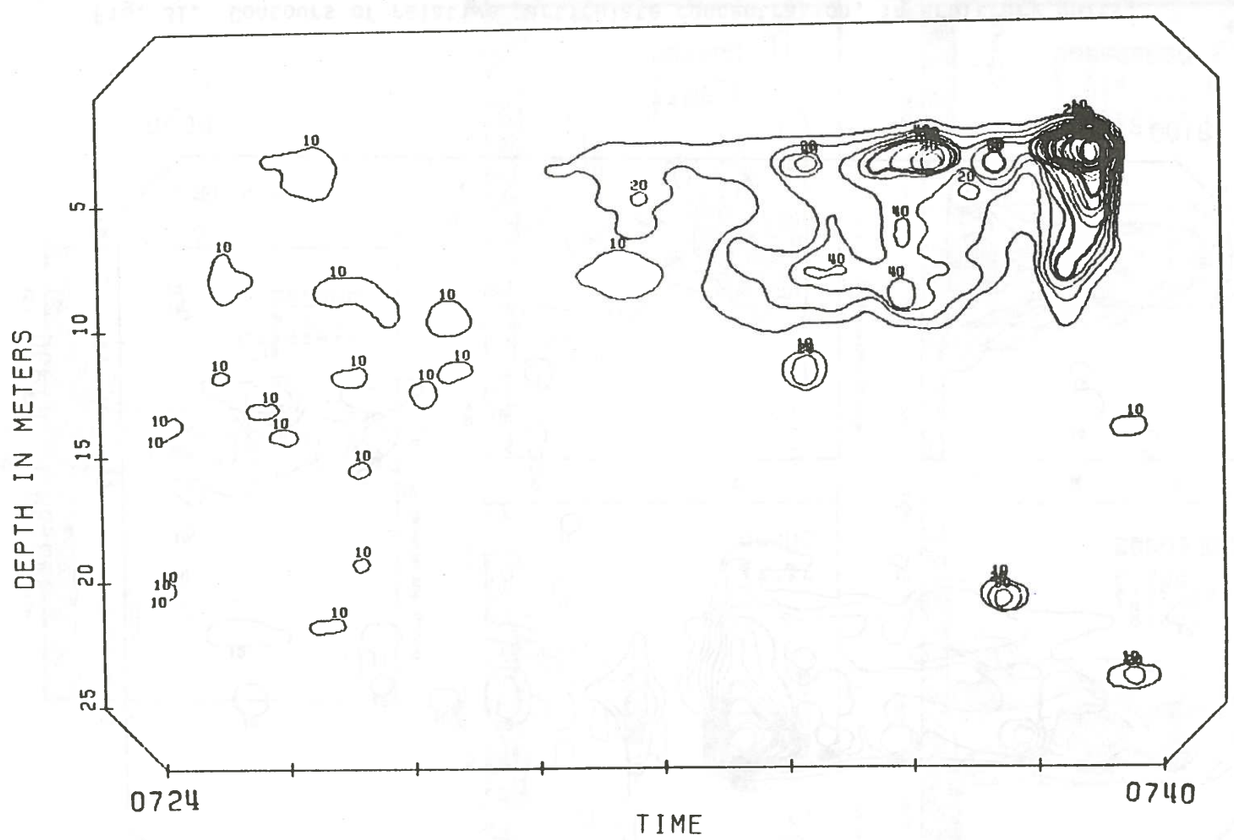

Fig. 30. Contours of relative particulate concentration, in arbitrary units, corresponding to the acoustic transect in Fig. 9(a), for October 30, 1978.

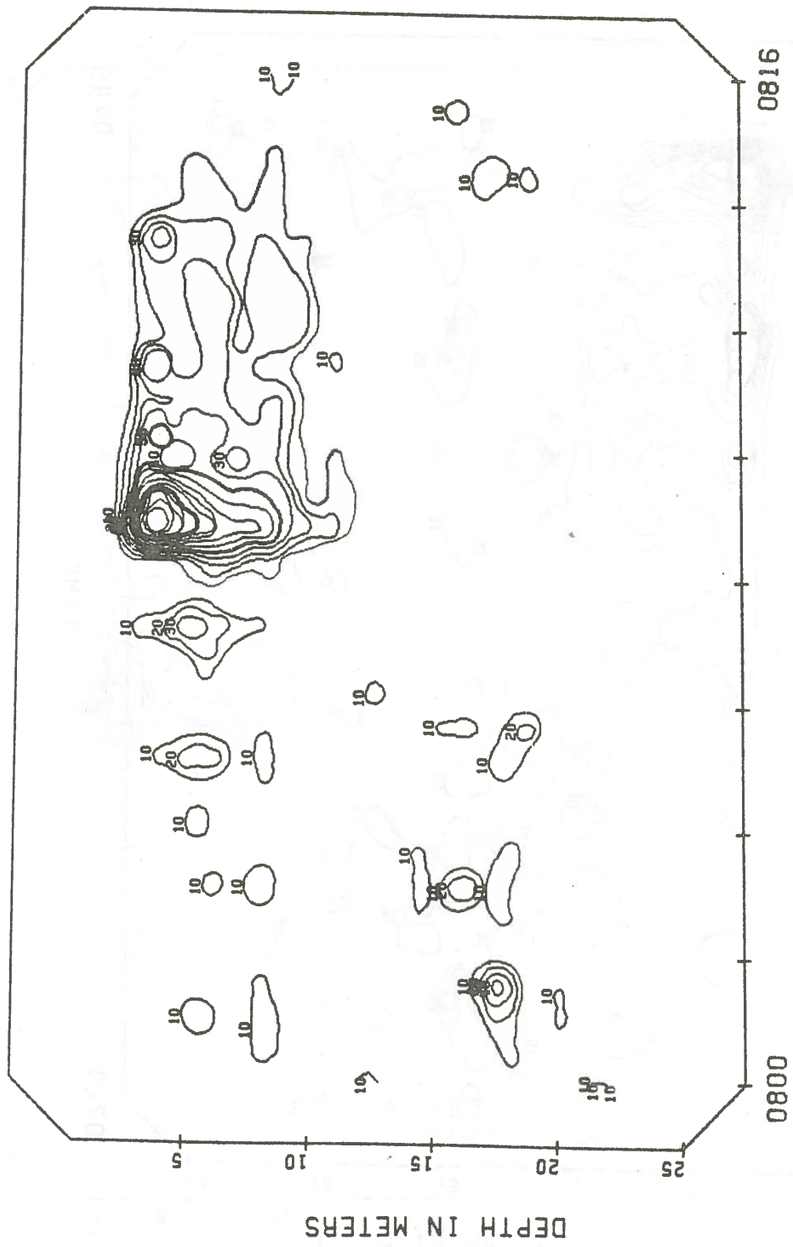

Fig. 31. Contours of relative particulate concentration, in arbitrary units, corresponding to the acoustic transect in Fig. 9(b), for October 30, 1978.

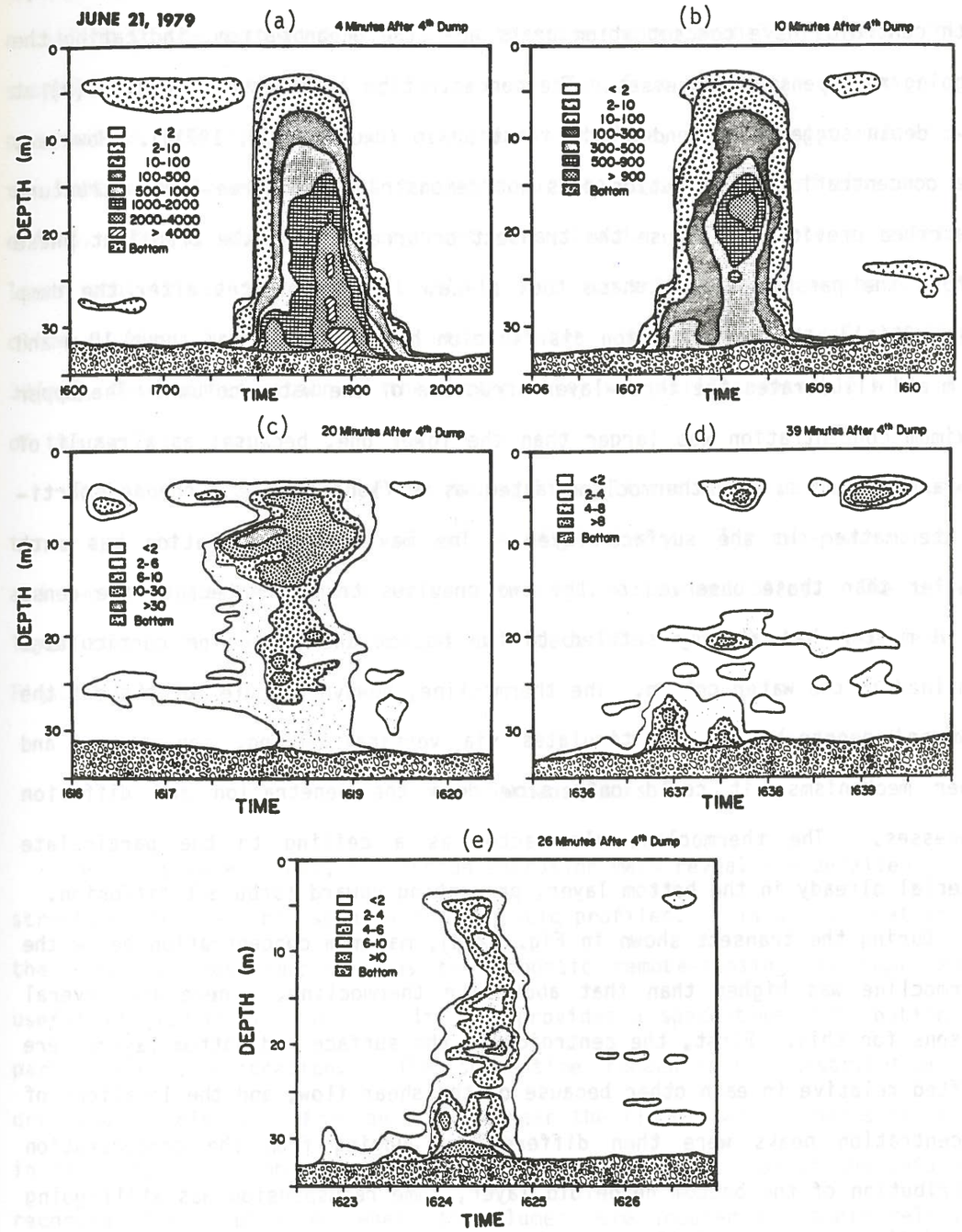

Fig. 32. Contours of relative particulate concentration, in arbitrary units, corresponding to the five acoustic transects in Fig. 16.

concentration centroids at different depths and positions shown in Fig. 32(a). Both centroids have concentration peaks near the ocean bottom, indicating the ongoing resuspension processes. The concentration peak shown in Fig. 32(b) at 17-m depth suggests the end of the first phase (Okubo, 1970, 1971a). However, the concentration distribution does not demonstrate the three-layer structure described previously because the transect occurred during the transient phase before the passive second phase took place. Twenty minutes after the dump [Fig. 32(c)], the concentration distribution has two maxima at about 10 m and 23 m and illustrates the three-layer structure of the water column. The upper maximum concentration was larger than the lower one, because, as a result of buoyancy effects, the thermocline acted as a floor to the suspended particulate matter in the surface layer. The maximum concentration was much smaller than those observed on the two previous transects because the dense solid matter had already settled to the bottom and only fine particulates remained in the water column. The thermocline, however, could not prevent the downward penetration of particulates via vertical mixing, convection, and other mechanisms; it could only slow down the penetration and diffusion processes. The thermocline also acted as a ceiling to the particulate material already in the bottom layer, preventing upward turbulent diffusion.

During the transect shown in Fig. 32(d), maximum concentration below the thermocline was higher than that above the thermocline. There are several reasons for this. First, the centroids of the surface and bottom layers were shifted relative to each other because of the shear flow, and the locations of concentration peaks were then different. Judging from the concentration distribution of the bottom nepheloid layer, some resuspension was still going on and the transect probably took place exactly across the initial dumpsite. However, the concentration peak of the surface layer was moving downstream and

was no longer at the initial dumpsite. Second, the thermocline was acting as a ceiling to the suspended materials within the bottom nepheloid layer. These suspended particulates, either by resuspension from the ocean bottom or by penetration from the surface above the thermocline, were constrained within the bottom layer and could not reach the surface layer because of this ceiling effect. Third, the high background concentration of the bottom nepheloid layer contributed to the relatively higher concentration below the thermocline. After the plume broke into patches for the fifth transect [Fig. 32(e)], peak concentration of the bottom layer was still comparable with that of the surface layer.

The plumes from the other two dumps (Figs. 17 and 18) have similar structure, and are shown in Figs. 33 and 34 respectively. The two-phase process and two-centroid feature are evident in Figs. 33(a) and 34(a). The three-layer structure, and the floor-ceiling effect of the thermocline are seen in Figs. 33(b) and 34(c).

C. Flower Gardens Banks

As illustrated above, the isoconcentration maps reveal the detailed plume structures that are not seen on the acoustic profiles. This quantification of the acoustic measurements makes the acoustic remote-sensing technique more useful in dispersion studies. It also provides a space-time distribution of particulate concentration. The space-time concentration distribution of drilling-mud discharge from an oil rig near the Flower Gardens Banks is shown in Fig. 35. The numbers are the times at which the position of the ship was recorded. The graph shows where the plumes were located and their relative concentrations. There are two segments of ship tracks in Fig. 35; one corresponds to the acoustic transect in Fig. 36, and the other to the acoustic

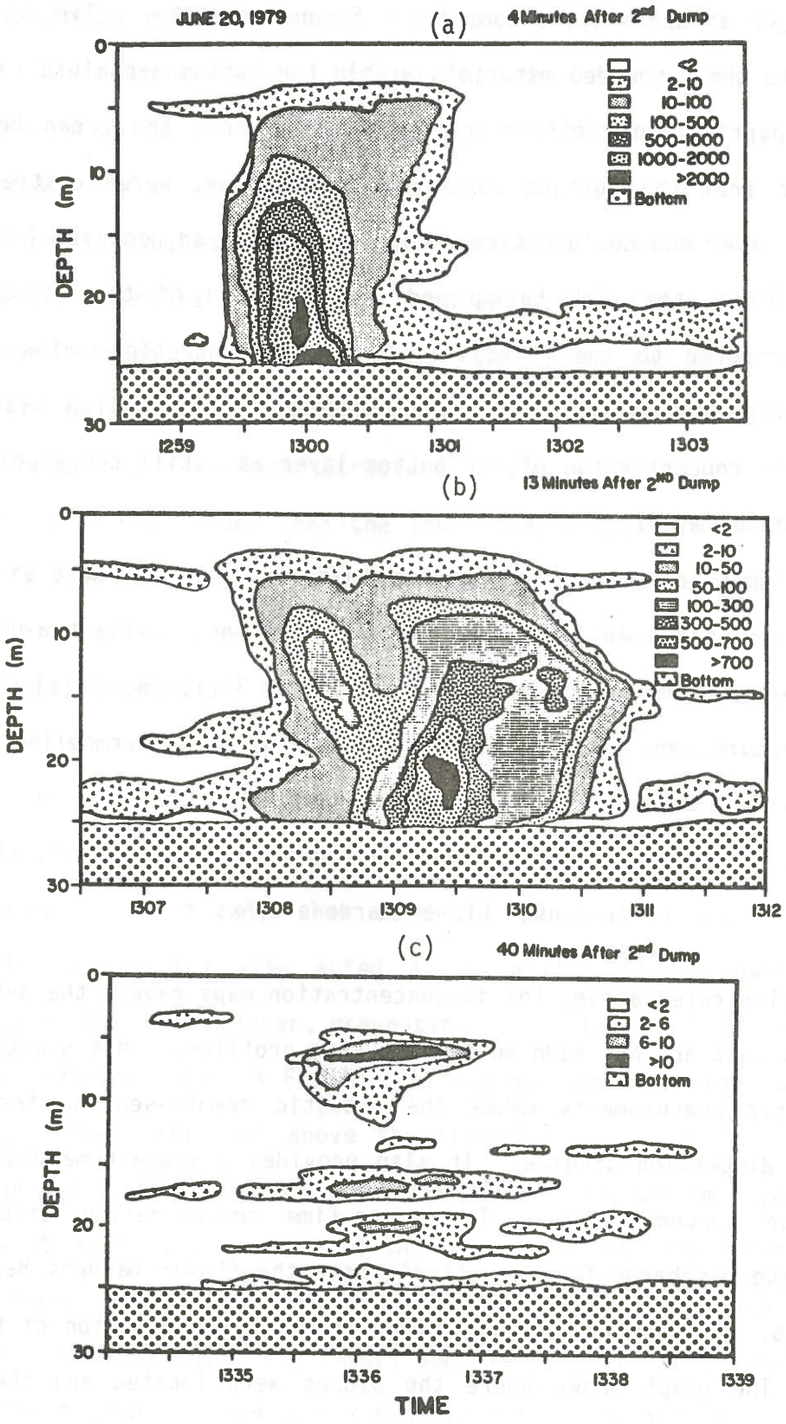

Fig. 33. Contours of relative particulate concentration, in arbitrary units, corresponding to the three acoustic transects in Fig. 17.

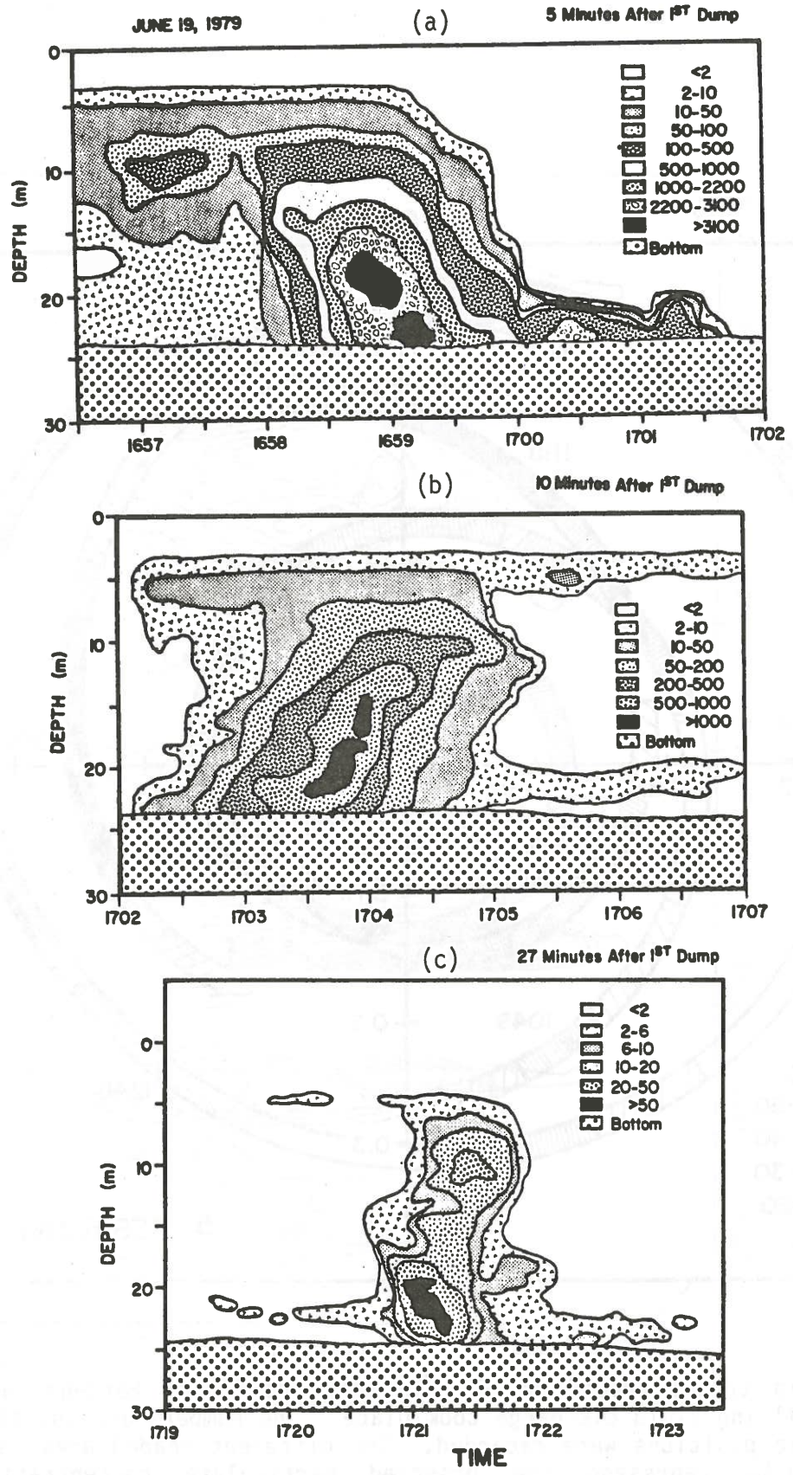

Fig. 34. Contours of relative particulate concentration, in arbitrary units, corresponding to the three acoustic transects in Fig. 18.

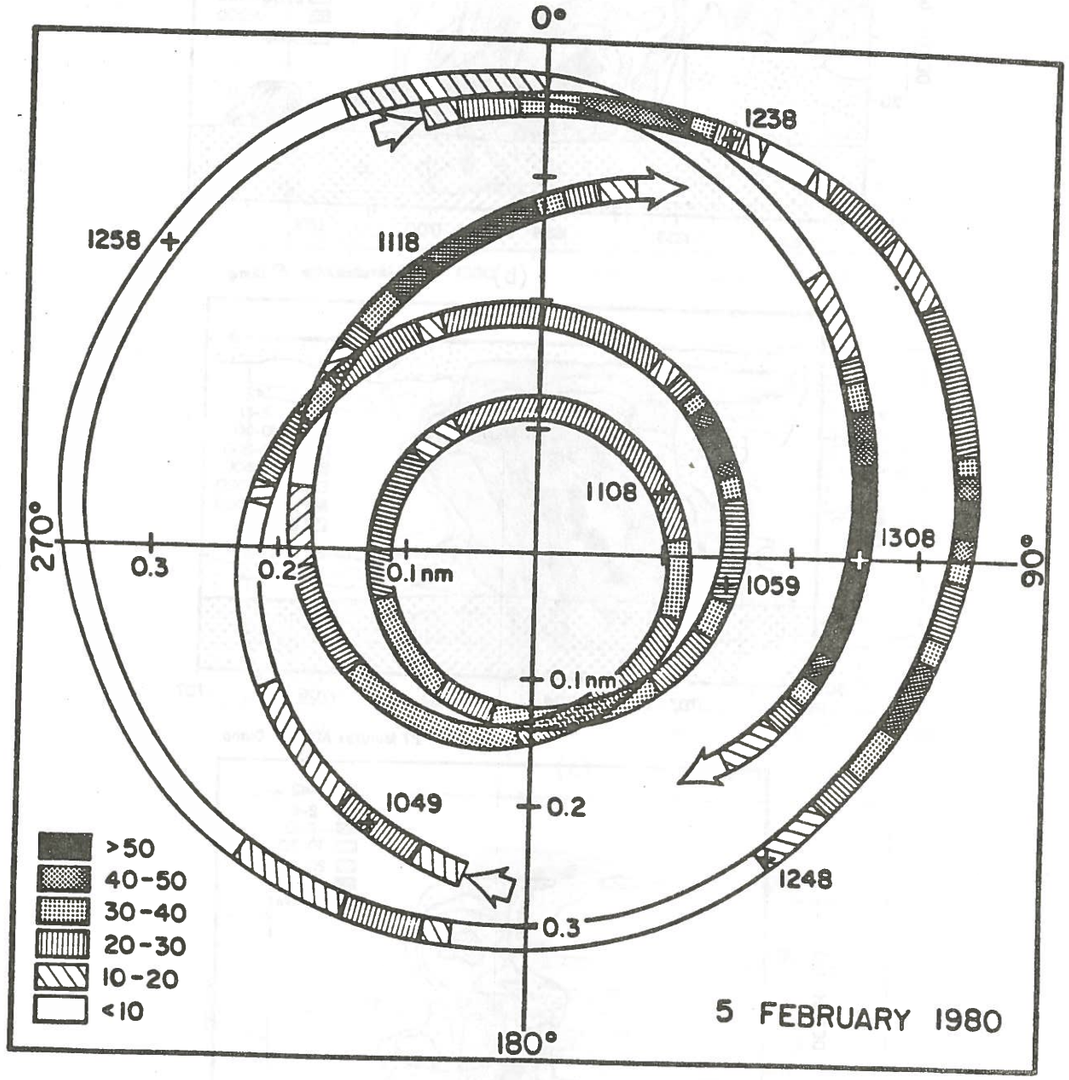

Fig. 35. Ship tracks around an oil rig near the Flower Gardens Banks when drilling fluid discharge took place. The numbers are the times when ship positions were recorded. The different shaded areas along the tracks represent the observed particulate concentrations, in arbitrary units, of the discharged plume in Fig. 20.

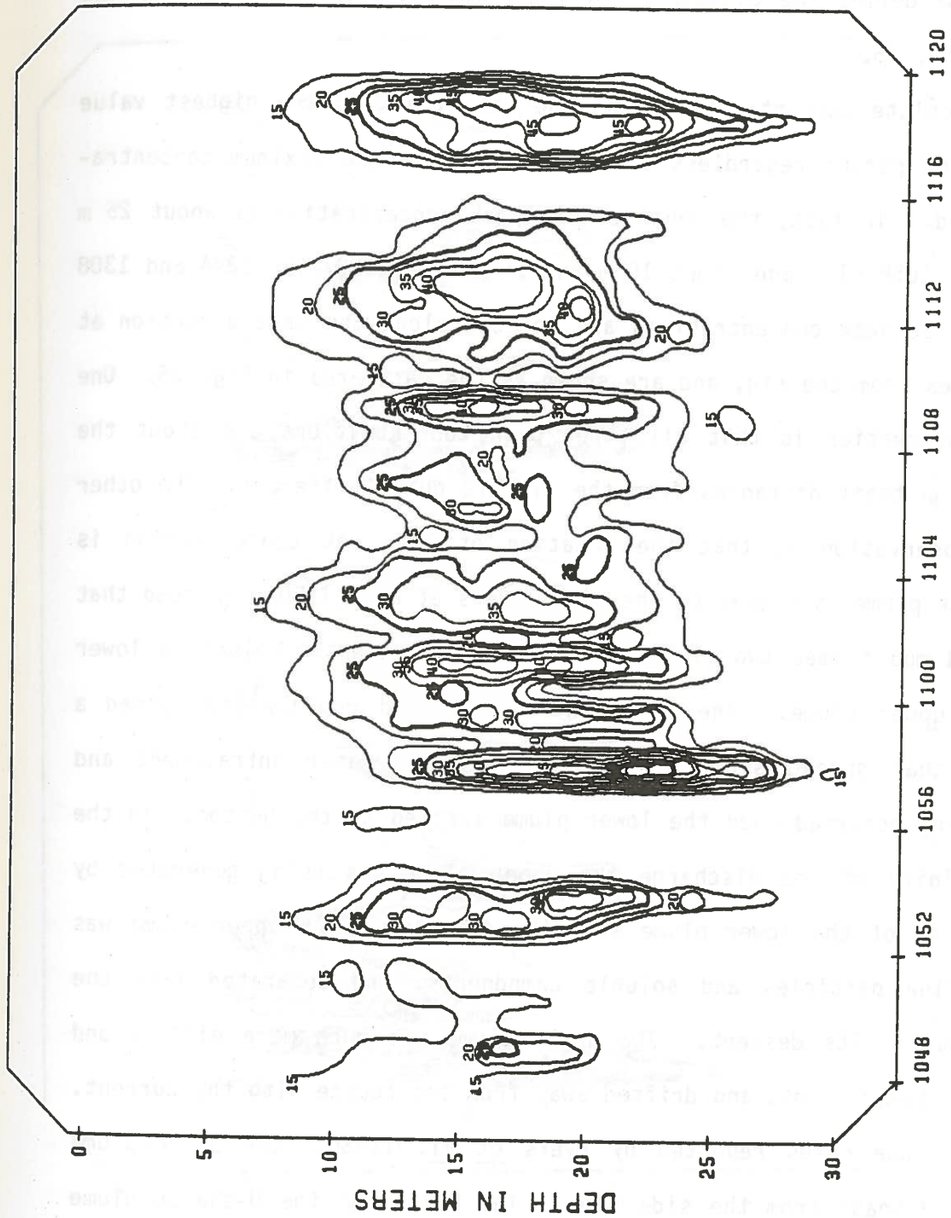

Fig. 36. Contours of relative particulate concentration, in arbitrary units, corresponding to acoustic transects in Fig. 20(a) and to one of the two ship tracks in Fig. 35.

transect in Fig. 37. The acoustic profiles for these two transects were discussed previously and are shown in Fig. 20. The isoconcentration lines in Figs. 36 and 37 define the boundaries of the plumes and the locations of the centroids in Fig. 35.

The particulate concentration along the ship track is the highest value during that time period regardless of the depth where the maximum concentration is located. In fact, the depth of the peak concentration is about 25 m in Fig. 36 (at 1058 LT), and about 10 m and 15 m in Fig. 37 (at 1244 and 1308 LT). These three peak concentrations are located along the same direction at different ranges from the rig, and are shown as the dark area in Fig. 35. One interesting observation is that all three peak concentrations are about the same even though their distances from the rig are quite different. The other interesting observation is that the location of the peak concentration is deeper when the plume is closer to the rig. Ayers et al. (1980) reported that the discharged mud formed two plumes as it entered the water column, a lower plume and an upper plume. The lower plume descended rapidly and formed a fluffy cloud that spread slowly along the bottom. Water entrainment and turbulent mixing occurred when the lower plume settled to the bottom. In the immediate vicinity of the discharge the upper plume was being generated by turbulent mixing of the lower plume with the seawater. The upper plume was composed of fine particles and soluble components, and separated from the lower plume during its descent. The upper plume was much more diffuse and puffy than the lower plume, and drifted away from the source with the current.

In one of the cases reported by Ayers et al. (1980), the upper plume appeared as a U shape from the side view. The bottom of the U-shaped plume was located about 300 m from the source. In our case, the peak concentration at deeper water in Fig. 36 is about 0.15 mi or 280 m from the rig. The peak

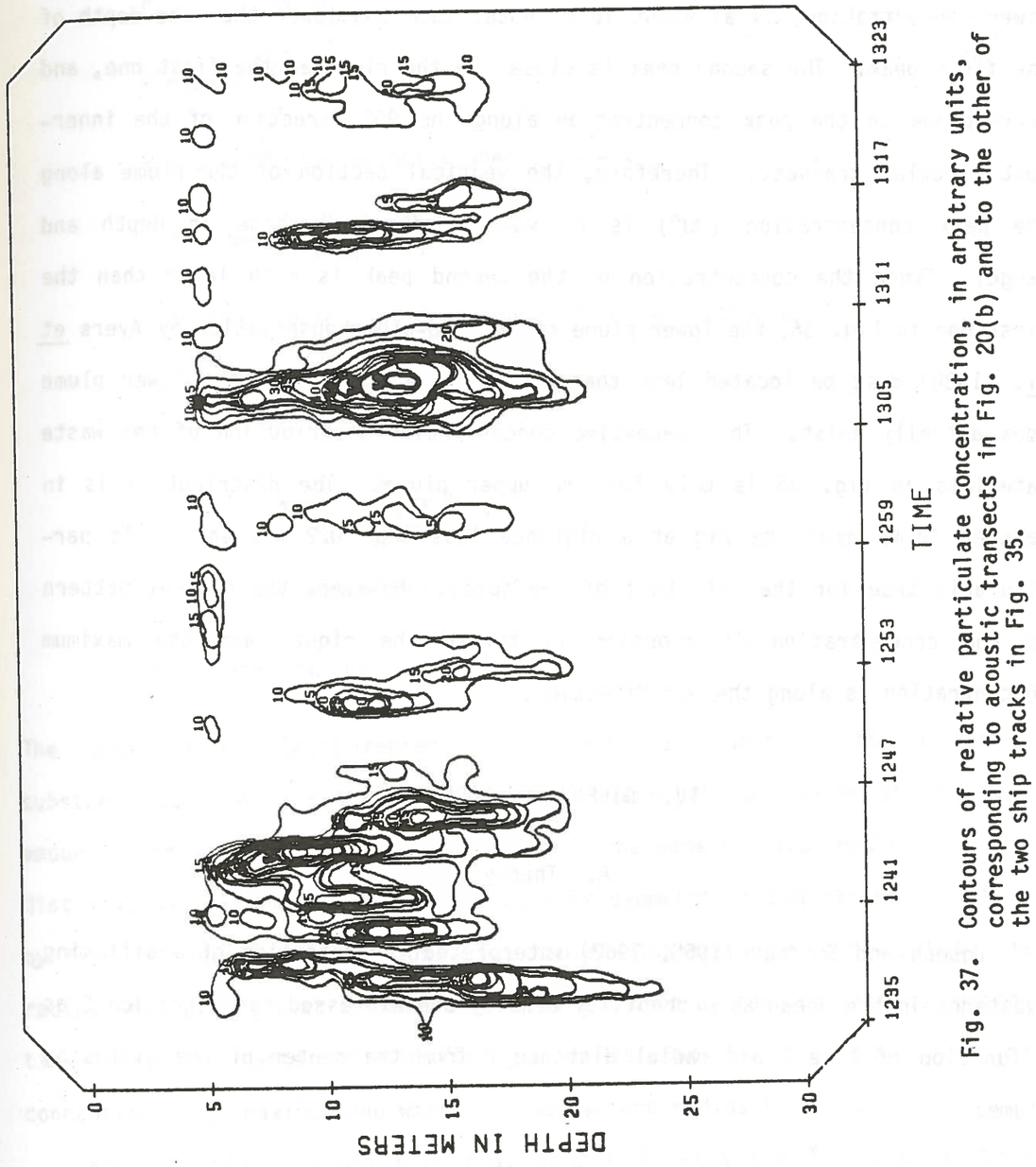

Fig. 37. Contours of relative particulate concentration, in arbitrary units, corresponding to acoustic transects in Fig. 20(b) and to the other of the two ship tracks in Fig. 35.

concentrations in shallower water in Fig. 37 are beyond 0.25 mi or at least 350 m from the rig. At 1110 LT in Fig. 36, there is another concentration peak of lower value than the first peak at 1058 LT. This second peak, of lower concentration, is at about 15 m depth, much shallower than the depth of the first peak. The second peak is closer to the rig than the first one, and corresponds to the peak concentration along the 90° direction of the innermost circular transect. Therefore, the vertical section of the plume along the peak concentration (90°) is a two-dimensional U shape in depth and range. Since the concentration of the second peak is much lower than the first one in Fig. 36, the lower plume of the two-plume observation by Ayers et al. (1980) must be located less than 0.1 mi from the rig if the lower plume does actually exist. The space-time concentration distribution of the waste materials in Fig. 35 is only for the upper plume. The distribution is in patched forms near the rig at a distance less than 0.2 mi, and it is particularly true for the left half of the space. However, the general pattern of the concentration distribution is toward the right, and the maximum concentration is along the 90° direction.

IV. DIFFUSION PROCESSES

A. Theory

Joseph and Sendner (1958, 1962) interpreted concentration of a diffusing substance in the ocean as probability density and expressed concentration C as a function of time t and radial distance r from the center of the diffusing plume:

$$C(r,t) = S_o(T) \exp\left[-\alpha(T)\, R^{2-\lambda}\right], \qquad (3)$$

where

R equals $\frac{r}{r_o}$;

r_o is a constant;

T equals $\frac{P_o t}{r_o}$;

P_o is diffusion velocity when r equals r_o;

$\alpha(T)$ equals $\frac{1}{(2-\lambda)^2}\left(\frac{1}{T}\right)$;

λ is the exponent of dependence of concentration on R;

$S_o(T)$ equals $C_o[\alpha(T)]^{\frac{2}{2-\lambda}}$;

C_o equals $\frac{2-\lambda}{2\pi r_o^2}\frac{M}{\Gamma\left(\frac{2}{2-\lambda}\right)}$;

$\Gamma(a)$ is the Gamma function of a;

M is total substance.

The concentration C(r,t) represents averaged distribution of the diffusing substance at t when a sufficiently large number of substances of the same amount is introduced into a small area under the same oceanic conditions. The distribution is then assumed to be radially symmetrical and can be described by lines of equal concentration. The radial distance r is equivalent to the radius of a circle that has the same area enclosed by the constant concentration line. The center of a diffusing plume is always at the point where the concentration is maximum and where the equivalent radius is zero.

Equation (3) is plotted in Fig. 38 for fixed λ and T. Concentration approaches zero as the radius goes to infinity. The slope of the concentration curve at a particular R not only depends on the concentration at that

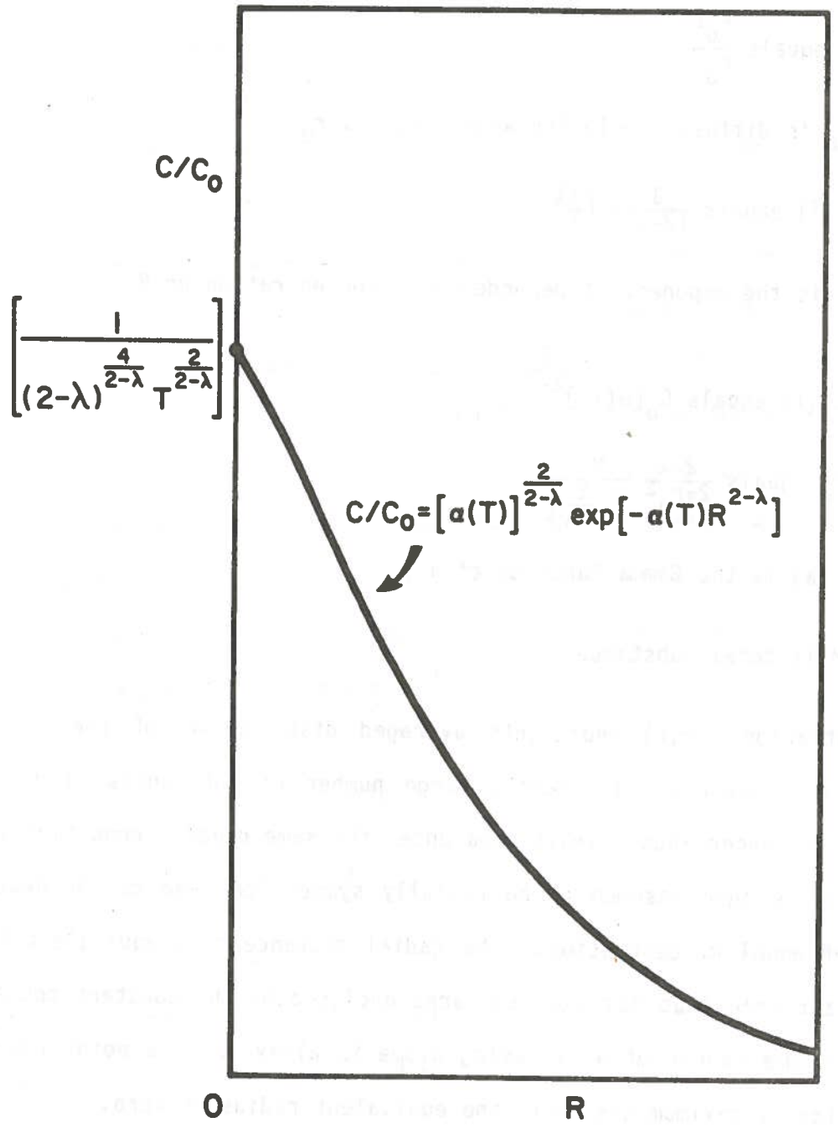

Fig. 38. Theoretical curve of particulate concentration vs. equivalent radius from equation (3).

point, but also depends on λ and T. The maximum concentration (at R = 0) also depends on λ and T. The dependence is illustrated in Figs. 39 and 40 for selected λ and T. Although the values of λ are between 0 and 2, in practice most interesting problems have values of λ between 0 and 1. When $\lambda = 1$, the concentration curves in semilogarithmic scales are straight lines [Fig. 39(c)] and correspond to the original model of Joseph and Sendner (1958). For fixed λ, the maximum C/C_0 decreases as T increases (Fig. 39). For fixed T, the maximum $C'C_0$ can decrease or increase as λ decreases (Fig. 40). The turning point is at $T = T_M$. When $T < T_M$ and fixed, the maximum C/C_0 decreases as λ decreases. When $T > T_M$ and fixed, the maximum C/C_0 increases as λ decreases. T_M is determined by the following equation:

$$T_M = \frac{R^{2-\lambda}}{2(2-\lambda)} . \tag{4}$$

Actually T_M is the time for the concentration to be maximum for fixed R and λ. The maximum concentration is

$$C_M = C(R, T_M) = C_0\left(\frac{2}{2-\lambda}\right)^{\frac{2}{2-\lambda}} \frac{\exp\left[-\frac{2}{2-\lambda}\right]}{R^2} . \tag{5}$$

Figure 41 shows the functional relationship between concentration and time. The locus of C_M is also plotted in Fig. 41 as the heavy broken line. When R and λ vary, the concentration curve in Fig. 41 will change accordingly, but its maximum will move along this broken line. The concentration curves are plotted in Fig. 42 for different values of R at fixed λ, and in Fig. 43 for $\lambda = 0$ and 1 at fixed R. Since T_M is larger for larger R, the maximum of concentration moves to higher T as R increases, and also decreases its value for fixed λ.

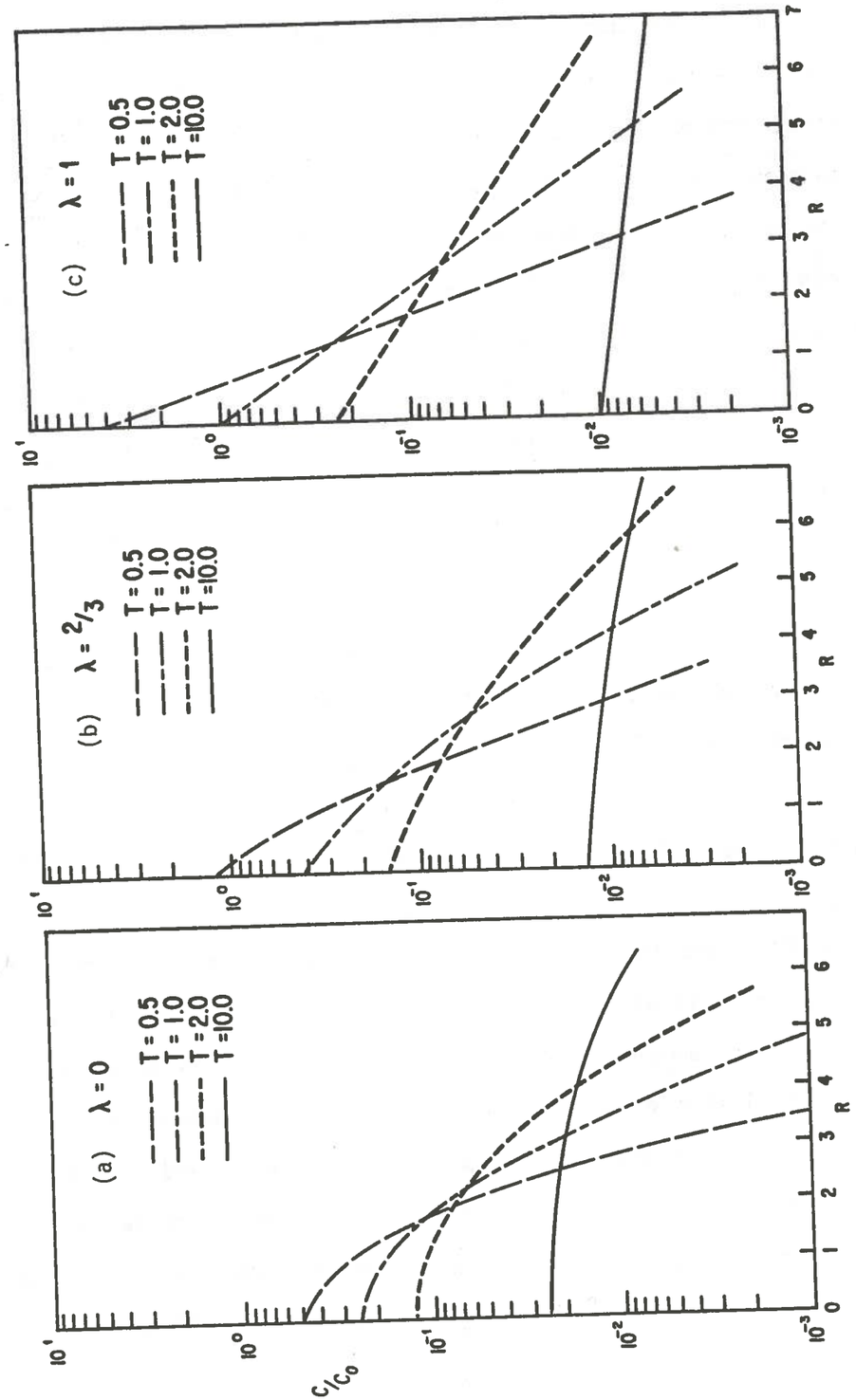

Fig. 39. Theoretical curves of particulate concentration vs. equivalent radius for different times at fixed λ values of (a) 0, (b) 2/3, and (c) 1.

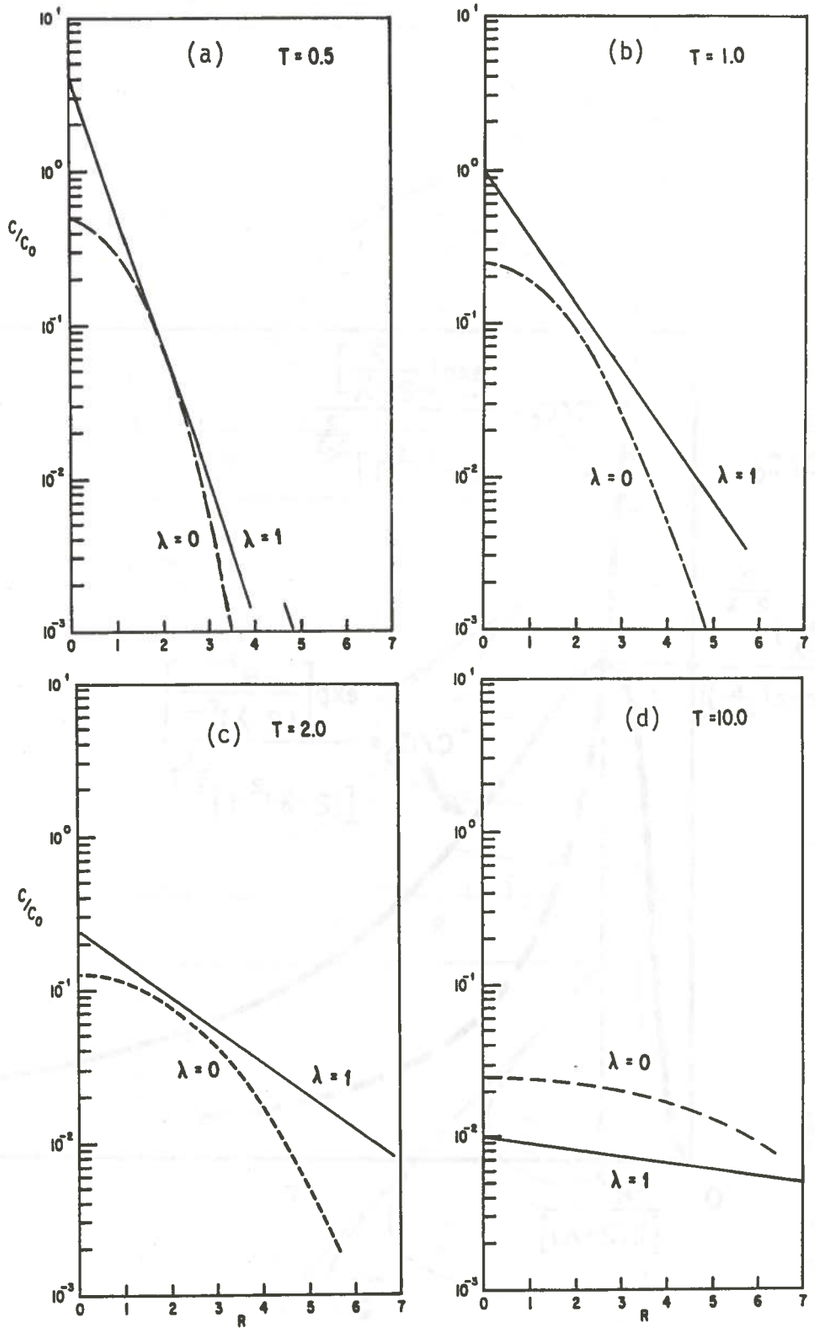

Fig. 40. Theoretical curves of particulate concentration vs. equivalent radius for λ = 0 and 1 at different fixed times.

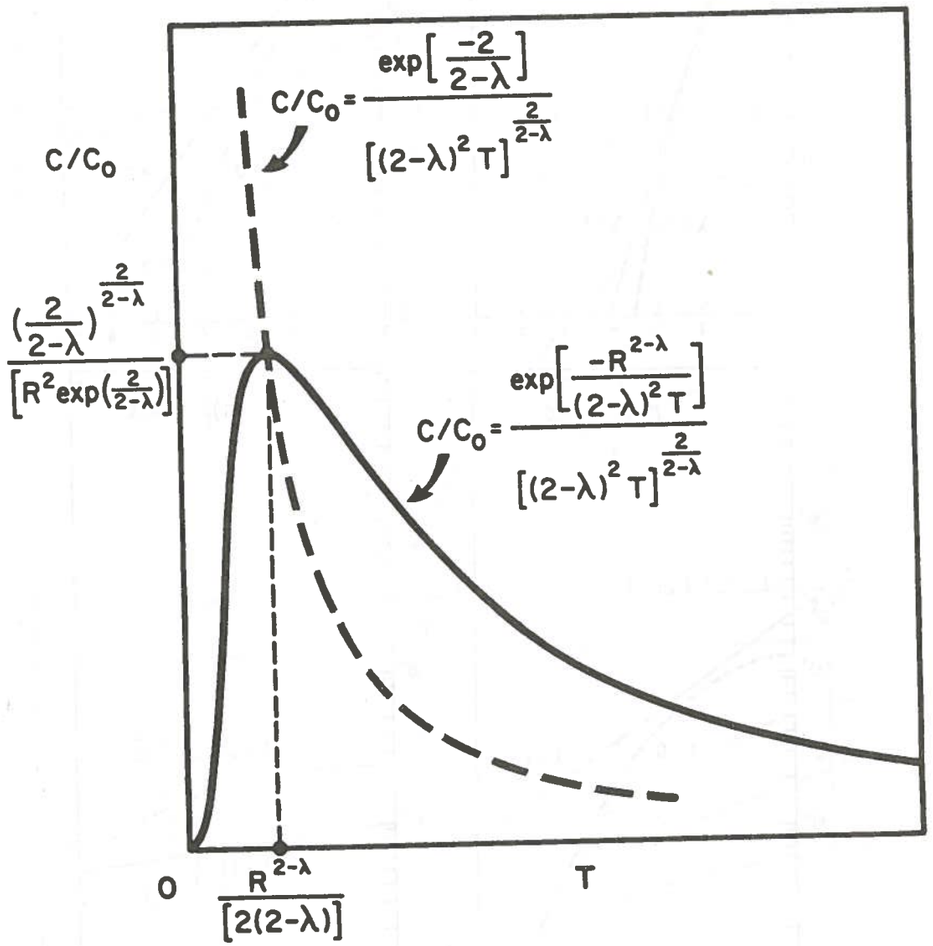

Fig. 41. Theoretical curve of particulate concentration vs. time from equations (3), (4), and (5).

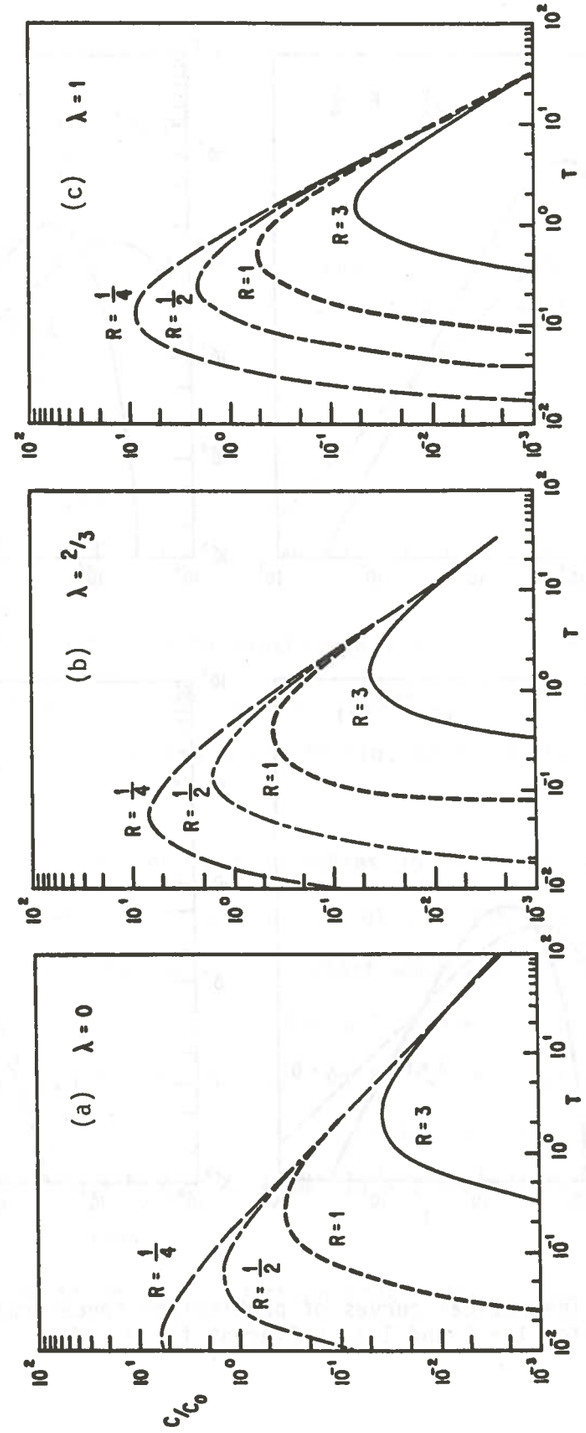

Fig. 42. Theoretical curves of particulate concentration vs. time for different radii at fixed λ values of (a) 0, (b) 2/3, and (c) 1.

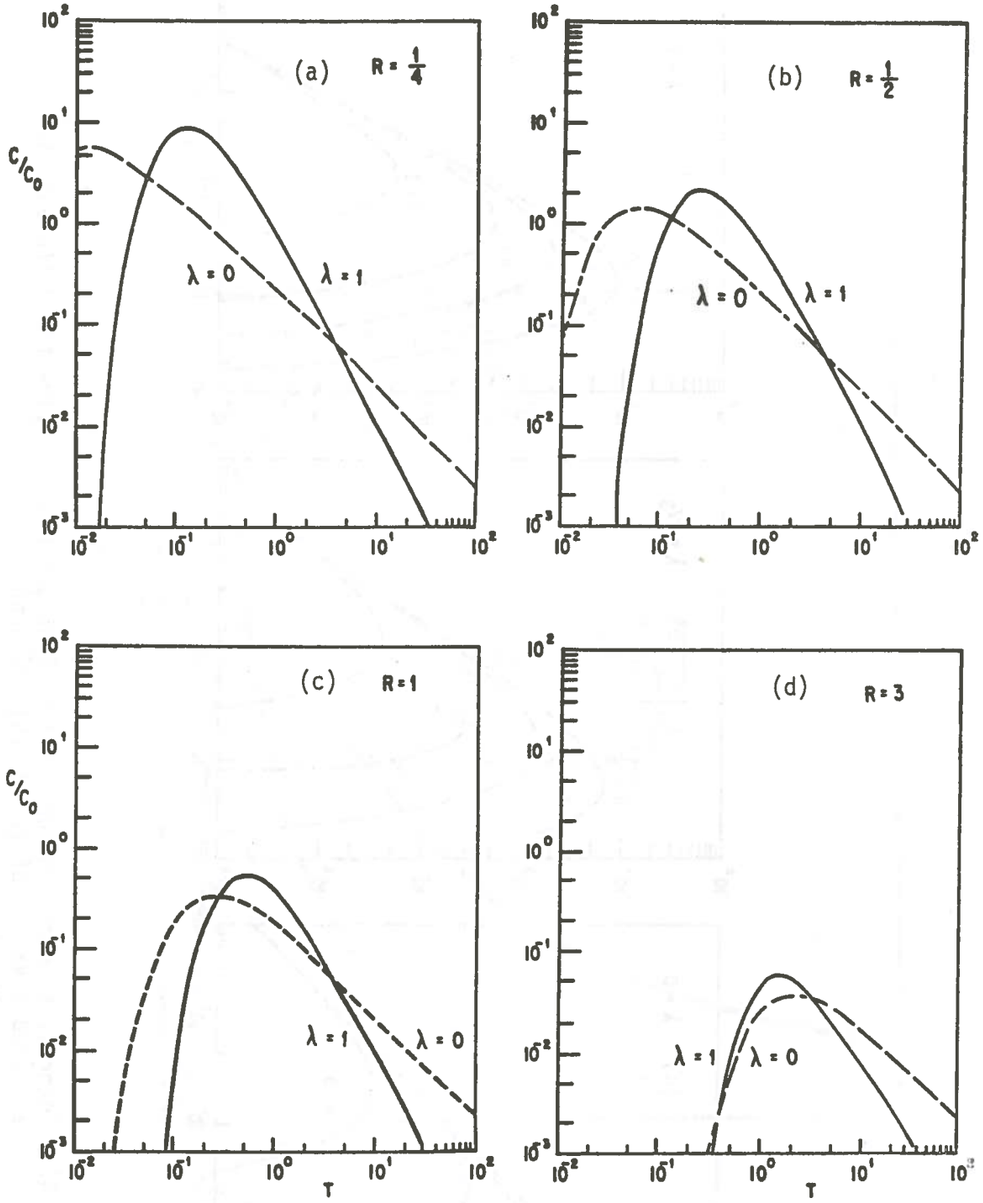

Fig. 43. Theoretical curves of particulate concentration vs. time for $\lambda = 0$ and 1 at different fixed radii.

If we look at the change of radius with time at certain concentrations, we can solve for R from equation (3) to get

$$R = \left[\frac{1}{\alpha(T)} \ln \frac{S_o(T)}{C(R,T)}\right]^{\frac{1}{2-\lambda}} . \tag{6}$$

Equation (6) is plotted in Fig. 44. The maximum radius at $T=T_R$ is

$$R_M = \left[2(2-\lambda)T_R\right]^{\frac{1}{2-\lambda}} \tag{7}$$

where

$$T_R = \frac{1}{(2-\lambda)^2 e}\left(\frac{C_o}{C}\right)^{\frac{2-\lambda}{2}} . \tag{8}$$

The locus of maximum radius is also plotted in Fig. 44, as the heavy broken line. This is a straight line when $\lambda = 1$. Equation (6) is also plotted in Fig. 45 for different C/C_o at fixed λ and in Fig. 46 for different λ at fixed C/C_o.

The characteristic parameters and variables in Figs. 38, 41, and 44 are summarized in Tables 2 and 3 for six values of λ. The case for $\lambda = 2$ is excluded because the concentration C is constant when $\lambda = 2$. From Table 2 we notice that $\alpha(T)$ is proportional to T for all values of λ. The maximum concentration C_M is inversely proportional to R^2 for all values of λ. The time T_M at which $C = C_M$ depends on $R^{2-\lambda}$. This is the same as the exponent dependence on R for the concentration. From Table 3 we notice that R_M depends on C as $(C_o/C)^{1/2}$ for all values of λ.

Equation (3) is based on the assumption that diffusion velocity depends on r and

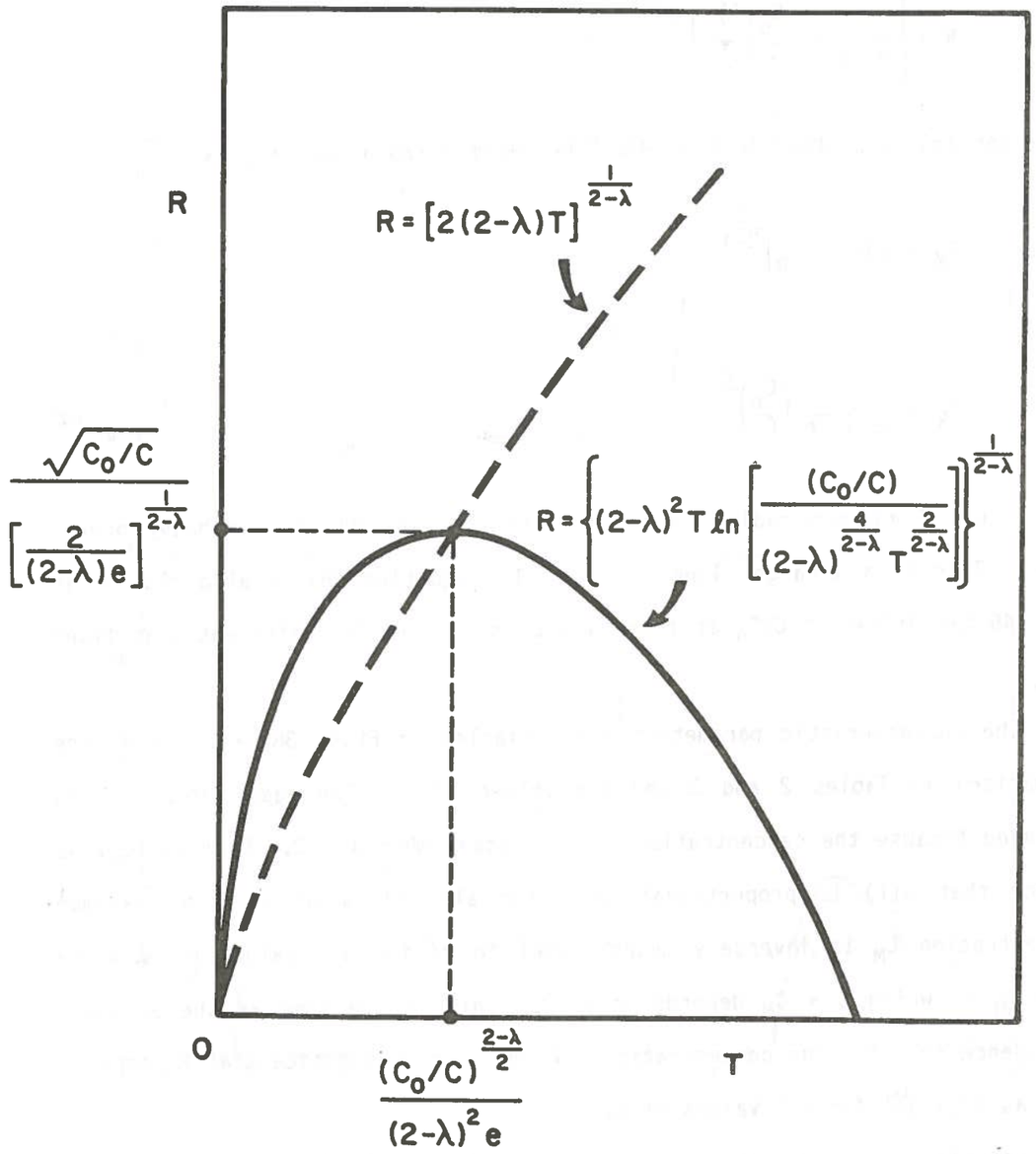

Fig. 44. Theoretical curve of equivalent radius vs. time from equations (6), (7), and (8).

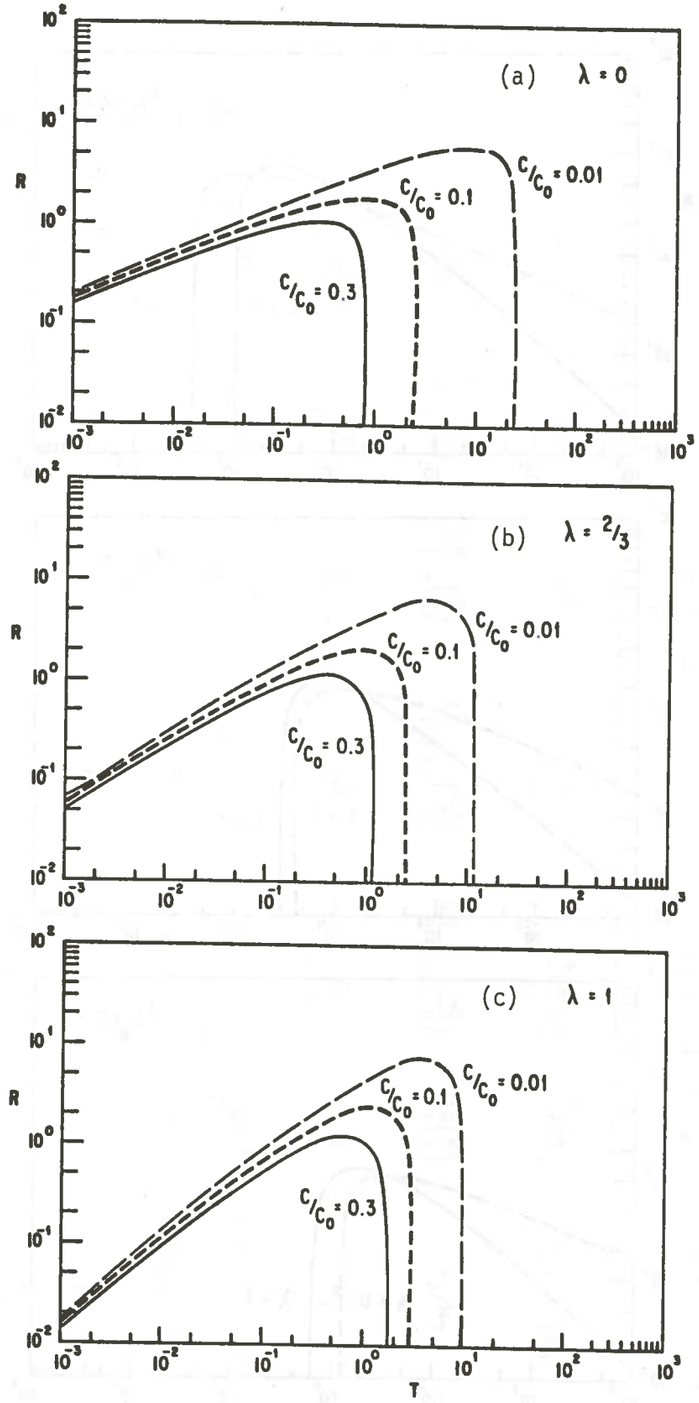

Fig. 45. Theoretical curves of equivalent radius vs. time for different concentration levels at fixed λ values of (a) 0, (b) 2/3, and (c) 1.

Fig. 46. Theoretical curves of equivalent radius vs. time for $\lambda = 0$ and 1 at different fixed concentration levels.

Table 2. Characteristic parameters for six values of λ when concentration is expressed as a function of time*.

0	1/3	2/3	1	4/3	5/3
$\frac{2}{2-\lambda}$	1	6/5	3/2	2	3	6
$\alpha(T)/T$	1/4	9/25	9/16	1	9/4	9
$S_o(T)/C_o$	α	$\alpha^{6/5}$	$\alpha^{3/2}$	α^2	α^3	α^6
$C(R,T)/S_o(T)$	$e^{-\alpha R^2}$	$e^{-\alpha R^{5/3}}$	$e^{-\alpha R^{4/3}}$	$e^{-\alpha R}$	$e^{-\alpha R^{2/3}}$	$e^{-\alpha R^{1/3}}$
T_M	$\frac{1}{4}R^2$	$\frac{3}{10}R^{5/3}$	$\frac{3}{8}R^{4/3}$	$\frac{1}{2}R$	$\frac{3}{4}R^{2/3}$	$\frac{3}{2}R^{1/3}$
C_M/C_o	$\left(\frac{1}{e}\right)\frac{1}{R^2}$	$\left(\frac{6}{5e}\right)^{6/5}\frac{1}{R^2}$	$\left(\frac{3}{2e}\right)^{3/2}\frac{1}{R^2}$	$\left(\frac{2}{e}\right)^2\frac{1}{R^2}$	$\left(\frac{3}{e}\right)^3\frac{1}{R^2}$	$\left(\frac{6}{e}\right)^6\frac{1}{R^2}$
$C_M(T_M)/C_o$	$\left(\frac{1}{4eT_M}\right)$	$\left(\frac{9}{25eT_M}\right)^{6/5}$	$\left(\frac{9}{16eT_M}\right)^{3/2}$	$\left(\frac{1}{eT_M}\right)^2$	$\left(\frac{9}{4eT_M}\right)^3$	$\left(\frac{9}{eT_M}\right)^6$

$$C_M = C_o\left(\frac{2}{2-\lambda}\right)^{\frac{2}{2-\lambda}}\left[\frac{1}{R^{\frac{2}{2-\lambda}}e^{\frac{2}{2-\lambda}}}\right] = \frac{C_o}{e^{(2-\lambda)^2}(T_M)^{\frac{2}{2-\lambda}}}$$

* $C = C(T) = S_o(T)\, e^{-\alpha(T)R^{(2-\lambda)}}$

$$T_M = \frac{R^{(2-\lambda)}}{2(2-\lambda)}$$

Table 3. Characteristic parameters for six values of λ when radius is expressed as a function of time*.

	0	1/3	2/3	1	4/3	5/3
$2-\lambda$	2	5/3	4/3	1	2/3	1/3
$\alpha(T)/T$	1/4	9/25	9/16	1	9/4	9
$S_o(T)/C_o$	α	$\alpha^{6/5}$	$\alpha^{3/2}$	α^2	α^3	α^6
T_R	$\frac{1}{4e}\left(\frac{C_o}{C}\right)$	$\frac{9}{25e}\left(\frac{C_o}{C}\right)^{5/6}$	$\frac{9}{16e}\left(\frac{C_o}{C}\right)^{2/3}$	$\frac{1}{e}\left(\frac{C_o}{C}\right)^{1/2}$	$\frac{9}{4e}\left(\frac{C_o}{C}\right)^{1/3}$	$\frac{9}{e}\left(\frac{C_o}{C}\right)^{1/6}$
R_M	$\left(\frac{1}{e}\right)^{1/2}\left(\frac{C_o}{C}\right)^{1/2}$	$\left(\frac{6}{5e}\right)^{3/5}\left(\frac{C_o}{C}\right)^{1/2}$	$\left(\frac{3}{2e}\right)^{3/4}\left(\frac{C_o}{C}\right)^{1/2}$	$\frac{2}{e}\left(\frac{C_o}{C}\right)^{1/2}$	$\left(\frac{3}{e}\right)^{3/2}\left(\frac{C_o}{C}\right)^{1/2}$	$\left(\frac{6}{e}\right)^{3}\left(\frac{C_o}{C}\right)^{1/2}$
$R_M(T_R)$	$\left(4T_R\right)^{1/2}$	$\left(\frac{10}{3}T_R\right)^{3/5}$	$\left(\frac{8}{3}T_R\right)^{3/4}$	$\left(2T_R\right)$	$\left(\frac{4}{3}T_R\right)^{3/2}$	$\left(\frac{2}{3}T_R\right)^{3}$

* $R(T)^{2-\lambda} = \frac{1}{\alpha(T)} \ln \frac{S_o(T)}{C}$ $\qquad T_R = \frac{1}{(2-\lambda)^2 e}\left(\frac{C_o}{C}\right)^{\frac{2-\lambda}{2}}$

$$R_M = \left[\frac{2}{(2-\lambda)e}\right]^{\frac{1}{2-\lambda}}\left(\frac{C_o}{C}\right)^{1/2} = \left[2(2-\lambda)T_R\right]^{\frac{1}{2-\lambda}}$$

$$P(r) = P_o\left(\frac{r}{r_o}\right)^{\lambda-1}. \qquad (9)$$

Okubo (1962a) derived a similar expression to equation (3) without explicitly defining $\alpha(t)$ and $P(r)$. Various solutions of different diffusion models can be derived from Okubo's results, including Joseph and Sendner's original solution (1958). Different solutions correspond to different values of λ and have different time dependences for $\alpha(t)$. Table 4 compares Joseph and Sendner's model with Okubo's model, based on their respective definitions and assumptions. The quantity $C(0,t)$ is actually $S_o(T)$ defined in equation (3). Table 5 compares Joseph and Sendner's solution with other solutions listed by Okubo (1962a,b), including the Fickian solution and Okubo's original solution.

We will use Joseph and Sendner's generalized solution to interpret the data from the Puerto Rico and New York Bight Ocean dumping experiments, by assuming that the relative concentration is proportional to the acoustic backscattering intensity as described in Section III. Since Joseph and Sendner's model actually describes the horizontal diffusion of a point source within a thin layer, several additional assumptions are needed so that equation (3) can be applied. The major question is whether the lines of equal concentration, represented by equation (3), describe the horizontal or vertical diffusion.

Okubo (1971a) and Okubo and Carter (1966) proposed a simplified model of the shear effect on horizontal mixing in a bounded sea. The result of shear effect is that an effective longitudinal dispersion is produced by the combination of a gradient of velocity with turbulent mixing in the same direction. A characteristic time τ is defined so that the shear effect produces a homogeneous layer throughout the water column after time τ, and disperses the substance in the longitudinal direction repeatedly at intervals of τ (see Fig. 4.12 in Okubo, 1971a). We assume that no direction is preferred in the field

Table 4. Comparison of Joseph and Sendner's (1962) model with Okubo's (1962a,b) model.

	Okubo	Joseph and Sendner
$\frac{\partial C}{\partial t}$	$\frac{1}{r}\frac{\partial}{\partial r}\left(kr^{m+1}f\frac{\partial C}{\partial r}\right)$	$\frac{1}{r}\frac{\partial}{\partial r}\left(r^{2p}\frac{\partial C}{\partial r}\right)$
	m	λ
M	$\int_0^\infty C\ 2\pi r dr$	$\int_0^\infty C\ 2\pi r dr$
A	$k(m+1)r^{m-1}f$	$\frac{1}{r}\frac{\partial}{\partial r}(r^2P) = (\lambda + 1)P$
B	$kr^m f$	$\frac{2}{r}\int_0^r P(r)rdr = rP$
$k\Psi$	$k\int_0^t f(t)dt$	$kft = P_o t r_o^{1-\lambda}$
P	kfr^{m-1}	$P = P_o\left(\frac{r}{r_o}\right)^{\lambda-1}$
C(0,t)*	$\frac{(2-m)M}{2\pi(2-m)^{\frac{4}{2-\lambda}}\Gamma\left(\frac{2}{2-m}\right)(k\Psi)^{\frac{2}{2-m}}}$	$\frac{(2-\lambda)M}{(2\pi)(2-\lambda)^{\frac{4}{2-\lambda}}\Gamma\left(\frac{2}{2-\lambda}\right)(P_o t)^{\frac{2}{2-\lambda}} r_o^{\frac{2(\lambda-1)}{2-\lambda}}}$
$\ln \frac{C(r,t)}{C(0,t)}$	$-\frac{r^{2-m}}{(2-m)^2(k\Psi)}$	$-\frac{r_o(r/r_o)^{2-\lambda}}{(2-\lambda)^2(P_o t)}$
α	$\frac{r_o^{2-m}}{(2-m)^2(k\Psi)}$	$\frac{r_o}{(2-\lambda)^2(P_o t)}$

*C(0,t) is actually $S_o(T)$ defined in equation (3).

Table 5. Comparison of Joseph and Sendner's (1958) solution with other solutions listed in Okubo (1962a,b).

	λ	$\alpha(t)$	$S_o(t)/M$	$\ln C/S_o$
JS	1	$\frac{r_o}{P_o t}$	$\frac{t^{-2}}{2\pi P_o^2}$	$-\frac{r}{P_o t}$
Oz	4/3	$\frac{r_o^{2/3}}{\gamma t}$	$\frac{t^{-3}}{6\pi\gamma^3}$	$-\frac{r^{2/3}}{\gamma t}$
OP	0	$\frac{r_o^2}{\omega^2 t^2}$	$\frac{t^{-2}}{\pi\omega^2}$	$-\frac{r^2}{\omega^2 t^2}$
Ok	2/3	$\frac{r_o^{4/3}}{\alpha_o^2 t^2}$	$\frac{t^{-3}}{\frac{3}{4}\pi^3\ ^2\alpha_o^3}$	$-\frac{r^{4/3}}{\alpha_o^2 t^2}$
Ob	0	$\frac{r_o^2}{\beta^3 t^3}$	$\frac{t^{-3}}{\pi\beta^3}$	$-\frac{r^2}{\beta^3 t^3}$
Fi	0	$\frac{r_o^2}{4Kt}$	$\frac{t^{-1}}{4\pi K}$	$-\frac{r^2}{4Kt}$

JS = Joseph and Sendner
Oz = Ozmidov
OP = Okubo and Pritchard
Ok = Okubo
Ob = Obukhov
Fi = Fickian

of turbulence in the time average and that the acoustic transects across the plume from different directions shall give the same concentration contours at a particular time. The time for completing one acoustic transect is short compared with the time between the dumping and the transect.

In shallow water, at the commencement of dumping, the dumped materials reach the bottom almost instantaneously. At any instant, the disappearing of dumped materials into the ocean bottom and resuspension of particulate matter from the bottom give net zero contribution to the total suspended material within the water column. This assumption is weak, not only because the materials that disappear and that resuspend are different particulate matter, but because they have different rates of contribution and may actually act as a source or sink to the entire diffusion process. However, the time interval is very short during the period when exchange of material between the bottom and the water column is taking place. Before the first acoustic transect, the exchange process would cease to occur and the diffusion and mixing within the water column would dominate the distribution of particle concentration. The two phases, dynamically active and passive, are hard to determine.

In the deep water case, most of the dumped materials will penetrate the thermocline and reach the deep ocean at the initial phase. The fine particulate matter will then be trapped within and above the thermocline, and undergo the diffusive process. The initial detection of the plume by acoustic systems can only occur after the diffusive process.

B. Analysis

The relative particulate concentration within each plume from an ocean disposal experiment can be expressed as the distance from the center of the plume, and be described by equations (3) and (9) with proper definitions of

the variables and the parameters in the equations. The distance is the equivalent radius of a circle that has the same area enclosed by the isoconcentration lines. The relative concentration is the measured acoustic backscattered intensity. The concentration is plotted against the radius for experimental data and from theoretical prediction. Instead of an arbitrary value of λ, we chose λ to be multiples of 1/3 and of a value between 1 and 0. The zero value of λ corresponds to the Fickian solution of constant diffusivity. The diffusivity is just $r_o P_o$. When λ is equal to 1, it represents Joseph and Sendner's solution of constant diffusion velocity. The parameters α and C_o are determined with the best-fitted curve to the measured acoustic data.

The short-term fate of the dumped dredged materials in the New York Bight in June 1979 was discussed in section III. The isoconcentration maps for three particular dumps were shown in Figs. 32 to 34; the corresponding concentration plots as a function of radius are shown now in Figs. 47(a) to 47(c) respectively. It turns out that the relative particulate concentration cannot be described by a single set of parameters. Two theoretical curves are needed to fit the experimental data points for all acoustic transects. The intercept of the two curves is assumed to be located at $r = r_o$, with r_o being defined in equation (3). This point illustrates a two-process diffusion and defines an imaginary boundary within the plume. The boundary moves inward toward the center, as time goes on, and characterizes the two different processes of diffusion with different λ values. The two processes are called mixed diffusion and normal diffusion, respectively, for $r < r_o$ and $r > r_o$. For mixed diffusion inside the boundary, settling and resuspension take place continuously at the early stage after the dump and eventually cease after a short duration. The required time t_o is on the order of seconds for the

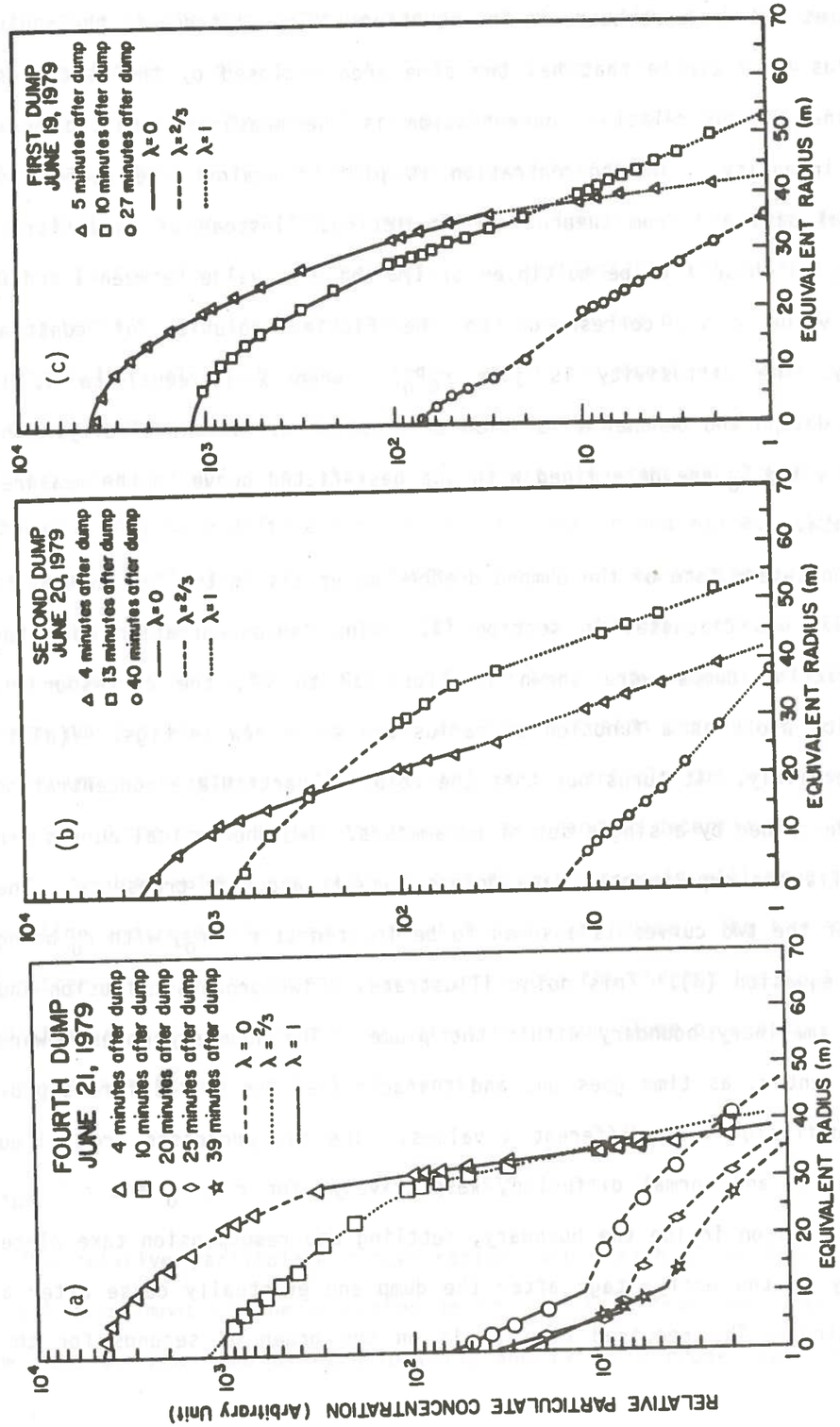

Fig. 47. Relative particulate concentration vs. equivalent radius from the experimental data with the best-fitted curves of equation (3). The experimental data are taken from (a) Fig. 32, (b) Fig. 33, and (c) Fig. 34.

shallow water at the New York Bight Dumpsite. Dispersion begins after this short period and equation (3) can then be applied. For normal diffusion outside the boundary, little or no settling, resuspension, and mixing occur from the beginning of the dump; the dumped waste is regarded as being neutrally buoyant so that the substances diffuse with constant velocity. The diffusion diagram of radioactive test material in the ocean (Fig. 2 in Joseph and Sendner, 1958) might also be interpreted in terms of the two-process diffusion. The boundary point is located at approximately 16 km from the center of the dispersion plume.

For all different acoustic observations in the New York Bight Dumping Experiments, the dependence of particulate concentrations on r changes with time for both regions. Tables 6 to 8 summarize these changes along with other diffusion parameters of the plumes for the three dumps shown in Fig. 47. The primed quantities are for $r > r_0$. The λ values generally increase with time for $r < r_0$ and decrease for $r > r_0$. That is to say that mixed diffusion follows Fickian law at the beginning of the dump and later on approaches Joseph and Sendner's model with constant diffusion velocity. It occurs in the opposite way in normal diffusion. As the concentration is interpreted as probability density, the concentration distribution immediately after the dump should be more random and have equivalent Gaussian distribution with r^2 dependence in the exponent. When dynamic processes and vertical mixing cease to dominate, the concentration distribution more or less deviates from the Gaussian and tends to approach the r^n dependence with $n < 2$. The boundary point for each transect is different and decreases as a function of time after the dump. Figure 47(a) seems to indicate that only two values of r_0 exist, one value for the first two transects and the other value for the other three transects. Values from the first dump on June 19 [Fig. 47(c)] do support this

Table 6. Summary of diffusion parameters for the fourth dredged material dump on June 21, 1979, for five transects.

	1	2	3	4	5
t(s)	240	600	1200	1500	2340
r_o(m)	29	29	10	6	10.5
$\lambda(r < r_o)$	0	2/3	1	1	1
$\lambda'(r > r_o)$	1	2/3	0	0	0
$\alpha(r < r_o)$	2.61	2.46	1.58	1.43	1.79
$\alpha'(r > r_o)$	16.4	8.08	0.116	0.056	0.147
P_o(cm s^{-1})	1.16	1.11	0.53	0.28	0.25
P_o'(cm s^{-1})	0.74	0.34	1.80	1.79	0.76
C_o	4499	1216	65	34	28
σ^2(cm^2)	2.6×10^6	2.7×10^6	7.8×10^6	6.6×10^6	8.2×10^6
K(cm^2 s^{-1})	2.7×10^3	1.1×10^3	1.6×10^3	1.1×10^3	8.7×10^2
ℓ(cm)	4.8×10^3	4.9×10^3	8.4×10^3	7.7×10^3	8.6×10^3

Table 7. Summary of diffusion parameters for the second dredged material dump on June 20, 1979, for three transects.

	1	2	3
t(s)	240	780	2400
r_o(m)	25.5	36	17.5
$\lambda(r < r_o)$	0	2/3	2/3
$\lambda'(r > r_o)$	1	1	1
$\alpha(r < r_o)$	4.1	2.79	1.35
$\alpha'(r > r_o)$	5.76	8.24	1.16
P_o(cm s^{-1})	0.65	0.93	0.30
P_o'(cm s^{-1})	1.84	0.56	0.63
C_o	2498	888	15
σ^2(cm^2)	6.1×10^6	2.4×10^5	1.9×10^7
K(cm^2 s^{-1})	6.3×10^3	7.7×10^1	2.0×10^3
ℓ(cm)	7.4×10^3	1.5×10^3	1.3×10^4

Table 8. Summary of diffusion parameters for the first dredged material dump on June 19, 1979, for three transects.

	1	2	3
t(s)	300	60	1620
r_o(m)	36	35	8
$\lambda(r < r_o)$	0	0	2/3
$\lambda'(r > r_o)$	1	1	2/3
$\alpha(r < r_o)$	4.77	3.82	0.95
$\alpha'(r > r_o)$	19.30	6.04	0.53
P_o(cm s^{-1})	0.63	0.38	0.29
P_o'(cm s^{-1})	0.62	0.97	0.53
C_o	4335	1159	78
σ^2(cm^2)	2.7×10^6	3.0×10^6	3.6×10^6
K(cm^2 s^{-1})	2.2×10^3	1.3×10^3	5.6×10^2
ℓ(cm)	4.9×10^3	5.2×10^3	5.7×10^3

conjecture. However, the second dump on June 20 indicates three different values of r_o for the same plume.

It is obvious that the diffusion velocity, according to equation (9), is discontinuous at $r = r_o$. For each transect, the value of α is different because the λ value is found to be different for the two diffusion processes. The diffusion velocity parameter P_o is then different and gives distinct P(r) at $r = r_o$. Despite the fact that the concentration is continuous at the boundary point, the discontinuity of diffusion velocity at the same point generates some difficulties of interpretation without more measurements and understanding of short-term dredged-material dumping. The magnitude of P_o is between 0.1 to 1.9 cm s^{-1} and agrees with the general spectrum of diffusion velocities (Joseph and Sendner, 1962). However, P_o decreases with time for $r < r_o$ and fluctuates for $r > r_o$.

The peak concentration $C_o(t)$, defined as C(r,t) at $r = 0$, decreased rapidly with time as $t^{-2.29}$ for all transects. Okubo (1971a) and Pritchard et al. (1966) reported a two-slope variation of maximum concentration with time for instantaneous dye-release experiments in the sea off Cape Kennedy. Csanady (1966) also observed different behaviors of axial concentration at different locations in Lake Huron. In fact the concentration behaves according to different laws at three regions of distance from the source, and decreases more sharply at larger distances. Our data shown in Fig. 48(a) seem to illustrate a two-slope variation, with the breaking point at 10^3 seconds. This differs from Okubo's (1971a) results only in the time scale.

For comparison with other results, we calculate the variance σ^2 and apparent diffusivity K similar to those by Okubo (1971b)

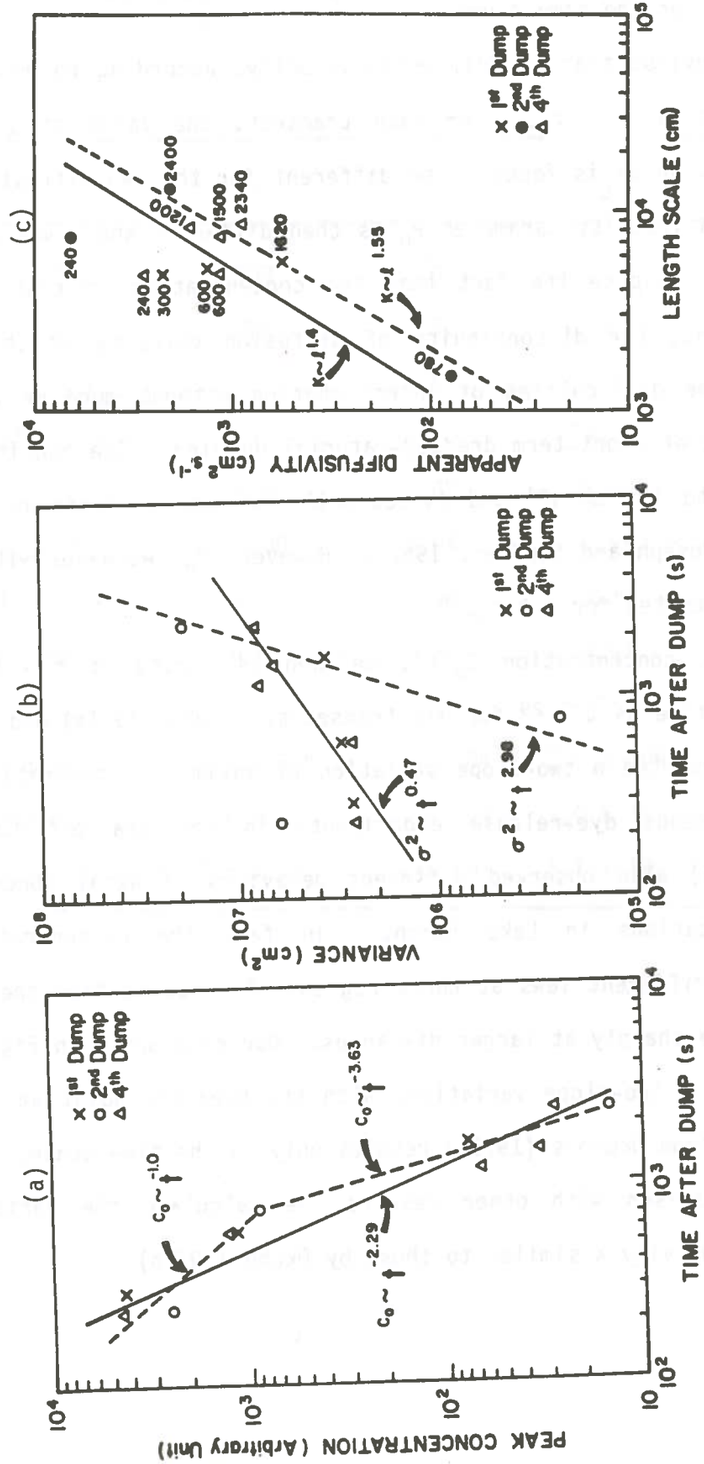

Fig. 48. (a) Peak concentration and (b) variance as a function of time after each dump, and (c) apparent diffusivity as a function of length scale for the three different dumps in the New York Bight. The solid lines represent all data. The dotted lines represent data for time larger or smaller than 10^3 seconds. K is defined as $\sigma^2/4t$ and ℓ is 3σ. The number with each datum point in (c) is the time in seconds after each dump.

$$\sigma^2 = r_o^2 \left\{ \frac{\int_0^1 R^2 C \, 2\pi \, RdR + \int_1^\infty R^2 \, C' \, 2\pi \, RdR}{\int_0^1 C \, 2\pi \, RdR + \int_1^\infty C' \, 2\pi \, RdR} \right\} , \tag{10}$$

$$K = \frac{1}{4} \frac{\sigma^2}{t} . \tag{11}$$

The variance is about one order larger than those reported by Okubo (1971b), but increases at a much slower rate for the time period of the measurements. For all measurements of the three dumps, taken from Tables 6 to 8 and shown in Fig. 48(b), the variance increases only as $t^{0.47}$. However, the variance increases as $t^{2.98}$ when variance is computed only for time larger than 10^3 seconds. That is, there probably exists a time limit for which the third power law dependence of variance on time cannot hold valid. This time limit coincides with the transient time for the change of the diffusion process from $\lambda = 0$ to $\lambda = 1$. It corresponds to the break point in time for the maximum concentration mentioned above. Gifford (1957) reported similar results for the spreading of smoke puffs in the atmosphere. His calculated mean-square particle dispersion as a function of time follows second and third power laws for different time intervals.

The apparent diffusivity, corresponding to Fig. 48(b), is shown in Fig. 48(c). The length scale ℓ is taken to be 3σ. Neither diffusivities for all transects nor diffusivities for transects at times larger than 10^3 seconds follow the 4/3 law. In fact, both increase with length scale more rapidly than predicted by the 4/3 law.

The concentration vs. radius for the Puerto Rico Dumping Experiments is shown in Fig. 49. The three transects from February 6, 1978 (Figs. 22 and 23), are plotted in Fig. 49(a). The other five transects from October 29-30, 1978 (Figs. 27 to 31), are plotted in Figs. 49(b). The best-fitted theoretical

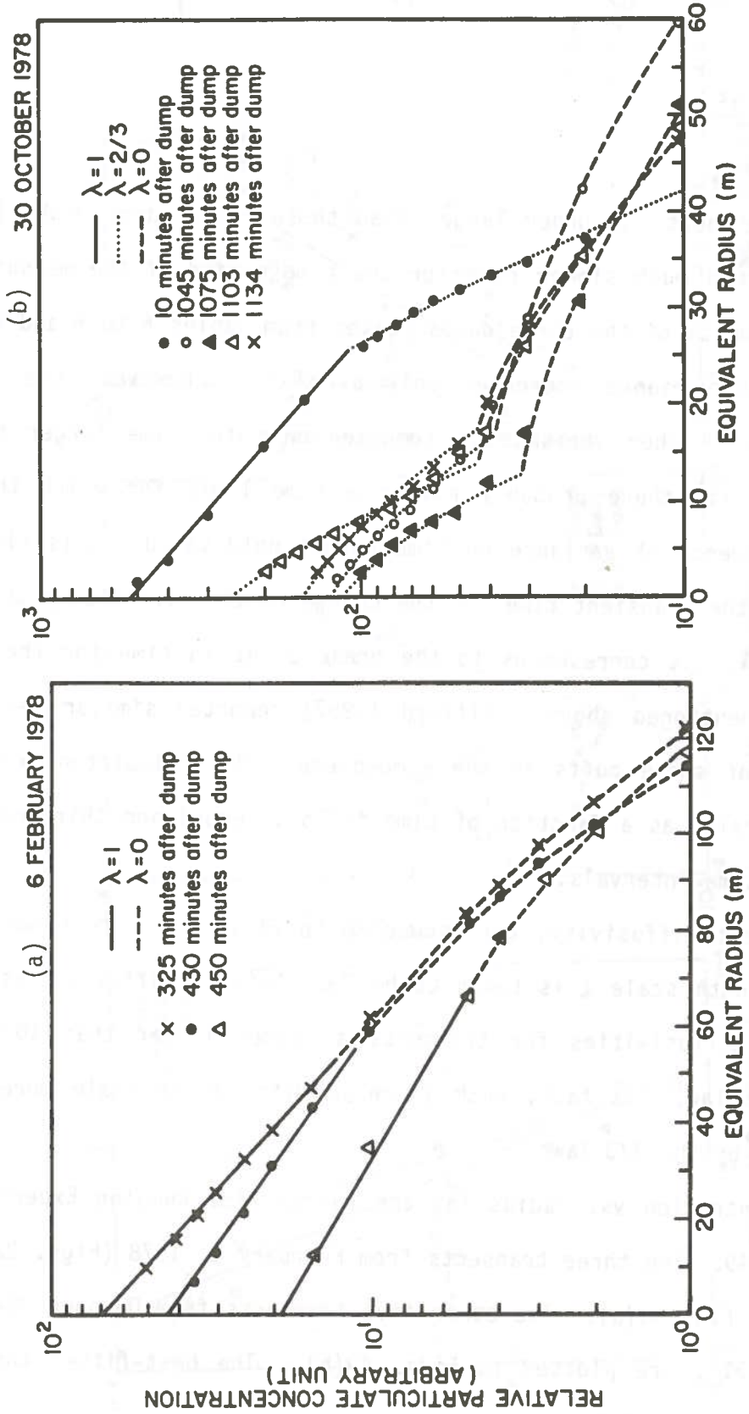

Fig. 49. Relative particulate concentration vs. equivalent radius from the experimental data with the best-fitted curves of equation (3). The experimental data are taken from (a) Figs. 22 and 23, and (b) Figs. 27 to 31.

curves from equation (3) give only two values of λ, 0 and 1. The two-phase diffusion process is apparent, but the boundary point r_o is quite different from those in the New York Bight water. The water depths and time scales are different for the two cases. The New York Bight water is much shallower than the Puerto Rico water. The dumping is different in nature and procedure too. One is a spot dump of dredged materials (New York Bight) and the other is a line dump of industrial waste. The plots of concentration vs. radius are also different for the two line dumps at the same Puerto Rico Dumpsite [Figs. 49(a) and 49(b)]. In particular, the four transects at 1045 minutes and later after the dump [Fig. 49(b)] have very sharp boundaries at $r = r_o$. It appears that the rapid slope change at $r = r_o$ is due to the current effect on plume structure, which we discussed in Figs. 28 to 30.

The diffusion parameters from Fig. 49(a) are summarized in Table 9. The peak concentration and the calculated variance and apparent diffusivity from equations (10) and (11) are shown in Fig. 50. The peak concentration depends on time to the fourth power [Fig. 50(a)]. The variance approximately follows the third power law of dependence on time. The apparent diffusivity approximately follows the 4/3 law. We added the variance and apparent diffusivity from Fig. 50 to the same graphs of Okubo (1968, 1971b) for comparison. The Puerto Rico data fall closely to Okubo's data as shown in Figs. 51 and 52.

V. PARTICLE BUDGET AND TOTAL SUSPENDED MATERIAL

As described before, one of the essential assumptions for the particulate concentration analysis based on measured acoustic backscattering intensities is equation (1). How true this direct relationship holds is unclear; further studies definitely are needed. Besides the direct calculation of total particle budget, other results and calculations based on acoustic intensities can

Table 9. Summary of diffusion parameters for the Puerto Rico industrial waste dumping on February 6, 1978, for three transects.

	1	2	3
t(s)	1.95×10^4	2.58×10^4	2.70×10^4
r_o(m)	52	56	60
$\lambda(r < r_o)$	1	1	1
$\lambda'(r > r_o)$	0	0	0
$\alpha(r < r_o)$	1.70	1.39	1.22
$\alpha'(r > r_o)$	0.558	0.742	0.571
P_o(cm s^{-1})	0.16	0.16	0.18
P_o'(cm s^{-1})	0.12	0.07	0.10
C_o	69.4	42.4	19.1
σ^2(cm^2)	5.4×10^8	2.8×10^8	1.0×10^9
K(cm^2 s^{-1})	6.9×10^3	2.7×10^3	9.6×10^3
ℓ (cm)	7.0×10^4	5.0×10^4	9.7×10^4

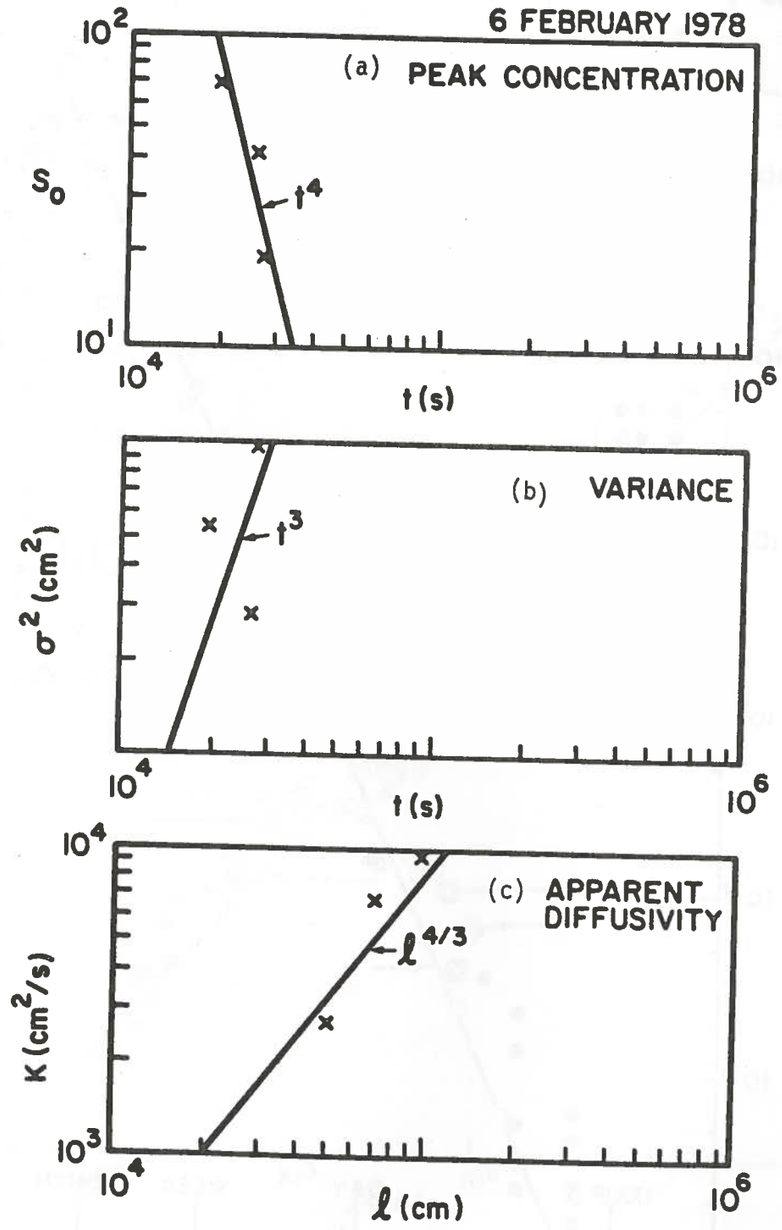

Fig. 50. (a) Peak concentration and (b) variance as a function of time, and (c) apparent diffusivity as a function of length scale for the Puerto Rico Arecibo Industrial Waste Dumping Experiment.

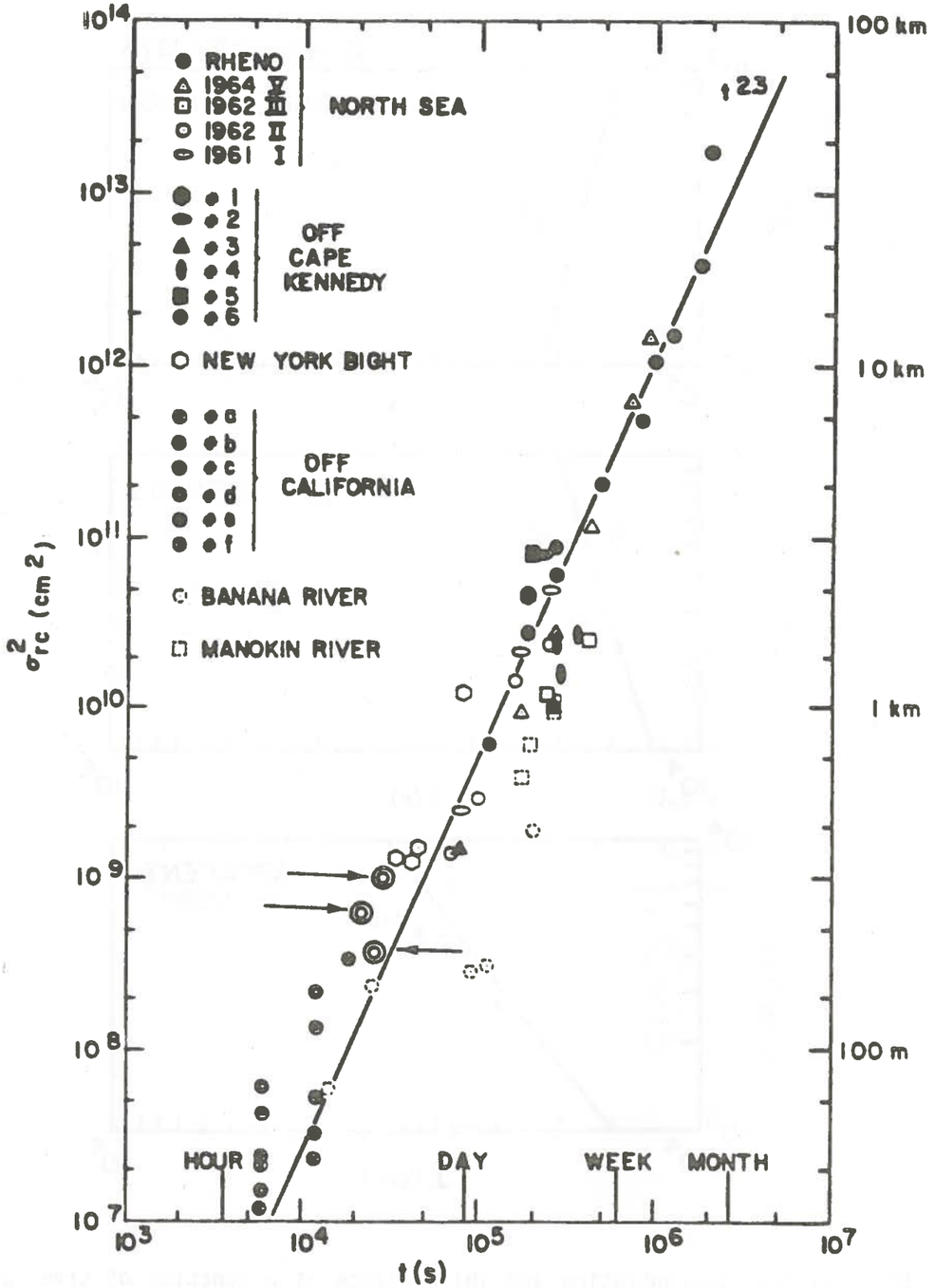

Fig. 51. Variance as a function of time from Okubo (1968, 1971b) and from Fig. 50(b). Data from Fig. 50(b) are plotted as double circles and indicated by arrows.

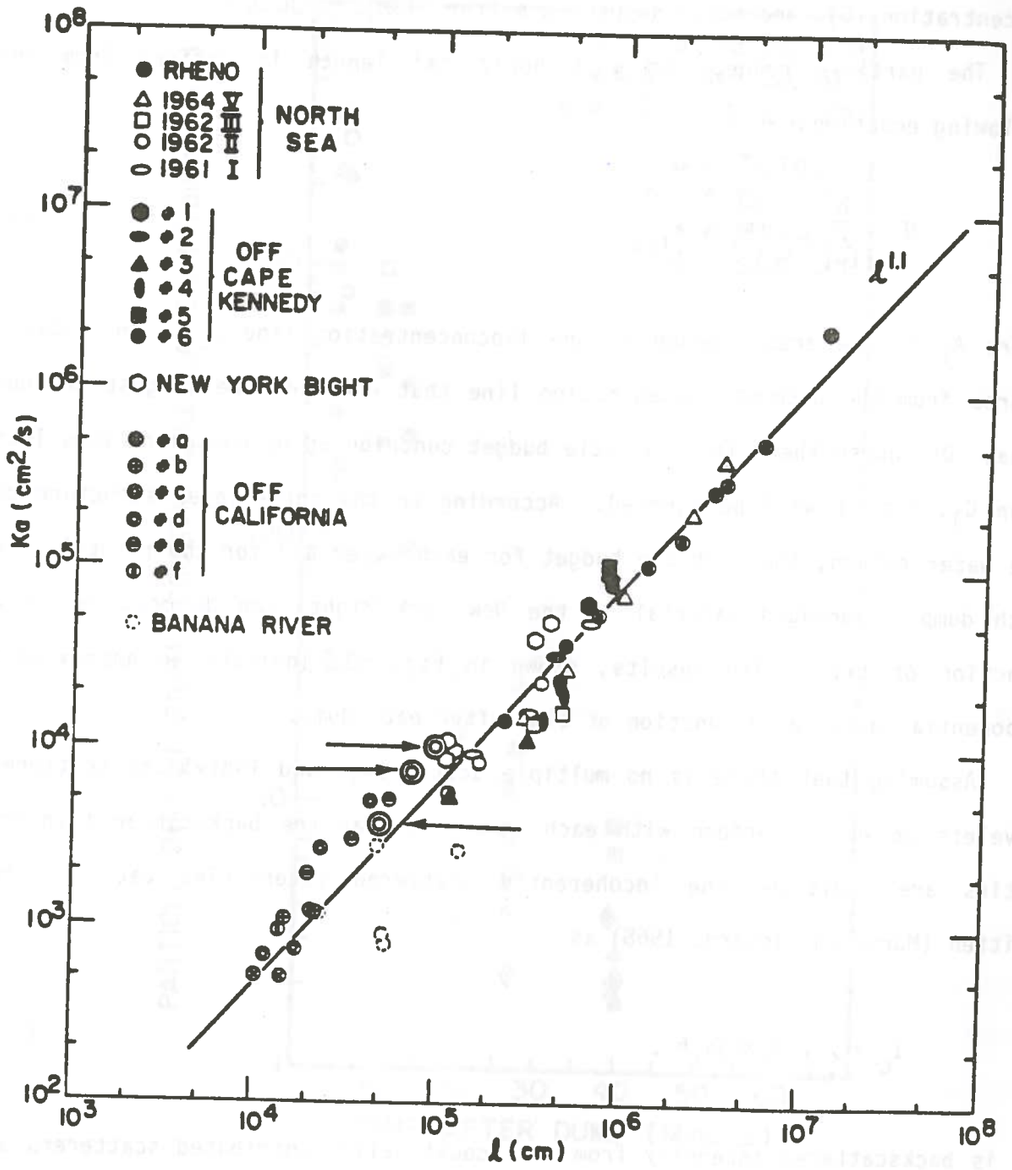

Fig. 52. Apparent diffusivity as a function of length scale from Okubo (1968, 1971b) and from Fig. 50(c). Data from Fig. 50(c) are plotted as double circles and indicated by arrows.

be compared with chemical measurements in several aspects. We will use the New York Bight data to demonstrate the relationships among intensity (I), concentration (C), and total suspended matter (TSM).

The particle budget for unit horizontal length is derived from the following equation:

$$\overline{N} = \sum_{i=1}^{n} C_i \left(A_i - A_{i+1}\right) \qquad (12)$$

where A_i is the area bounded by the isoconcentration line C_i. The index i starts from the outmost concentration line that encloses the largest contour area. Of course there is a particle budget contributed by concentrations less than C_1, but it will be ignored. According to the three-layer structure of the water column, the particle budget for each layer and for their total, for each dump of dredged material in the New York Bight, can be measured as a function of time. The results, shown in Fig. 53, indicate an approximate exponential decay as a function of time after each dump.

Assuming that there is no multiple scattering, and individual scattered wavelets do not interfere with each other so that the backscattered intensities are additive, the incoherently scattered intensities can then be written (Morse and Ingard, 1968) as

$$I_c = \sum_i \beta (N_i z^2) a_i^6 \ . \qquad (13)$$

I_c is backscattered intensity from all acoustically contributed scatterers at depth z. N_i is the number of particles with size a_i. β is taken to be constant and independent of particle size and depth. Assuming constant density ρ regardless of the difference in particle sizes, the TSM at depth z can be approximated by

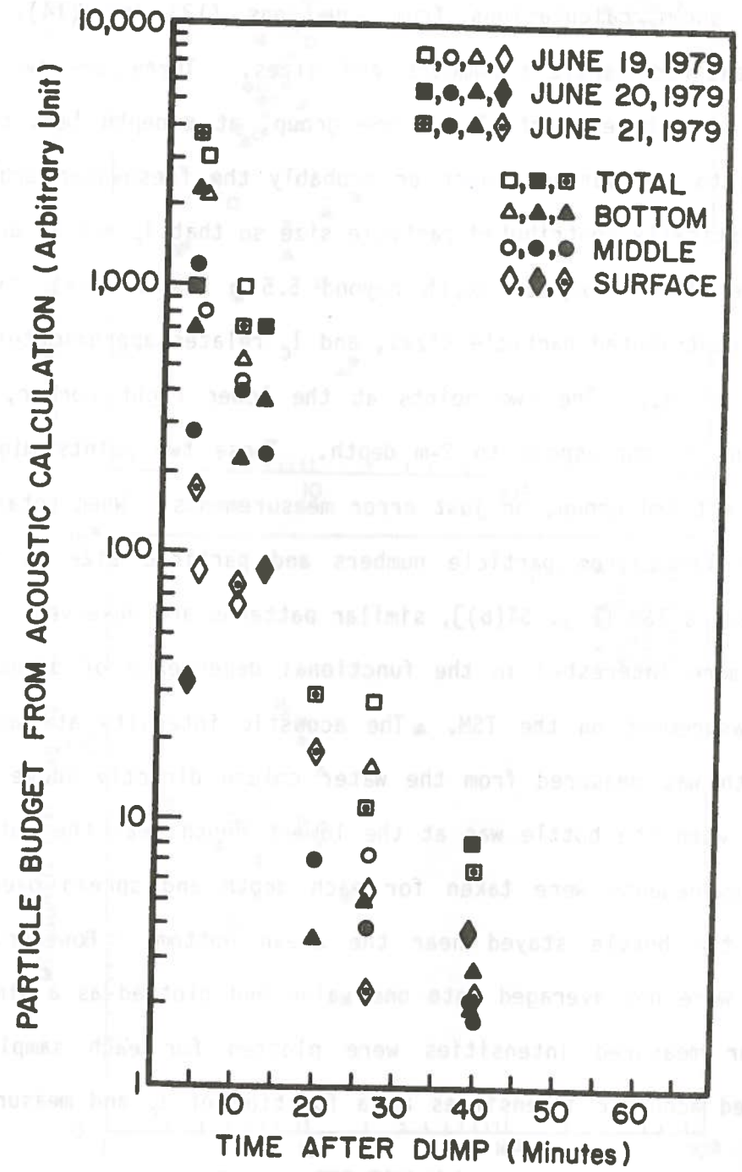

Fig. 53. Particle budget, calculated from acoustic intensity measurements of the three spot dumps in the New York Bight, as a function of time after each dump. The three dumps are the same as those in Figs. 16 to 18 and Figs. 32 to 34.

$$M_C = \sum_i N_i \left(\frac{4}{3} \rho a_i^3\right). \qquad (14)$$

Figure 54(a) shows calculations from equations (13) and (14), using the chemically measured particle numbers and sizes. There are two groups of acoustically contributed particles. One group, at a depth less than 5.5 m, corresponding to the surface layer or probably the freshwater sublayer, has only one acoustically contributed particle size so that I_C and M_C are linearly related. The other group at depth beyond 5.5 m has at least two or more acoustically contributed particle sizes, and I_C relates approximately with the second power of M_C. The two points at the lower right corner, data from stations 5 and 6, correspond to 2-m depth. These two points might suggest existence of a third group, or just error measurements. When total suspended material calculated from particle numbers and particle size is related to directly measured TSM [Fig. 54(b)], similar patterns are observed.

We are more interested in the functional dependence of direct acoustic intensity measurement on the TSM. The acoustic intensity at each chemical sampling depth was measured from the water column directly above the Niskin water bottle when the bottle was at the lowest depth near the bottom. Four intensity measurements were taken for each depth and spread over the time period when the bottle stayed near the ocean bottom. However, the four measurements were not averaged into one value and plotted as a single point; instead, four measured intensities were plotted for each sampling depth. These measured acoustic intensities as a function of I_C and measured TSM are

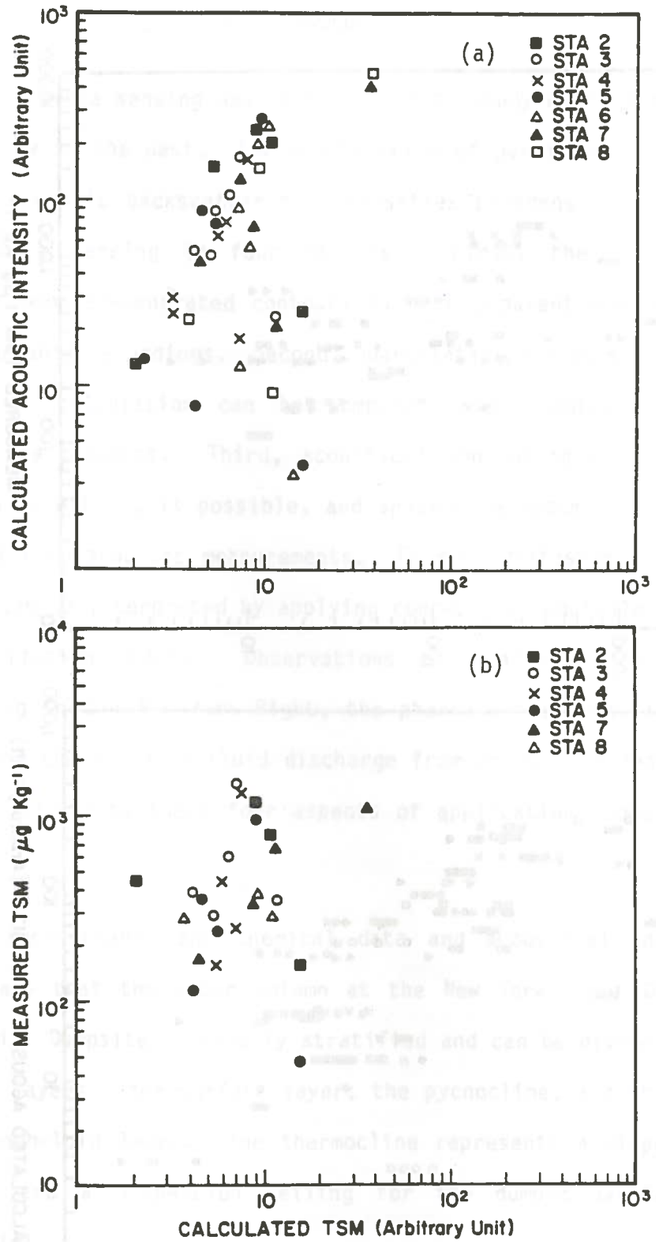

Fig. 54. (a) Acoustic intensity vs. total suspended material, both calculated from chemically measured particle numbers and particle sizes, and (b) measured TSM vs. TSM calculated from particle numbers and particle sizes for the seven stations during the 3-day Dredged Material Dumping Experiment in the New York Bight.

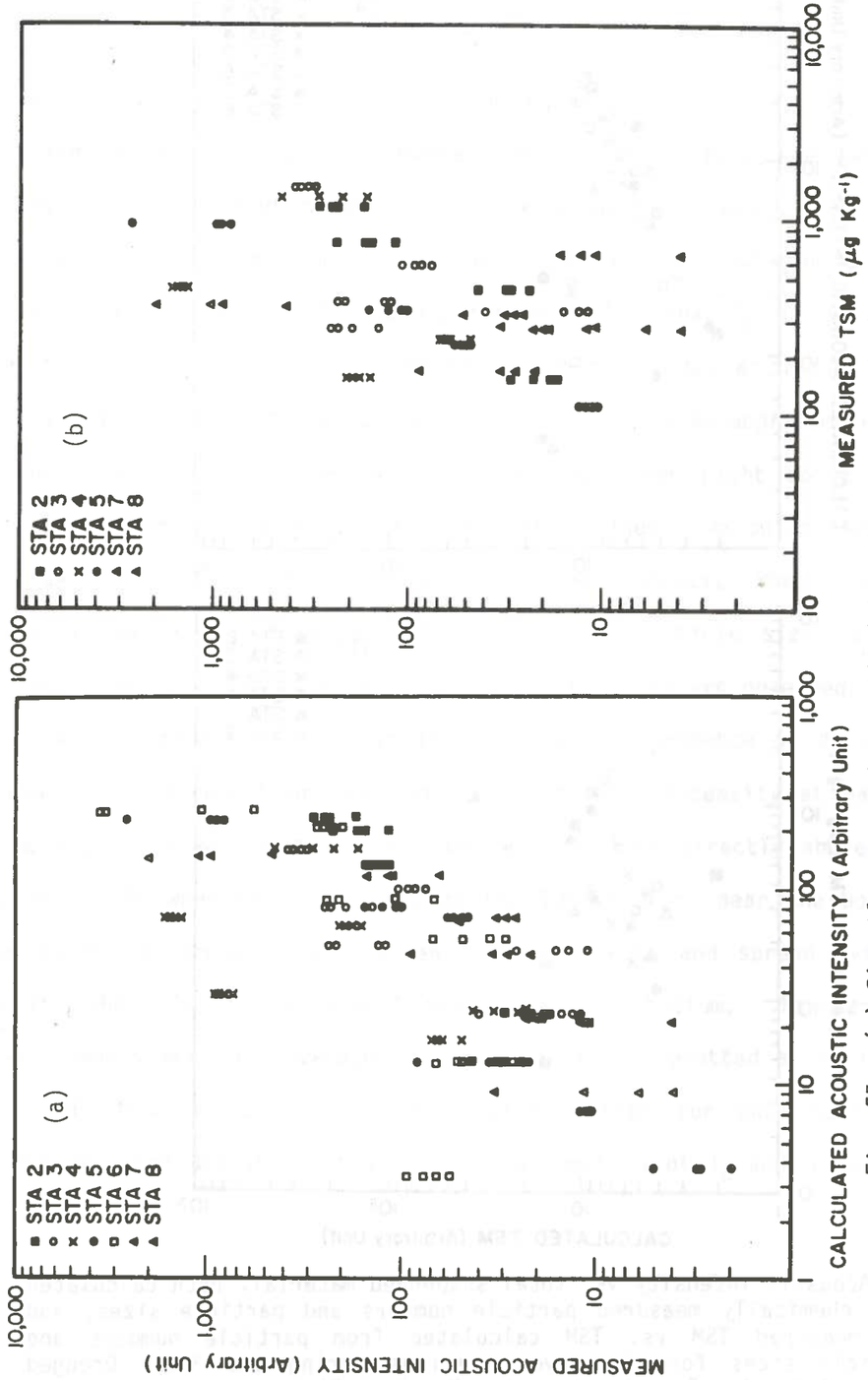

Fig. 55. (a) Directly measured acoustic intensity vs. acoustic intensity calculated from particle numbers and particle sizes, and (b) measured acoustic intensity vs. measured total suspended material for the same stations in Fig. 54. For each station, there is one calculated value of acoustic intensity at each depth, but there are four measured values of acoustic intensity taken from the same depth.

VI. CONCLUSIONS

Acoustical remote sensing has been applied to study waste disposal in the ocean succesfully in the past. The construction of particulate concentration contours from acoustic backscattering intensities broadens the usefulness of acoustical remote sensing in four aspects. First, the plume structure obtained from computer-generated contours is more apparent and detailed than in real-time graphic recordings. Second, quantitative analysis is possible so that results of calculation can be compared with chemical and physical oceanographic measurements. Third, acoustical monitoring of drilling-fluid discharge from an oil rig is possible, and space-time waste distributions can be constructed from acoustic measurements. Fourth, diffusion processes from ocean dumping can be interpreted by applying concepts of equivalent radius and theoretical diffusion models. Observations and analysis from the dredged material dumping in the New York Bight, the pharmaceutical waste dumping off Puerto Rico, and the drilling-fluid discharge from an oil rig near the Flower Gardens Banks illustrate these four aspects of application; some conclusions can be made:

(1) Both hydrographic and chemical data and acoustical analysis indicate that the water column at the New York Bight Dredged Material Dumpsite is clearly stratified and can be divided into three layers: the surface layer, the pycnocline, and the bottom nepheloid layer. The thermocline represents a dispersion floor and a dispersion ceiling for the dumped particulate material.

(2) The Antilles Current at the Arecibo Industrial Dumpsite off Puerto Rico has a strong effect on the plume structure when

dumping takes place at the dumpsite. The westward current always creates a sharp boundary at the eastern edge of the plume.

(3) Acoustic measurements of drilling fluid discharged from an oil rig north of the Flower Gardens Banks indicate a complicated plume structure near the rig. Away from the rig, the space-time distribution generally follows the current pattern at the rig. The vertical section of the discharged plume has a U shape similar to the one observed by Ayers et al. (1980).

(4) Using Joseph and Sendner's (1962) model, a two-process diffusion is observed for dumping of dredged materials in shallow water and industrial wastes in deep water, with different diffusion velocities and spatial variations at a given time. A boundary point is found and interpreted as the characteristic distance r_0 defined in Joseph and Sendner's solution. As time goes on, one of the two diffusion processes changes from Fickian diffusion with constant diffusivity to Joseph and Sendner's solution of constant diffusion velocity, and the other process undergoes the opposite change. This is particularly true in the shallow water of the New York Bight. Both peak concentration and variance also show a break point in time at which the functional dependence changes.

(5) A particle budget calculated from acoustic intensity measurements of the dumped dredged materials in the New York Bight shows an approximate exponential decrease as a function of time for each of the three layers and the water column as a whole.

(6) Acoustic intensity and total suspended material can be calculated from the chemically measured particle numbers and particle sizes. The relation between the calculated intensity and total suspended material (TSM) from the New York Bight Dumping Experiment indicates that there are two groups of particulate substance. Direct and linear relationships are found among the calculated acoustic intensity and TSM, chemically measured TSM, and observed acoustic intensity.

ACKNOWLEDGMENTS

Data used in this report are from several projects led by Dr. John R. Proni, Chief, Ocean Acoustic Division. Special thanks are given to all members of the division for the success in the team work.

REFERENCES

Ayers, R. C., Jr., T. C. Sauer, Jr., and D. O. Stuebner, 1980. An environmental study to assess the effect of drilling fluids on water quality parameters during high rate, high volume discharges to the ocean. In: Proceedings of Research and Environmental Fate and Effects of Drilling Fluids and Cuttings, Vol. 1, Lake Buena Vista, Florida, Symposium Committee, Washington, D.C., pp. 351-381.

Bowman, N. J., and L. D. Wunderlich, 1976. Hydrographic properties. MESA New York Bight Atlas Monograph, 1, New York Sea Grant Institute, Albany, 78 pp.

Csanady, G. T., 1966. Accelerated diffusion in the skewed shear flow of lake currents. J. Geophys. Res., 71(2), 411-420.

Gifford, F., Jr., 1957. Relative atmospheric diffusion of smoke puffs. J. of Meteor., 14, 410-414.

Joseph, J., and H. Sendner, 1958. Uber die horizontale Diffusion im Meere. Deutsche Hydrographische Zeitschrift, 11(2), 49-77. (Also, English translation by G. I. Roden. Horizontal diffusion in the sea, unpublished manuscript.)

Joseph, J., and H. Sendner, 1962. On the spectrum of the mean diffusion velocities in the ocean. J. Geophys. Res., 67, 3201-3205.

Kester, D. R., B. H. Ketchum, I. W. Duedall, and P. K. Park (Eds.), 1983. Dredged Material Disposal in the Ocean. John Wiley and Sons, Inc., New York, 384 pp.

Mamayev, O. I., 1975. Temperature-Salinity Analysis of World Ocean Waters. Elsevier Scientific Publishing Co., Amsterdam, 374 pp.

Morse, P. M., and K. U. Ingard, 1968. Theoretical Acoustics. McGraw-Hill, Inc., New York, 927 pp.

Mukherji, P., D. R. Kester, and R. W. Zuehlke, 1981. Chemical investigations of dredged material disposal in the marine environment. Unpublished Report, University of Rhode Island, Kingston, Rhode Island. Submitted to National Oceanic and Atmospheric Administration-Office of Marine Pollution Assessment, Rockville, Maryland, 48 pp.

Okubo, A., 1962a. A review of theoretical models for turbulent diffusion in the sea. J. Oceanogr. Soc. Japan, 20th Anniversary Volume, 286-320.

Okubo, A., 1962b. Horizontal diffusion from an instant point-source due to oceanic turbulence. Technical Report 32, Chesapeake Bay Institute, The Johns Hopkins University, Maryland, 124 pp.

Okubo, A., 1968. A new set of oceanic diffusion diagrams. Technical Report 38, Chesapeake Bay Institute, The Johns Hopkins University, Maryland, 45 pp.

Okubo, A., 1970. Ocean mixing. Technical Report 62, Chesapeake Bay Institute, The Johns Hopkins University, Maryland, 119 pp.

Okubo, A., 1971a. Horizontal and vertical mixing in the sea. In: Impingement of Man on the Oceans, D. W. Hood (Ed.), Wiley-Interscience, New York, 89-168.

Okubo, A., 1971b. Oceanic diffusion diagrams. Deep-Sea Res., 18, 789-802.

Okubo, A., and H. H. Carter, 1966. An extremely simplified model of the "shear effect" on horizontal mixing in a bounded sea. J. Geophys. Res., 71, 5267-5270.

Pritchard, D. W., A. Okubo, and H. H. Carter, 1966. Observations and theory of eddy movement and diffusion of an introduced tracer material in the surface layers of the sea. In: Proceedings of the Symposium on the Disposal of Radioactive Wastes into Seas, Oceans and Surface Waters, Vienna, May 1966, International Atomic Energy Agency, Vienna, pp. 397-424.

Proni, J. R., D. C. Rona, C. A. Lauter, and R. L. Sellers, 1975. Acoustic observations of suspended particulate matter in the ocean. Nature, 254, 413-415.

Proni, J. R., F. C. Newman, D. C. Rona, D. E. Drake, G. A. Berberian, C. A. Lauter, and R. L. Sellers, 1976a. On the use of acoustics for studying suspended oceanic sediment and for determining the onset of the shallow thermocline. Deep-Sea Res., 23, 831-837.

Proni, J. R., F. C. Newman, R. L. Sellers, and C. Parker, 1976b. Acoustic tracking of ocean-dumped sewage sludge. Science, 193, 1005-1007.

Proni, J. R., F. C. Newman, E. R. Meyer, H. B. Stewart, D. J. Walter, R. L. Sellers, and C. A. Lauter, 1977. On the use of acoustics in applied oceanographic and coastal engineering problems with emphasis on the oceanic transport of particulate materials. Thalassia Jugoslavica, 13, 389-393.

Proni, J. R., and J. B. Stewart, Jr. 1978. Acoustic techniques for ocean pollution studies and their easy transferability to developing nations. Interciencia, 3 24-27.

Trefry, J. H., and J. R. Proni, 1984. Drilling fluid discharge near the Texas Flower Gardens, Northwest Gulf of Mexico. In: Wastes in the Ocean, vol. 1, Energy Wastes in the Ocean, I. W. Duedall et al. (Eds.), Wiley-Interscience, New York, in press.